11 Reactive Polymer Processing and Compounding

One can view *polymerization* as the "structuring" of monomeric molecules into macromolecular structures and *polymer processing* as the "structuring" of polymeric molecules, since it results in products of specific macromolecular orientation and morphology distributions. These two processes require very different types of process equipment and are carried out at different manufacturing facilities. *Reactive polymer processing*, in the broadest sense, is the execution of both processes simultaneously, in equipment normally associated with polymer processing. In reactive polymer processing we go either from monomer to polymer, or more often, from polymer to *modified* polymer, to shaped and structured finished products (1). Extruders, both single and twin rotor, have unique advantages in that they are capable of handling high viscosity reacting systems. On the other hand, extruders also have limitations, which must be considered when selecting equipment for a given reacting polymer stream. Following Todd (2), the advantages are easy handling and melting of polymeric particulates; rapid laminar distributive and dispersive mixing of the reactants; good temperature and residence-time distribution control; the ability to react in one or more stages under appreciable pressure levels; and also the ability to remove by the devolatilization elementary step (3) volatile unreacted species, or reaction by-products. Finally, such devices are very good drag pressurization devices and affect easy viscous melt discharge and shaping. The two main limitations are (a) difficulty in handling large heats of reaction, and (b) the high equipment cost, because of the need that the process provide for long reaction times. It is because of these two limitations that only few classic polymerization reactions are carried out in continuous reactive polymer equipment and go from monomer to finished polymer. On the other hand, single and twin rotor processing equipments are uniquely suited as *reactors* for carrying out *polymer chain modification reactions*. In this chapter, we concentrate on such reactive polymer systems, which create novel, value-added, or "designer pellet polymers," needed to meet specific product properties.

The equipment in which reactive polymer processing is carried out, is in fact a *chemical reactor*. The performance, design, analysis, and control of such reactors have been dealt

Principles of Polymer Processing, Second Edition, by Zehev Tadmor and Costas G. Gogos

with extensively in the chemical engineering literature (4). We follow the standard chemical engineering reactor design approach, pointing out both the similarities and the profound differences between classic chemical engineering *low viscosity* reactor design and that which is necessary in *high viscosity* reactors as the ones used in reactive processing. The main differences between the two are the conditions required for achieving adequate mixing: in low-viscosity reactors, with their turbulent flow regimes, mixing times for achieving composition uniformity, although they have to be addressed, are short compared to the *characteristic reaction times*. Whereas in high viscosity reactors, in which only laminar creeping flows are attainable, we have to secure efficient low-energy–consuming distributive flow kinematics to achieve mixing times that are commensurate to the reaction times of the reacting components. In this chapter we make use of the *ratios of characteristic times* of the competing processes of mixing, diffusion, reaction, and heat generation/transfer, pioneered by Biesenberger and Sebastian (5).

11.1 CLASSES OF POLYMER CHAIN MODIFICATION REACTIONS, CARRIED OUT IN REACTIVE POLYMER PROCESSING EQUIPMENT

There are many polymer chain modification reactions of different types that have been carried out on polymer melts processed in single and twin rotor extruders. This activity, (4–6) in the analysis of polymerization reactors, driven by market forces seeking to create value-added polymers from commodity resins, started in the mid-1960s in industrial research laboratories (7). Indeed much of the early work is to be found in the patent literature.[1] Although in recent times more publications, both industrial and academic can be found in the open literature, there is still a good deal of industrial secrecy, because the products of reactive polymer processing are of significant commercial value to industry. Below we will deal briefly with two important examples of such reactions.

Chain Functionalization Reactions

Chain functionalized polymers or graft copolymers are of great technological importance. They are used as compatibilizing agents for immiscible polymer blends (8) and adhesive layers between polymer–polymer co-extruded surfaces (8). Currently, of all polymers sold, about 30% are in the form of compatibilized immiscible blends (9–12). Next we discuss a few examples of chain functionalization.

Reactive polymer processing has been used extensively in the manufacture of carboxyl-containing polymers (8). The *carboxylation of unsaturated polymers* with maleic anhydride (MAH) proceeds through the ''ene'' reaction where succinic anhydride is attached to the polymer with a shift of the double bond to the adjacent site.

1. Kowalski (7), commenting on the early period of work in this area, stated as follows: ''At Exxon Chemical we measured the level worldwide interest in reactive extrusion via a patent and literature survey for the period 1966–1983. We found a total of more than 600 different patents granted to 150 companies—many Japanese. In comparison only 57 papers were found in the open literature, mostly by extruder vendors . . . only three papers were from the above 150 companies!''

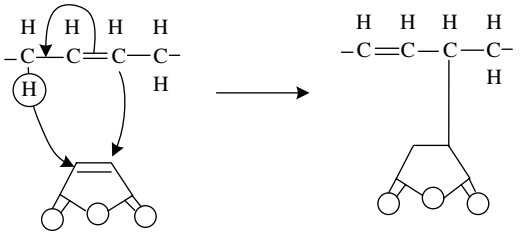

The carboxylated ethylene–propylene–diene elastomeric terpolymer (EPDM) with MAH (13)

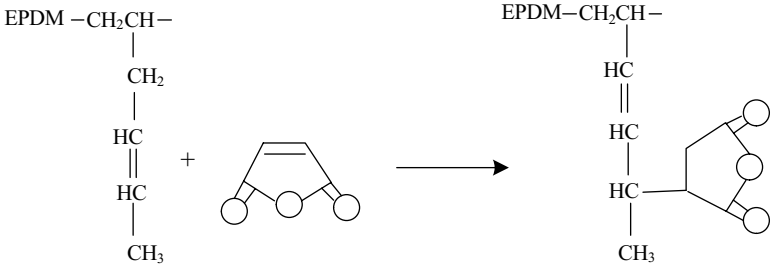

is one of the components of producing the impact modified Dupont SuperTough™ Nylon 6-6 compatibilized polymer blend. The blend components are: EPDM–MAH–Nylon–EPDM, EPDM and Nylon 6-6 (Zytel™ST) (14,15). The two amine groups of Nylon 6-6 (one at each end) are capable of reacting and cross-linking the EPDM, creating the compatibilizing first blend component in the preceding formula. The dispersed 20% elastomeric phase is of the order of one micron and is the main toughening agent.

Hydroxylation of saturated polymers can also take place in polymer processing equipment. As a first example, MAH in the presence of a free-radical initiator will attach succinic or anhydride groups on the saturated chain (16)

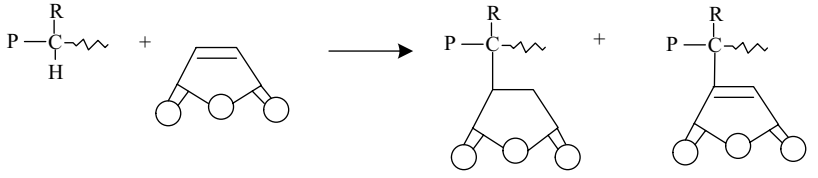

Although this reaction does not involve MAH homopolymerization, the reaction conditions used are those promoting homoplymerization. Thus, the MAH homopolymerization mechanism has to be understood in order to properly carry out the MAH carboxylation of saturated polymers in the presence of a free radical initiator. In other words, maleation of polyolefins represents a rather complex reaction, involving dimethyl formmanide (DMF) to inhibit the undesirable MAH homopolimerization (17) and diamyl peroxide (DCP) to partially cross link the polyolefins being maleated (18). About 0.2% of the MAH is grafted onto polyolefins using peroxide (POX) concentrations of 100–500 ppm. We discuss the decomposition rate requirements in Section 11.2 in a process scheme shown in Fig. 11.1. Higher levels of POX achieve higher bonded MAH concentrations, but result in chromophoric reactions, which are product-undesirable. Colorless maleated polyolefins can be produced at concentrations greater than 0.2% in

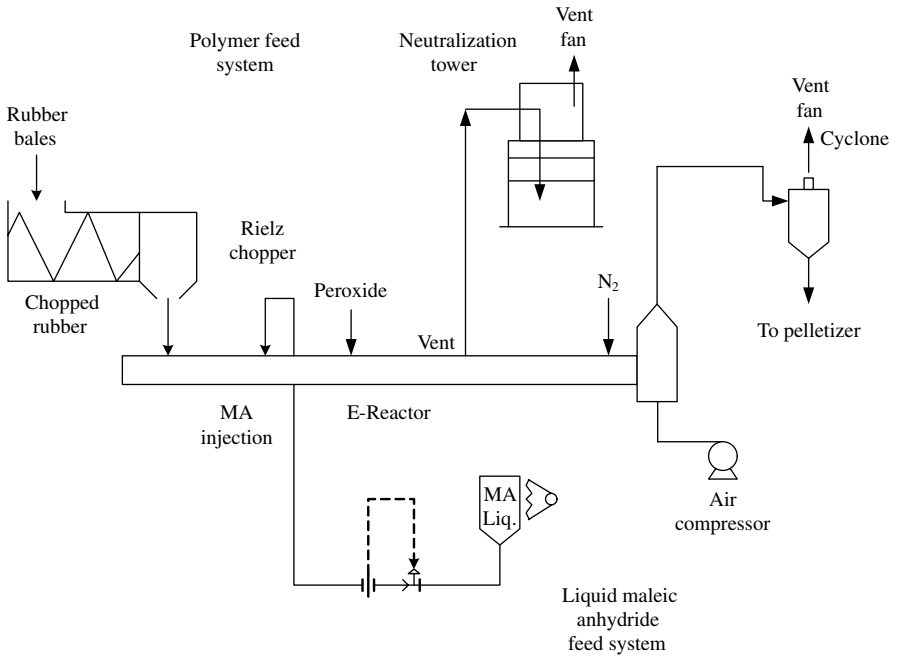

Fig. 11.1 Maleic anhydride graft process for baled EP rubber. [Reprinted by permission from R. C. Kowalski, "Fit the Reactor to the Chemistry," in *Reactive Extrusion,* M. Xanthos, Ed., Hanser, New York, 1992.]

dilute solution; it is obvious, therefore, that maleation, carried out in reactive polymer processing equipment taking place under evolving degrees of mixedness and in nonuniform temperature fields that are difficult to control, is a more complex reaction scheme. We will be discussing the roles and control of the competing phenomena of laminar mixing, temperature increases, diffusion, and reaction in Sections 11.2 and 11.3. Saturated polymers are also commonly carboxylated with acrylic acid (AA) monomer, which is itself polymerizable, since the reaction takes place in the presence of a free-radical initiator. The result is a graft copolymer, where the polyacrylic acid is the graft, produced simultaneously with polyacrylic acid. The mechanisms are, for homodymerization (19,20):

$$
\begin{aligned}
R\cdot + (AA) &\xrightarrow{k_a} (AA)\cdot \\
(AA)\cdot + M &\xrightarrow{k_p} (AA)_2\cdot \\
&\vdots \\
&\vdots \\
(AA)_x\cdot + M &\xrightarrow{k_p} (AA)_{x+1}\cdot \\
(AA)_x\cdot + (AA)_y\cdot &\longrightarrow (AA)_{x+y}
\end{aligned}
$$

or

$$
\longrightarrow (AA)_x + (AA)_y
$$

The simultaneous and desired grafting of polyacrylic acid onto the saturated host polymer proceeds as:

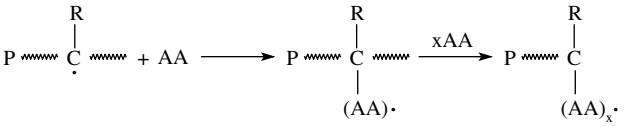

followed by the termination step(s).

Common saturated polymers-forming copolymers with AA are HDPE, PP and ethylene–propylene copolymer (EPR), the last being a grafted elastomer. All are blend compatibilizers, high density polyethlene (HDPE)–g–AA, PP–g–AA, and EP–g–AA. Producing these copolymers through reactive processing is the only reaction route available, because copolymerization between AA and the olefin monomers just given is not possible since the polar AA reacts and inactivates the metal-based olefin polymerization catalysts (8).

Polymer Macromolecular Chain Modification Reactions

Soon after the Ziegler–Natta catalyst enabled the commercial production of isotactic polypropylene (PP), it became apparent that it was a difficult polymer to melt process, especially in producing thin fibers at acceptable rates. Kowalski (21) carrying out retarded elastic melt recovery experiments with an instrument developed by Bryce Maxwell showed that PP has an unusually high melt elasticity that results in both extrudability problems and extruded products with high levels of retained orientation. Later, Kowalski and his co-workers at Esso Research and Engineering (22–25) extruded PP using a ''reverse'' temperature profile by setting high barrel temperatures of 370–425°C at the single screw extruder (SSE) melting zone. Such high temperatures near the feed zone will generate oxygen free radicals from the air in the particulates solid bed. Such free radicals may initiate a β chain scission reaction at the ternary carbon backbone sites of the PP melt. Since chain scission is more likely to occur with longer PP chains, the product of the preceding reaction will be of lower weight-average molecular weight ($\bar{M}_W$) *and* narrower molecular weight distribution (MWD). In turn, these polymer chain modifications have a profound effect on both melt viscosity and melt elasticity, as shown in Fig. 11.2, where melt flow rate (MFR), indicative of viscosity and extrudate swell, indicative of melt elasticity, are plotted against MW and MWD (21,9). It is evident from this figure that the *entire viscoelastic behavior* is affected by the chain ''degradation path,'' that is, each of the five cures on Fig. 11.2, where the parameter MFR is indicative of the viscous nature and the extrudate swell is indicative of the elastic nature of the PP viscracked melts. They are plotted against $\bar{M}_W$ and MWD. It is evident on this figure that the entire viscoelastic behavior is affected in every one of the degradation paths, that is, each of the five curves on Fig. 11.2. It is for this reason that the free radical polymer chain modification of PP carried out by reactive processing is commonly referred to in practice as ''controlled rheology'' (CR–PP) or viscracking processes. In practice, the *amount and rate* of the free radical POX initiator can be controlled, as can the *protocol and mode of addition* of the POX stream, mixed with the feed, or introduced as a diluted or undiluted liquid at an appropriate axial position, usually after melting is completed. It must be noted, though, that the presence of oxygen and process stabilizers (free-radical scavengers) may interfere through radical

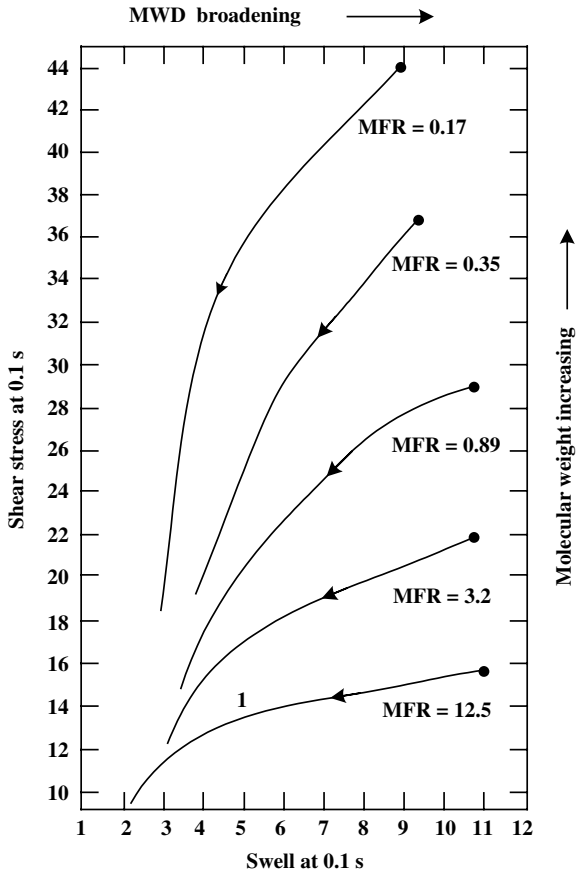

Fig. 11.2 The effect of the PP controlled rheology (CR) or ''viscracking'' process on the ''viscoelastic grid''; each curve represents a PP macromolecular ''degradation path.'' [Reprinted by permission from R. C. Kowalski, ''Fit the Reactor to the Chemistry,'' in *Reactive Extrusion*, M. Xanthos Ed., Hanser, New York, 1992.]

competing reaction (26). Hence, closed-loop viscracking control schemes, based on the linear relationship between POX concentrations and MFR, have been developed by industry (27–29) as well as by academic research (30,31). Of course, in-line or on-line measurement of MFR is required in these control schemes. Information on the ''process technology'' of CR–PP processes can be found in Xanthos (26), and the accepted PP degradation reaction with peroxides ROOR is given by Dorn (32) and Tzoganakis, Vlachopoulos, and Hamielec (33).

Since the peroxide decomposition may be the rate-controlling reaction step in the preceding, it is of paramount importance to choose the peroxide that has the ''required'' decomposition rate at the real or expected melt processing temperatures. Such rates for dialkylperoxides are determined from decomposition kinetic data carried out in dilute decane or dodecane solutions in the form of half-lives, $t_{½}$, which is the time required for the decomposition of 50% of the POX (34), as shown in Figure 11.3.

High temperature and low reactivity host substances (e.g., polymers) are known to favor secondary decompositions, leading to other active radicals and nonreactive volatiles

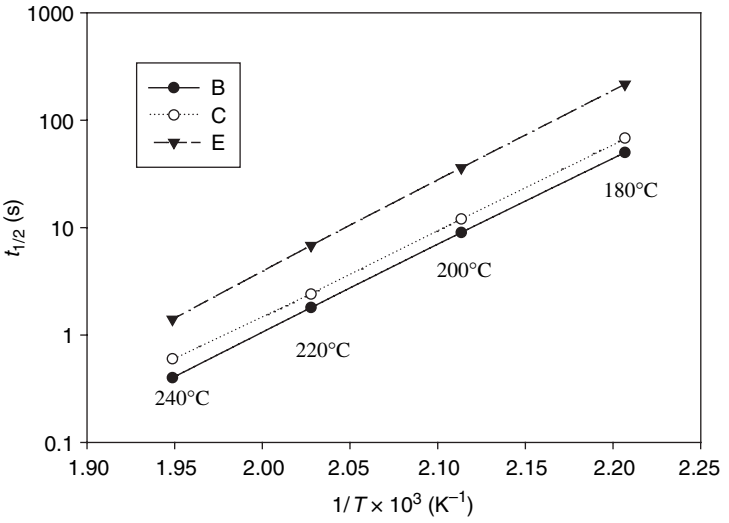

Fig. 11.3 Arrhenius plots of the half-lives of three different POX showing that despite the difference in half-lives among them, their activation energies are of the same value and equal to 155 KJ/mol.

(32). Thus, is it not surprising that the dilute solution, half-lives shown in Fig. 11.3 are different from the experimentally obtained effective half-lives in molten flowing polymers, which may be 2 to 5 times longer than the dilute solutions $t_{½}$ (34,35). An additional reason for this difference is the gradual and, at times, incomplete laminar mixing of the POX in polymer melts, compared to the ''instantaneous'' and homogeneous mixing obtained with very low-viscosity diluents, such as decane. We discuss this further in Section 11.2. Finally, half-lives, $t_{½}$ (T) are important to the semiquantitative *specification* of the required residence time of the polymer in *molten form*, that is, the ''*age*'' of the melt from the time of its formation to the die exit at the prevailing processing temperatures. For 99% POX decomposition, the average residence time of the melt in the reactive polymer processing equipment must be of the order of six to seven times its half-life at the process temperature.

Recalling the profound differences in the melting mechanisms in SSEs and in co-rotating twin-screw extruders (Co-TSE) (Chapter 5), we see that the latter one creates all of the melt almost instantaneously, resulting in a very narrow ''melt age distribution,'' while in SSE the age distribution is very broad. Thus, Co-TSEs and twin rotor *melting* devices [e.g., continuous mixers (CMs)] are better suited to be ''reactors'' of polymer melts, as is reflected in the current industrial reactive polymer processing practice.

Experiments conducted in laboratory-scale batch-intensive mixers can be suitable for following the kinetics of CR–PP. PP pellets or powder are introduced and are completely melted in these hot co-rotating batch devices, under a blanket of nitrogen. Following melting, the POX is introduced all at once and is mixed into the polymer melt. The ensuing PP degradation will cause the torque required to drive the mixer shafts at the process speed to drop, due to the reduction of the melt viscosity of the reacting melt. Figure 11.4 shows the torque reduction rate, which is very similar to the POX (Lupersol 101) decomposition in dodecane (36). The result that the kinetics of the controlling POX decomposition in an isothermal dilute solution environment is the same as the viscracking kinetics in a melt

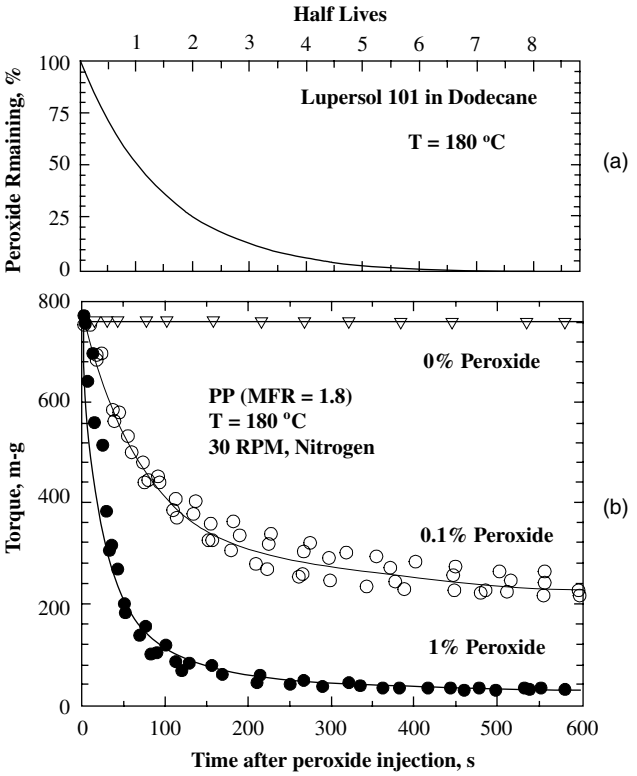

Fig. 11.4 Comparison of (a) the POX decomposition rate in dodecane at 180°C with (b) the rate of reduction of the batch mixer torque, that is, reduction of the viscosity of the reacting PP, indicates that the two are identical; the POX decomposition is *rate controlling* and the CR-PP reactions are practically complete after 6–7 POX half-lives. [Reprinted by permission from D. W. Yu, ''Polyolefin Blends Modified through Peroxide Initiated Reactions,'' Ph.D Dissertation, Department of Chemical Engineering, Stevens Institute of Technology, Hoboken, NJ, 1991.]

continuously mixed at 180°C and 30 rpm indicates that (a) the mixing rate in the batch mixer is fast, compared to the Lupersol decomposition rate, and (b) there is little melt temperature increase during this reactive processing.

Ryu et al. (37) and Xanthos et al. (38) prepared thin films of sintered PP, 200–300 micron diameter, precoated at room temperature with POX ''E''. The films were allowed to react in a constant-temperature oven and samples were withdrawn and analyzed to determine $\bar{M}_W$ and MWD. It was found that the reduction rates of the $\bar{M}_W$ and MWD became essentially zero after six to seven half-lives of POX ''E'' as measured in dodecane. The conclusion is, since there is no mixing during reaction, the diffusion rate of the POX coating onto the PP particulates is not rate controlling, that is, CR–PP for those coated 200–300-μm PP powder particulates is not diffusion controlled. In reactive processing one should strive for process conditions and reaction kinetics where the reactive polymer processing environment is uniform, resulting in uniform product. We discuss this in Sections 11.2 and 11.3.

Finally it is instructive to present the resulting macromolecular chain modifications (MWD) and their effect on the rate-dependent viscosity during viscracking, as shown in

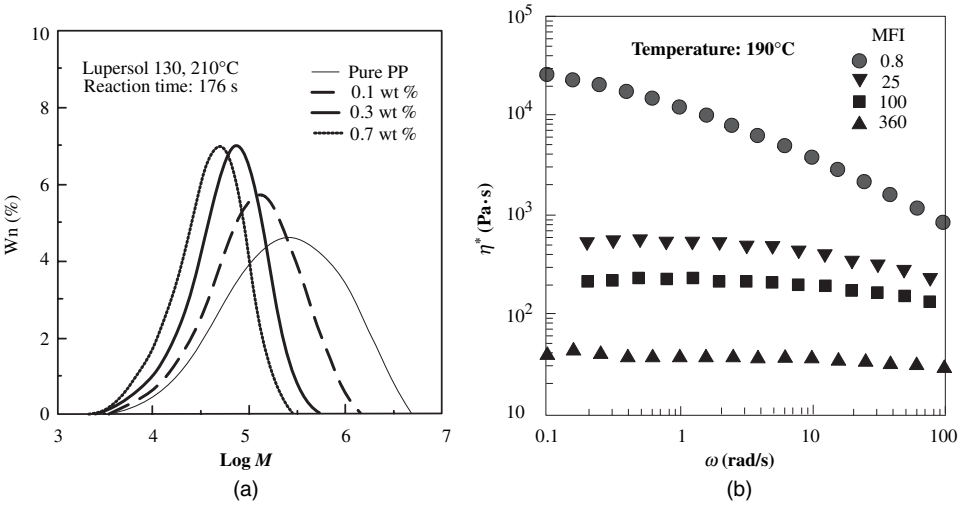

Fig. 11.5 (a) the MWD of a 0.8 MFR PP before and ''viscracking'' using three different POX E concentrations (b) the corresponding dynamic viscosities and MFR values af the original and three ''viscracked'' polypropylenes [Reprinted by permission from S. H. Ryu, C. G. Gogos, and M. Xanthos, ''Kinetic Studies on the Peroxide Initiated Polypropylene Controlled Degradation,'' *SPE ANTEC Tech. Papers*, **35**, 879–881 (1989).]

Figure 11.5 (37). At high POX concentrations, η^* at low frequencies can be reduced 100- to 1000-fold, and the polymer melts become essentially Newtonian. Such CR–PP products are very easily spinnable.

Another example of chain modification reactive processing reactions are those that induce *controlled long chain branching* or *(light) cross-linking*. Such reactions are carried out in the molten state in order to obtain specific melt rheological properties needed for specific polymer shaping methods. As an example, long chain branching incorporation onto (linear) polyethylene terephthalate (PET) chains, imparts sufficient levels of melt elasticity to the long chain branched PETs and make them suitable for extruding foamed or blow molded products (39), both of which require appreciable levels of melt elasticity.

11.2 REACTOR CLASSIFICATION

Chemical reactors are normally classified into *batch* and *continuous* reactors. In *batch* reactors all the species of the ''batch'' of compounds placed into the reactor have the same *residence time*, since the reactor forms a ''closed system'' with no material exchange with the surroundings. If the reactive fluids are agitated and are of monomeric level viscosities, then the resulting turbulent flow imparts *uniform* and practically *instantaneous mixing*. Turbulent flow is also necessary, but not sufficient, to achieve an efficient heat transfer and obtain a uniform batch reactor temperature field. For this to happen, first the heat of reaction has to be relatively small to moderate and second, the rate of heat conducted via both internal and ''jacketed'' vessel wall coolers has to be larger or much larger than the rate of reaction heat generation.

Batch Reactor Analysis

In batch reactors, for thermally simple types of reactions, that is, ones that can be attributed to a single reaction step, generally applicable to the propagation step of polymerization reactions, we can write the following thermal energy balance (6)

$$\frac{dT}{dt} = \frac{(-\Delta H_r)\dot{r}}{\rho C_p} - \frac{hA}{\rho C_p V}(T - T_c) \tag{11.2-1}$$

where $(-\Delta H_r)$ is the heat released by the reaction, $\dot{r}$ the reaction rate, h the overall heat transfer coefficient between fluid and coolant, A the heat transfer area, V the batch reactor volume, and T_e the coolant temperature. Equation 11.2-1 can be rewritten in dimensionless form as

$$\frac{d\hat{T}}{dt} = \frac{(-\Delta H_r)\dot{r}_{\text{ref}}\hat{\dot{r}}}{\rho C_p T_{\text{ref}}} - \frac{hA}{\rho C_p V}(\hat{T} - \hat{T}_c) \tag{11.2-2}$$

where the dimensionless temperature is defined as

$$\hat{T} = \frac{T - T_{\text{ref}}}{T_{\text{ref}}} \tag{11.2-3}$$

and the dimensionless reaction rate is defined as

$$\hat{\dot{r}} = \frac{\dot{r}}{\dot{r}_{\text{ref}}} \tag{11.2-4}$$

where T_{ref} is a reference temperature and $\dot{r}_{\text{ref}}$ is the rate of reaction at the reference temperature.

The two right-hand terms of Eq. 11.2-2 have units of reciprocal time. Physically, they are the inverse of the *characteristic times* for heat released by the reaction, t_G, and for heat removal, t_R. These can be written as

$$t_G = \frac{\rho C_p T_{\text{ref}}}{(-\Delta H_r)\dot{r}_{\text{ref}}} \tag{11.2-5}$$

and

$$t_R = \frac{\rho C_p V}{hA} = \frac{\rho C_p R_H}{h} \tag{11.2-6}$$

where $R_H = V/A$ is a "hydraulic radius." The ratio of these characteristic times gives good estimates on the thermal behavior of the reactor. Thus, Eq. 11.2-2 becomes

$$\frac{d\hat{T}}{dt} = t_G^{-1}\hat{\dot{r}} - t_R^{-1}(\hat{T} - \hat{T}_c) \tag{11.2-7}$$

If $t_G/t_R < 1$, the temperature field is expected to be nonuniform and the average batch-reactor temperature increases with time; whereas, if $t_G/t_R > 1$, the temperature field is

expected to be uniform and time independent, which, of course, is a desirable reactor condition to achieve from the point of view of both reaction control and product uniformity.

A very important characteristic of polymerization reactors is their thermal stability as discussed by Sebastian (6). Chain addition polymerizations are *thermally simple* reactions, in that the polymerization exotherm is attributable almost in its entirety to the chain propagation step. For chain addition polymerization reactors the rate of reaction $\dot{r}$ is proportional to the product of the square root of initiator concentration, c_i, and to monomer concentration, c_m

$$\dot{r} = \dot{r}_p = k_{ap} c_i^{1/2} c_m \tag{11.2-8}$$

where $\dot{r}_p$ is the rate of propagation, and k_{ap} the apparent reaction rate. By assuming that k_{ap} has an Arrhenius-type dependence on temperature characterized by the activation energy E, and substituting Eq. 11.2-8 into Eq. 11.2-7, results in

$$\frac{d\hat{T}}{dt} = t_G^{-1} \hat{\dot{r}}_p - t_R^{-1} (\hat{T} - \hat{T}_c) \tag{11.2-9}$$

where

$$\hat{\dot{r}}_p = e^{\left(\hat{E}\hat{T}/(1+\hat{T})\right)} \hat{c}_i^{1/2} \hat{c}_m \tag{11.2-10}$$

and the dimensionless activation energy and concentration are defined, respectively, as

$$\hat{E} = E/RT_{\text{ref}} \qquad \text{and} \qquad \hat{c}_k = c_k/c_{k0} \tag{11.2-11}$$

Next, following Semenov (40) we define another dimensionless temperature Θ, which is the product of the dimensionless temperature define in Eq. 11.2-3 with the dimensionless activation energy

$$\Theta = \frac{E}{RT_{\text{ref}}} \left(\frac{T - T_{\text{ref}}}{T_{\text{ref}}} \right) = \hat{E}\hat{T} \tag{11.2-12}$$

and in tems of Θ, Eq. 11.2-9 can be written as

$$\frac{d\Theta}{dt} = t_{AD}^{-1} \exp\left(\frac{\Theta}{1 + \varepsilon\Theta} \right) \hat{c}_i^{1/2} \hat{c}_m - t_R^{-1} (\Theta - \Theta_c) \tag{11.2-13}$$

where

$$t_{AD} = \hat{E}^{-1} t_G = \varepsilon t_G \tag{11.2-14}$$

Semenov noted that when $t_G/t_R <<< 1$, explosions may occur even before there is any appreciable depletion of the reactants, that is, when the dimensionless initiator and monomer concentrations are nearly unity and when $T_{\text{ref}} \approx T_0 \approx T_c$, where T_0 is the initial temperature. These conditions constitute the *early runaway approximation*

described by

$$\frac{d\Theta}{dt} \sim \exp\left(\frac{\Theta}{1+\varepsilon\Theta}\right) - a\Theta \tag{11.2-15}$$

where the ignition parameter, a, is the ratio of two characteristic times

$$a = \frac{t_{AD}}{t_R} = \varepsilon\frac{t_G}{t_R} = \varepsilon\frac{h}{(-\Delta H_r)\dot{r}_o R_H} \tag{11.2-16}$$

The dimensionless heat generation term $r_G = \Theta/(1-\varepsilon\Theta)$ is plotted as a function of the dimensionless temperature $\Theta = \hat{T}/\varepsilon$ for various values of the inverse dimensionless activation energy, ε, in Fig. 11.6.

We note two important features on this graph. First, the transition from stable to potentially "runway" conditions increases dramatically with decreasing ε, that is, increasing the reaction constant activation energy; in the limit at $\varepsilon \to 0$ we have explosive conditions. Second, the transition from stable to potentially unstable reactions occurs when the dimensionless at $\Theta = \hat{T}/\varepsilon \sim 1$. Furthermore, for $\Theta = 10^{-1}$ the reaction is stable with $\Theta/(1+\varepsilon\Theta) = 1$ and for $\Theta \geq 10^1$ there are is a significant increase (of the order of 10^4 to 10^{10}) in the dimensionless heat-generation term, denoting the potential of unstable, runway reactions.

Chain addition polymerizations have a typical value of $\varepsilon \approx 4 \times 10^{-2}$, and for such batch reactions r_G increase 10^6 times from $\Theta = 10^{-1}$ to $\Theta = 10$, with the plateau region at Θ values that are 10^{10} times higher. It is for this reason that chain addition polymerization reactions, although experimentally studied, as with methyl methacrylate (41,42), are rarely carried out in reactive polymer processing equipment.

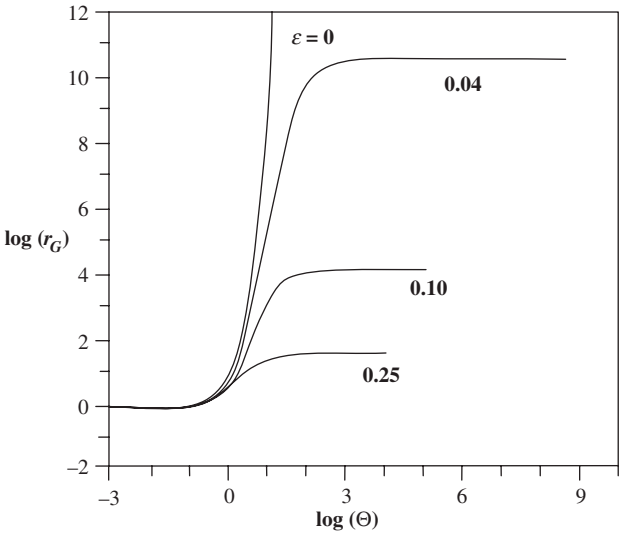

Fig. 11.6 Dimensionless heat generation rates for various values of the dimensionless activation energy. [Reprinted by permission from D. H. Sebastian, "Non-Isothermal Effects in Polymer Reaction Engineering," in *Temperature Control Principles for Process Engineers*, E. P. Dougherty, Ed., Hanser, Munich, 1993.]

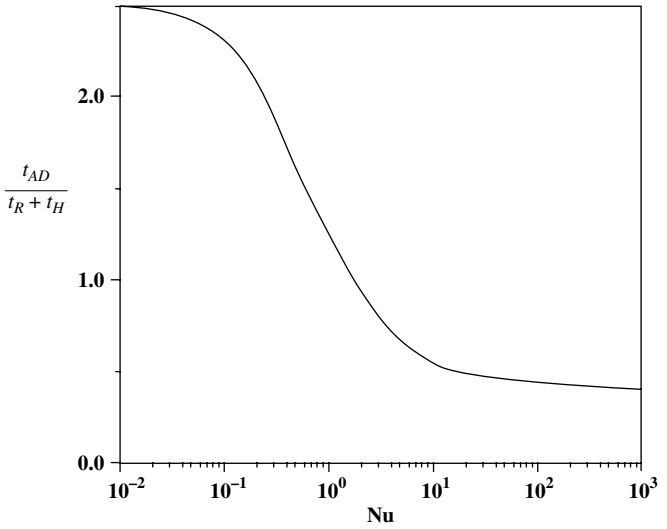

Fig. 11.7 Runaway boundary as a function of Nu number. [Reprinted by permission from D. H. Sebastian, "Non-Isothermal Effects in Polymer Reaction Engineering," in *Temperature Control Principles for Process Engineers*, E. P. Dougherty, Ed., Hanser, Munich, 1993.]

Sebastian (2,6) following Frank-Kamenetskii (43) arrived at the results depicted on Fig. 11.7, where the Nusselt (Nu) dimensionless number $\text{Nu} = hR_H/k$, k is the thermal conductivity, t_H is the characteristic time for removing the reaction-generated heat by conduction

$$t_H = \frac{\rho C_p R_H^2}{k} = \frac{R_H^2}{\alpha_T} \tag{11.2-17}$$

where $\alpha_T = k/\rho C_p$ is the thermal diffusivity. The heat removal in this case is a series process of the fluid conducting to the vessel followed by convective heat transfer to the surroundings. For this case a combined heat removal time is defined below

$$T_R = t_R + t_H \tag{11.2-18}$$

and the Nusselt number is

$$\text{Nu} = \frac{t_H}{T_R} \tag{11.2-19}$$

The ratio of the adiabatic heat generation characteristic time to that of heat removal is now $a = t_{AD}/(t_R + t_H)$ and related to the Nusselt number. For the chain addition polymerization this relation is shown graphically in Fig. 11.7.

It is noteworthy that the transition from large to small ignition parameter a transition is practically complete from $\text{Nu} \sim 10^{-1}$ to $\text{Nu} \sim 10$, and that the transition occurs when a is nearly unity. Both these results, because of their simplicity and because of the fact that they can be generalized to all competing processes, are very useful in understanding the results of the effects of competing processes—in this instance, the adiabatic reaction–generated heat characteristic time to the total heat-removal characteristic time. The

preceding simplified reaction kinetics and reactor behavior models cut to the core of illustrating competing phenomena in reactors. As suggested by Sebastian, the reader should not be deceived by this apparent simplicity. These models do not trivialize the results, but rather capture the essence that distinguishes principal cases of reaction and reactor behavior *without* obscuring the principles in intractable mathematics. Thus they are equally useful in determining dynamic similarity (44) in the process of scale-up as they are in reactor analysis and design.

The foregoing analysis holds for homogeneous single-phase reactions, but can also be applied to nonhomogenous, dispersed-phase morphology consisting of spatially well-distributed small spherical domains. Such systems can be considered, approximately, to be ''pseudocontinua.'' In the preceding analysis of thermally simple propagation reactions in batch reactors, t_m, the mixing characteristic time was assumed to be essentially zero because of the prevailing turbulent flow in the early reaction stages. We now address reactors where mixing is a most important consideration: The polymer processing equipment–reactor is used primarily to modify polymer chains in the molten state; thus, the resulting flows are laminar, mixing times can be considerable, and mixing spatial uniformity can be problematic to product stream quality.

Linear Continuous Flow Reactors

Most reactive polymer processing operations take place in single or twin rotor-type steady continuous-processing equipment or ''reactors.'' Following Biesenberger (3), all continuous flow reactors can be designated as either linear continuous flow reactors (LCFRs), or back-mixed flow reactors (BMFR). In LCFR, shown schematically in Fig.11.8, $L \gg H$ and the dominant flow direction axial. The axial distance downstream the feed inlet, z, corresponds to the time, t, in a batch reactor; that is, the reacting stream in a LCFR ''ages'' along the z direction as the batch material does with time.

The *plug flow reactor* (PFR) is conceptually the simplest example of a LCFR: all fluid elements have the same axial velocity, and therefore they have the same residence time or ''age'' at the exit, which would correspond to the batch reactor time. But, unlike the batch reactor in the CPFR there is no mixing of the species except by diffusion. Figure 11.9(a) schematizes a CPFR.

Tubular flow reactors (TFR) deviate from the idealized PFR, since the applied pressure drop creates with viscous fluids a laminar shear flow field. As discussed in Section 7.1, shear flow leads to mixing. This is shown schematically in Fig. 11.9(a) and 11.9(b). In the former, we show laminar distributive mixing whereby a thin disk of a *miscible* reactive component is deformed and distributed (somewhat) over the volume; whereas, in the latter we show laminar dispersive mixing whereby a thin disk of *immiscible* fluid, subsequent to being deformed and stretched, breaks up into droplets. In either case, diffusion mixing is superimposed on convective distributive mixing. Figure 11.9(c) shows schematically the

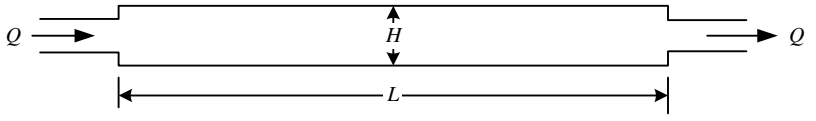

Fig. 11.8 Schematic representation of continuous flow reactors of length L, characteristic height H, and steady flow rate, Q.

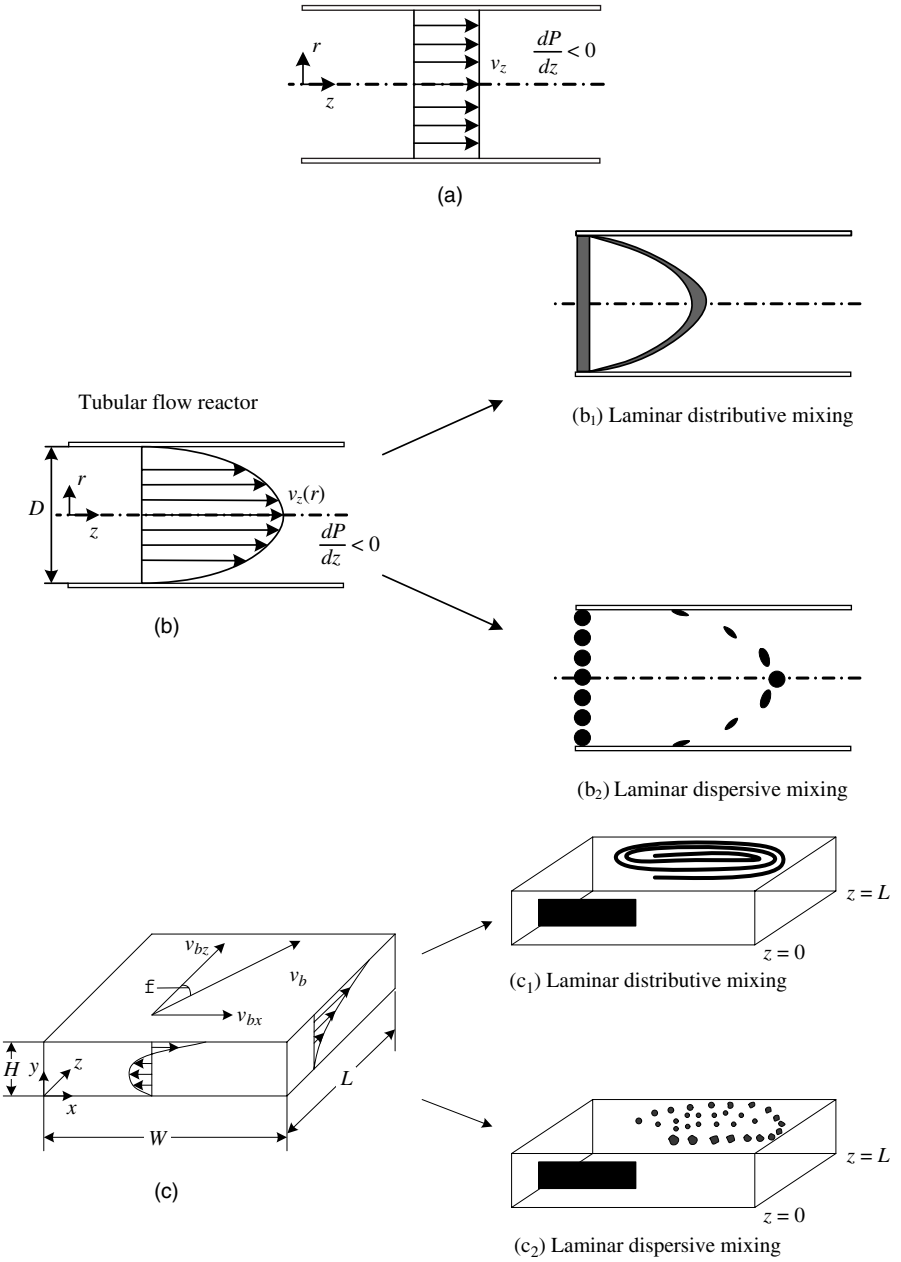

Fig. 11.9 Types of linear continuous-flow reactors (LCFRs). (a) Continuous plug flow reactor (CPFR) resembling a batch reactor (BR) with the axial distance z being equivalent to time spent in a BR. (b) A tabular flow reactor (TFR) with (b_1) miscible thin disk of reactive component deformed and distributed (somewhat) by the shear field over the volume, and (b_2) immiscible thin disk is deformed and stretched and broken up into droplets in a region of sufficiently high shear stresses. (c) SSE reactor with (c_1) showing laminar distributive mixing of a miscible reactive component initially placed at $z = 0$ as a thin slab, stretched into a flat coiled strip at $z = L$, and (c_2) showing dispersive mixing of an immiscible reactive component initially placed at $z = 0$ as a thin slab, stretched and broken up into droplets at $z = L$.

prevailing down-channel and cross-channel velocity profiles in the metering section of an SSE, with (c_1) showing laminar distributive mixing of a miscible reactive component initially placed at $z = 0$ as a thin slab, stretched into a flat coiled strip at $z = L$, and with (c_2) showing dispersive mixing of an immiscible reactive component initially placed at $z = 0$ as a thin slab, stretched and broken up into droplets at $z = L$.

The SSE is an important and practical LCFR. We discussed the flow fields in SSEs in Section 6.3 and showed that the helical shape of the screw channel induces a cross-channel velocity profile that leads to a rather narrow residence time distribution (RTD) with cross-channel mixing such that a small axial increment that moves down-channel can be viewed as a reasonably mixed differential batch reactor. In addition, this configuration provides self-wiping between barrel and screw flight surfaces, which reduces material holdback to an acceptable minimum, thus rendering it an almost ideal TFR.

If the striation thickness, r, becomes smaller than $(r)_{\text{crit}}$, which satisfies the relation below

$$t_{D_{\text{crit}}} = \frac{r_{\text{crit}}^2}{\mathscr{D}_{AB}} \ll t_{\text{res}} \tag{11.2-20}$$

then the ratio of the diffusion and residence characteristic times

$$\frac{t_{D_{\text{crit}}}}{t_{\text{res}}} \ll 1 \tag{11.2-21}$$

and the major portion of the LCFR is molecularly mixed. Since the rate of reaction changes continuously along the reactor as a result of concentration and temperature changes, some metric is required to represent the typical reactor characteristic, such as the familiar half-life. Sebastian (6) suggested that based on feed conditions we can devise a *characteristic* reaction time without solving any equations as follows:

$$t_r = \left(\frac{c}{\dot{r}}\right)\Big|_0 \tag{11.2-22}$$

where c is the reactive species concentration, for example, POX concentration in PP controlled-rheology reactive processing. For simple nth-order kinetics, $\dot{r} = kc^n$

$$t_r = \frac{1}{kc^{n-1}|_0} \tag{11.2-23}$$

which for first-order kinetics reduces to

$$t_r = \frac{1}{k} \tag{11.2-24}$$

and for second-order kinetics reduces to

$$t_r = \frac{1}{kc_0} \tag{11.2-25}$$

Equation 11.2-25 is the formal definition of *half-life*, the time the second-order reaction takes to reduce the initial concentration to half the initial c_0. Following the methodology of

gaining insights for reactive polymer processing systems by examining the ratios of characteristic times of competing phenomena taking place in such reactors, we define the Damkohler dimensionless number, Da, as

$$\mathrm{Da} = \frac{t_{\mathrm{res}}}{t_r} = \left(\frac{V}{Q}\right)\left(\frac{\dot{r}}{c}\right)\bigg|_0 \tag{11.2-26}$$

where V is the reactor volume and Q the volumetric flow rate.

In Fig. 11.10 the ratio of $c(t)/c_0$ is plotted against Da for well-mixed BR and LCFR with half-, first-, and second-order kinetics systems. Again, we observe that although each case has different concentration histories and flow conditions, we can have the following simple rule-of-thumb analysis for complex reactive processing systems: reactions are roughly half complete at $\mathrm{Da} = 1$; they are practically complete at $\mathrm{Da} = 10$; and the systems are essentially unreacted at $\mathrm{Da} = 0.1$. The entire dynamic state of the reaction is in the region $10^{-1} < \mathrm{Da} < 10$; this is a similar conclusion to that on Fig. 11.7 earlier in this section.

Furthermore, using the conditions for ''complete'' conversion of $\mathrm{Da} \approx 10$, Sebastian (6) noted that, one can solve for any parameter in the Da number, given values of others, to provide a simple linearization of a potentially complicated kinetic analysis. One can generalize this simple approach and obtain adequate analysis of complex systems with competing physical phenomena, one ''driving'' and the other ''resisting''

$$0.1 \leq \frac{t_{\mathrm{resisting}}}{t_{\mathrm{driving}}} \leq 10 \tag{11.2-27}$$

Examples of the preceding for reactive systems, other than Da, are t_D/t_{mix} and t_r/t_D, both giving rise to molecularly mixed systems.

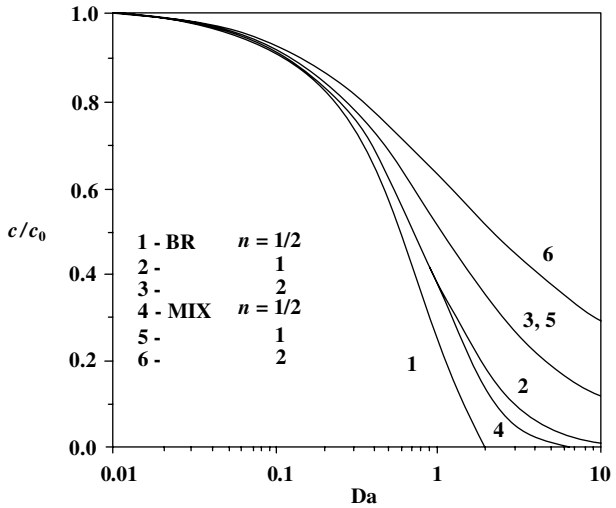

Fig. 11.10 The reduction of the initial reactant concentration as a function of the Da number, showing the unifying ability of the use of characteristic time ratios. The curves are solutions to the kinetic expressions for batch and LCFR with half-, first-, and second-order kinetics. [Reprinted by permission from D. H. Sebastian, ''Non-Isothermal Effects in Polymer Reaction Engineering,'' in *Temperature Control Principles for Process Engineers*, E. P. Dougherty, Ed., Hanser, Munich, 1993.]

Back-Mixed Continuous Flow Reactors

Following Biesenberger (3) "back-mixing" in a reactor is defined as *mixing of molecules in advanced stages of the reactor*, that is, low reactant and high product content, *with those in early stages*, that is, high reactant and low product concentrations. The main prerequisite for an ideally back-mixed reactor and continuous reacting stream is *complete* and *instantaneous mixing*, as is the case in the classic chemical engineering well-known *continuous stirred tank reactor* (CSTR). In such a reactor the exit probability of fluid particles, independent of its "age," is constant. Complete and instantaneous mixing can normally be achieved in low viscosity systems. Since the degree of mixing in CSTRs is instantaneous and the degree of mixedness is molecular and spatially uniform, the only requirement of reaction completion is

$$\mathrm{Da} = \frac{\bar{t}}{t_r} = \frac{V}{Q}\left(\frac{\dot{r}}{c}\right)\bigg|_0 \geq 10 \tag{11.2-28}$$

In a CSTR, as discussed in Section 7.3, the RTD is *exceptionally wide*, that is, the age, and thus the degree of reaction in the existing stream, at any time is very broad: 60% of the exiting stream has resided in the CSTR for a time less than the mean residence time, $\bar{t}$ and 10% less than $0.15\bar{t}$. For the reaction completion requirement given in Eq. 11.2-28 to be satisfied for this 10% young age exit element, $\mathrm{Da}|_{10\%} = 0.15\bar{t}/t_r > 10$. Thus, CSTRs must have a mean residence time of $\bar{t} > 67t_r$, and thus, they may not be desirable for all types of reactions.

It had widely been held by conventional wisdom, and reasonably so, that CSTR conditions cannot be achieved with high viscosity fluids in laminar flow fields, which as shown on Fig. 11.11, generally have narrower RTDs. However, in the early 1990s Biesenberger and Todd, working with Lu (45–47), and later on with Grenci (48), developed a laminar flow reactor physically resembling a LCFR, but one that achieves results close to those of a CSTR. For this reason they called it the *Back-mixed extruder*. The cumulative RTD function, evaluated experimentally by Lu (45), and shown in Fig. 11.12, is very close and slightly narrower than the theoretical CSTR.

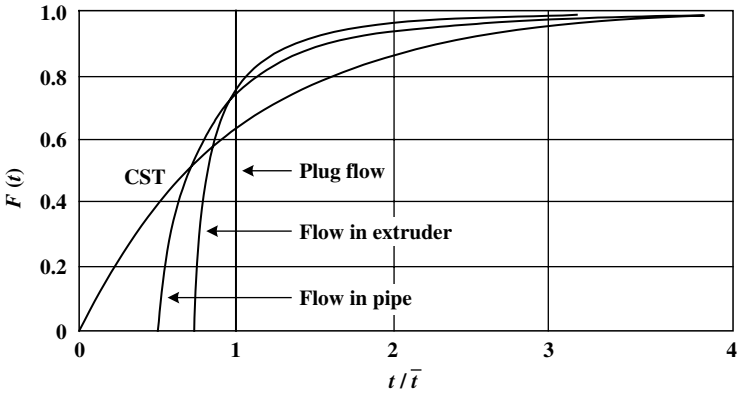

Fig. 11.11 The cumulative RTD function $F(t)$ versus dimensionless time, $t/\bar{t}$ for the metering zone of an SSE compared to plug flow, pipe flow (for Newtonian and isothermal conditions), and the very broad CSTR.

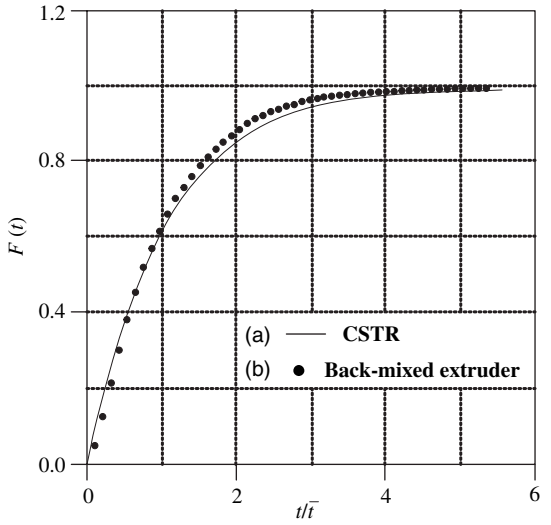

Fig. 11.12 Comparison between the theoretical cumulative RTD function for (a) CSTR and (b) the back-mixed extruder. [Reprinted by permission from Y. Lu, Ph.D Dissertation, Department of Chemical Engineering, Stevens Institute of Technology, Hoboken, NJ, 1993.]

The back-mixed extruder is a variant of the conventional nonintermeshing (tangential) counterrotating TSE represented on Fig. 11.13(a); both counterrotating screws in this LCFR create a dominant downstream flow with no back mixing and with some mixing screw-to-screw flow. By contrast, the two counterrotating screws of the back-mixed reactor

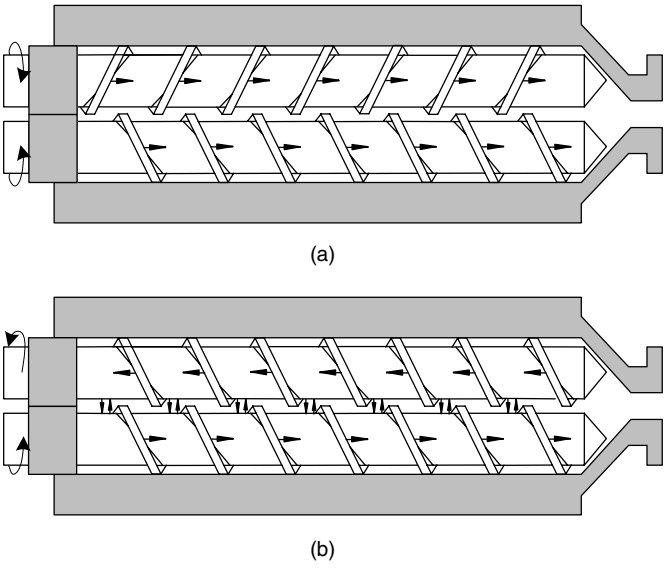

Fig. 11.13 Schematic representation of the twin-screw flow directions in (a) the conversional counterrotating nonintermeshing TSE, and (b) its ''back-mixed extruder'' variant. [Reprinted by permission from Y. Lu, Ph.D Dissertation, Department of Chemical Engineering, Stevens Institute of Technology, Hoboken, NJ, 1993.]

convey the material one forward and the other backward, as shown on Fig. 11.13(b). Such forward–backward flows occurring in parallel and side by side create the CSTR-type back-mix conditions. But, although this is an important feature of the back-mixed extruder, there is another feature, equally important, and it concerns the screw-to-screw material exchange, potentially leading to chaotic flows, and therefore well-mixed systems, represented by the vertical and reciprocal arrows between the two screws in Fig. 11.13(b). To understand the origins of these screw-to-screw material-exchange mixing flows we turn to Fig. 11.14 (45). The pressure ''profiles'' $P_b(z)$ for the backward- and $P_f(z)$ for the forward-pumping flows are created because of the circulatory cross-flows in each of the screws. Their slopes are $dP_f/dz < 0$ and $dP_b/dz > 0$. Therefore, the difference $P_b - P_f$ varies with z and can be negative or positive, and it is a function of the frequencies of rotation of the screws. When $P_b - P_f > 0$ melt in the backward-pumping screw at *that z location* is pushed into the forward-pumping screw flight. Of course, melt transfer from the forward- to the backward-pumping screw flight occurs at a z location when $P_b - P_f < 0$.

With the preceding arguments we see that the flow is three-dimensional with the added ''dimension'' of time periodicity, which as pointed out in Section 7.2, is a required condition for generating chaotic flows, as is the case in a two-dimensional cavity flow with periodic boundary conditions (49–51). Although apparently no fluid mechanical simulation has been done, there is strong experimental evidence of ''instantaneous'' mixing throughout the back-mixed extruder volume (45), and no composition drift is observed in copolymerization of two monomers with different reactivities, as expected only from a reaction occurring in a CSTR (48). Finally, in conventional tangential counter-rotating, either matched or staggered, TSEs the experimentally obtained $F(t)$ functions, as shown on Fig. 11.15, are very close to each other and very similar to that of

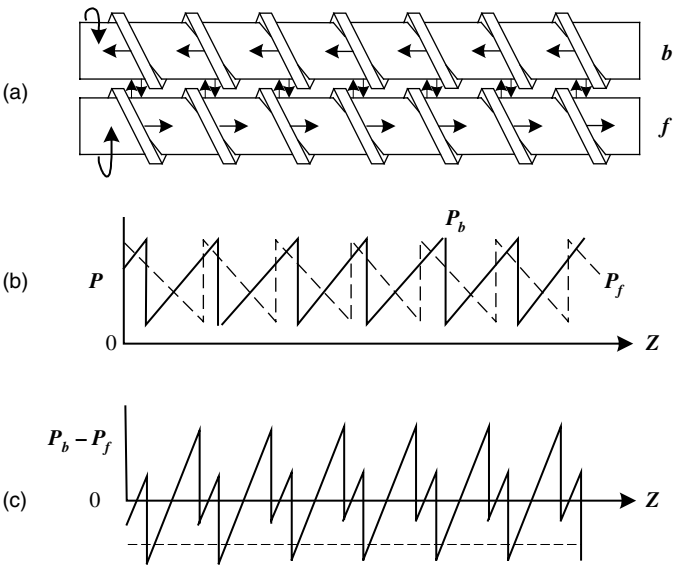

Fig. 11.14 Schematic representation of the local pressure and pressure difference at the ''interface'' between the two screws in the back-mixed extruder. The pressure difference changes periodically with varying amplitudes and frequencies. [Reprinted by permission from Y. Lu, Ph.D Dissertation, Department of Chemical Engineering, Stevens Institute of Technology, Hoboken, NJ, 1993.]

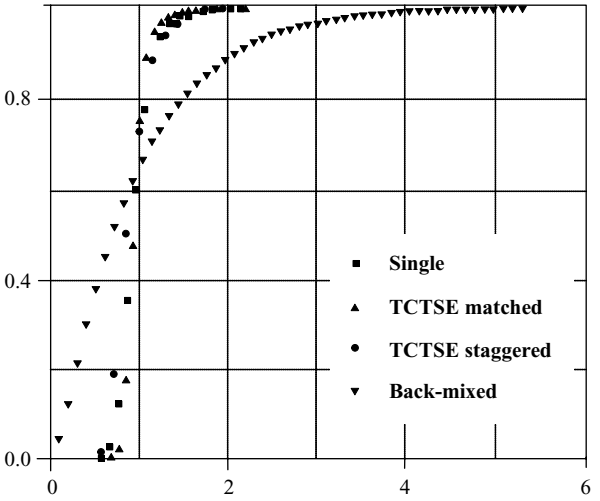

Fig. 11.15 RTD cumulative functions of a single screw; tangential counter-rotating twin-screw extruder (TCTSE) under matched and staggered conditions, and the back-mixed extruder reactor. [Reprinted by permission from Y. Lu, Ph.D Dissertation, Department of Chemical Engineering, Stevens Institute of Technology, Hoboken, NJ, 1993.]

the metering zone of the SSE, denoting parallel pumping along the two forward-pumping screws with no back mixing. Similarly there is experimental evidence of lack of "global," CSTR-like back mixing in co-rotating, intermeshing TSEs. There is "local" and limited-range back-mixing only in full kneading elements, due to the expansion–contraction squeezing flow that forces limited flows in the kneading elements of the next kneading element neighbors to the front and back of that element, as discussed in by Brouwer et al. (52). Thus both conventional counter- and co-TSEs, as well SSEs, are LCFRs.

11.3 MIXING CONSIDERATIONS IN MULTICOMPONENT MISCIBLE REACTIVE POLYMER PROCESSING SYSTEMS

Following the preceding discussions on the various types of reactors for reactive processing, we now discuss the requirements for attaining completed reactions, uniform reactor environment, and uniform reaction product.

First and foremost, the laminar mixing flow created in the reactive processing equipment, must reduce the striation thickness to a level where the diffusion characteristic time, $t_D = r^2/\mathscr{D}_{AB}$, is small compared to the reaction characteristic time. Since the molecular diffusivities of low molecular weight components in polymeric melts (see Section 8.3) are very small and of the order of $10^{-6}\,\mathrm{cm}^2/\mathrm{s}$, the striation thickness must be reduced to the micron level in order to get a characteristic time t_D of the order of 1 s. Shear flow can accomplish this in reasonable mixing times because the striation thickness is inversely proportional to the total shear (see Section 7.3)

$$r = \frac{r_0}{\gamma} \approx \frac{r_0}{\dot{\gamma} t_{\mathrm{mix}}} \tag{11.3-1}$$

and therefore the diffusion characteristic time is inversely proportional to the square of the total shear:

$$t_D = \frac{r^2}{\mathscr{D}_{AB}} = \frac{r_0^2}{\mathscr{D}_{AB}} \left(\frac{1}{\gamma}\right)^2 = \frac{t_{D_0}}{\dot{\gamma} t_{\text{mix}}} \tag{11.3-2}$$

This becomes evident from Figure 11.16, which gives the $t_D = 1\,\text{s}$ iso-t_D curves in the $\dot{\gamma}$-t_{mix} space for three initial t_{D_0} values of 10^1, 10^2, and 10^3 s. It is evident that for typical processing shear rates of $50 < \dot{\gamma} < 100\,\text{s}^{-1}$ at the t_{mix} needed to achieve $t_D = 1\,\text{s}$, and thus molecular mixing, are in the range of 1 s to 20 s. It is important to note that the iso-$t_D = 1\,\text{s}$ curves flatten out with decreasing shear rate. For example, for $t_{D_0} = 10^2$, $t_D = 1\,\text{s}$ is reached in about 1 s for $\dot{\gamma} = 100\,\text{s}^{-1}$ and in about 10 s at $\dot{\gamma} = 10\,\text{s}^{-1}$.

Thus, in nonuniform shear rate flows, as in drag- and pressure-induced LCFRs a binary miscible blend element flowing in regions of very low shear rate, for example, $\zeta = y/H \approx 2/3$ in the metering zone of the SSE (see Chapter 6), may exit the linear reactor with a striation thickness that has hardly changed from its initial t_{D_0} value, and since with polymer blends $10^3 < t_{D_0} < 10^6$, the reaction and resulting LCFR product will be quite nonuniform. Furthermore, as shown in Fig. 11.11, in the metering zone of SSEs the residence time is close to the minimum over a broad region of the channel *core*, with 75% of the exiting flow rate having experienced a residence time of less than the mean value, and only 5% of the flow rate stays more than twice the mean value.

The second requirement, for reactions that are *not* diffusion controlled to reach completion, is that the Damkohler number be larger than 10. The previous discussion and Fig. 11.12 strongly indicate that for SSEs, where at $t = 0.75\,\bar{t}$ there is an almost vertical ascent of $F(t)$, we use $\text{Da} = 0.75\,\bar{t}/t_r > 10$ as the requirement for completion.

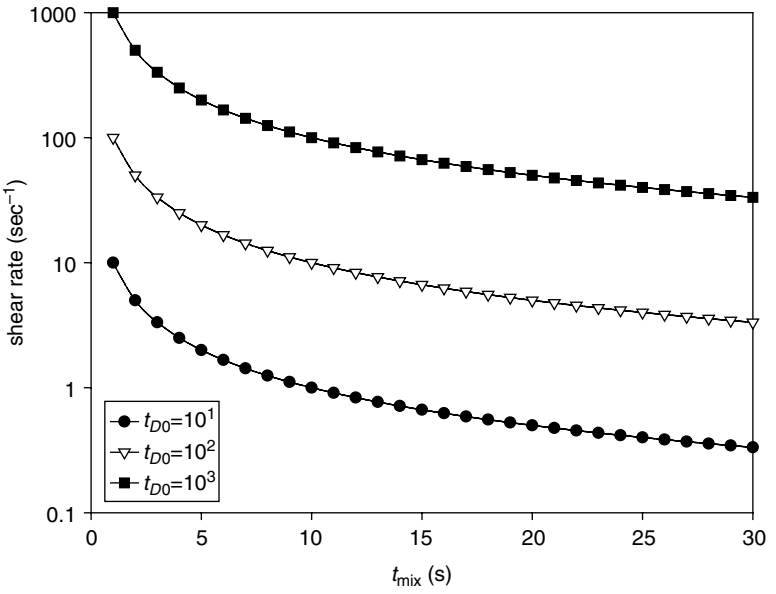

Fig. 11.16 Iso-$t_D = 1\,\text{s}$ curves for various $t_{D_0} = s_0^2/D_{AB}$ values, indicating that diffusion times of one second can be reached in short times for typical processing shear flow rates.

Example 11.1 Chain Modification (Branching and Partial Cross-linking) of PET with Triglycidyl Isocyanurate (TGIC) Dhavalkikar (39) conducted the reaction cited in the Example title on samples placed between the rheometrics mechanical spectrometer (RMS) parallel disks in the temperature-controlled chamber under nitrogen. He followed the reaction dynamics chemorheologically by measuring, in-line, the in- and out-of-phase dynamic moduli $G'(t)$ and $G''(t)$; they are indicative of the elastic and viscous nature of the molten reactive samples.

The reactive PET/TGIC 2.5-cm-diameter and 0.5-cm-thick disks were prepared by the following two methods: (a) a predried PET and 2000-ppm TGIC were dissolved in a few drops of hexafluoroisopropanol (HFIP); a thin film was cast and vacuum dried for 48 hours, resulting in a 2.5-cm diameter 0.05-cm thin sheets; ten of these sheets were stacked between the two parallel disks of the RMS where the reaction took place at 270°C after 300 s of sample heating in the RMS chamber; (b) the second method involved making spatially uniform, but microsegregated blends of 0.89-mm dried PET and 0.15 mm TGIC particulates; these blends were compression sintered into 2.5-cm by 0.5-cm disks, which were allowed to react in the RMS chamber, again under nitrogen.

The results obtained are shown in Fig. E11.1a. The elastic G' and loss (viscous) G'' moduli both increase with increasing branching and high cross-linking chain modification of PET by TGIC as expected, because the preceding macromolecular changes increase both the elastic and viscous responses. But there is a *notable difference*, between the responses of the homogeneous (solvent) and the initially heterogeneous (powder) samples. As expected, the homogeneous sample, after the needed time for thermal equilibrium, shows the expected response of a first-order kinetics of branching $dc_{\mathrm{TGIC}}/dt = kC_{\mathrm{TGIC}}$, through which the reaction kinetic constant at 270°C is found to be $k = 3 \times 10^{-3}\,\mathrm{s}^{-1}$.

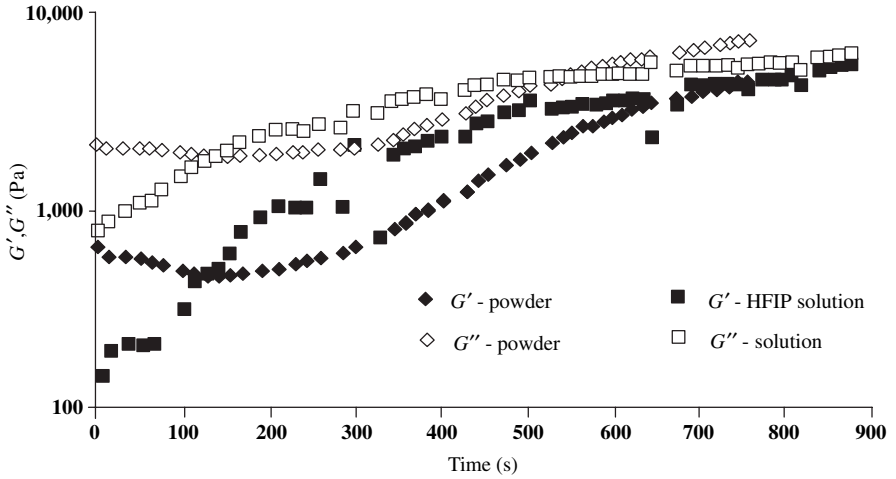

Fig. E11.1a The in-phase G' and out-of-phase G'' moduli of the PET/TGIC samples, one molecularly mixed (solution) and the other made of compressed and initially segregated PET. As expected, the homogeneous sample, after the required time for thermal equilibrium, shows the expected response of first-order kinetics. [Reprinted by permission from R. Dhavalkikar and M. Xanthos, ''Monitoring the Evolution of PET Branching Through Chemorheology,'' *Polym. Eng. Sci.*, **44**, 474 (2004).]

On the other hand, the initially heterogeneous ''powder'' (actually composed of 0.89-mm average-size particulates) sample response is virtually unchanged for the first 300 s, denoting the absence of a spatially uniform reaction and, thus, G' as well as G'' are dominated by the unreacted regions of PET and TGIC. The obvious conclusion is that for this microsegregated system the reaction will not take place uniformly before the required t_D of TGIC diffusing to the core of the PET particulates, (0.89/2) mm inwards.

For 10^{-6}-cm^2/s $< \mathscr{D}_{AB} < 10^{-4}$ cm^2/s, the characteristic time of diffusion falls in the range 200 s $< t_D <$ 2000 s. Thus, the observed ''delay'' time for the onset of the uniform reaction $t_D \approx 300$ s supports the assumption of a diffusion-controlled reaction for the initially segregated reactive system. Furthermore, the initial slopes of $G'(t)$ and $G''(t)$ for the homogeneous samples are larger than those of the segregated counterparts, 300 s later. This is because, for the latter, some nonuniform reaction is taking place in the mixed-sample regions with, presumably, the same reaction constant. Jeong and Gogos (53) analyzed these chemorheological results, simulating the following three cases

1. PET/TGIC reaction only ("solution" sample)

$$\frac{dc}{dt} = kc_{\text{TGIC}} \tag{E11.1-1}$$

2. Diffusion of TGIC into PET only (initially segregated "powder" sample)

$$\frac{\partial c}{\partial t} = \mathscr{D}_{AB}\frac{\partial^2 c}{\partial x^2} \tag{E11.1-2}$$

3. Coupled diffusion and reaction (actual initially segregated)

$$\frac{\partial c}{\partial t} = \mathscr{D}_{AB}\frac{\partial^2 c}{\partial x^2} + kc \tag{E11.1-3}$$

From Eq. E11.1-1, as mentioned earlier, the value of $k = 300$ s fits the ''solution'' data and with this k value one determines the time-dependent and spatially uniform drop in TGIC concentration, as shown on Fig. E11.1b. The reaction is complete in about 500 s, in agreement with experimental results. To appreciate the effect of the reaction in the coupled diffusion-reactions of the initially segregated ''powder'' sample, the pure diffusion of TGIC into PET is examined, Eq. E11.1-2. The results are plotted in Fig. E11.1c. The diffusion process, using $\mathscr{D}_{AB} = 10^{-6}$ cm^2/s is effectively complete in 500–900 s, close to the rough t_D calculation just given.

Turning now to the results of Eq. E11.1-3, the coupled diffusion-reaction process demonstrates the effect of reaction in depleting the TIGC concentrations, especially at longer t_{res} in the initially segregated sample, as shown in Fig. E11.1d.

Jeong and Gogos proceeded to answer the following question: If, instead of applying on the initially segregated sample an oscillatory deformation $\gamma = \gamma_0 \sin \omega t$, a steady shear flow $\gamma(t) = \dot{\gamma} \cdot t$ was applied, by rotating the top RMS disk, the effect of such a flow, according to Eq. E11.1-3, would be to reduce the initial striation thickness, r_0, with time $r(t) = r_0/(1 + \dot{\gamma}t)$ and consequently reduce the diffusion time from t_D to $t_D(t) = r^2(t)/D_{AB}$. The results of solving the coupled diffusion-reaction process (Eq. E11.1-3) in the presence of a steady shear-flow field, which reduces continuously the

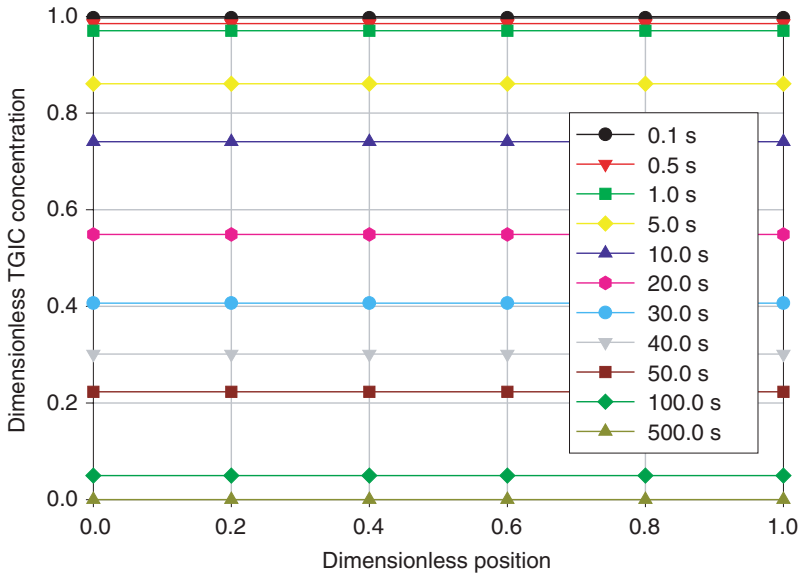

Fig. E11.1b Results of Eq. E11.1-1 with $k = 300\,\text{s}$. The uniform sample reaction at 270°C is complete in 500 s.

striation thickness and diffusion time, are shown on Fig. E11.1e for $\dot{\gamma} = 1\,\text{s}^{-1}$, that is, $\gamma = t$.

Comparing the preceding results with those of Fig. E11.1d, where the striation thickness is constant, demonstrates the *dramatic decrease of the reaction time*, with a modest $\dot{\gamma} = 1\,\text{s}^{-1}$ shear flow.

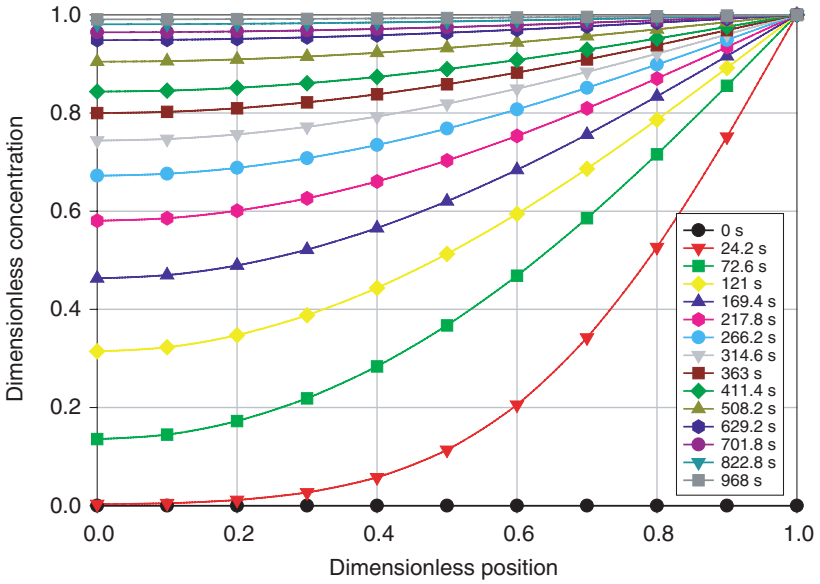

Fig. E11.1c Results of Eq. E11.1-2 for the pure diffusional process of TGIC in PET.

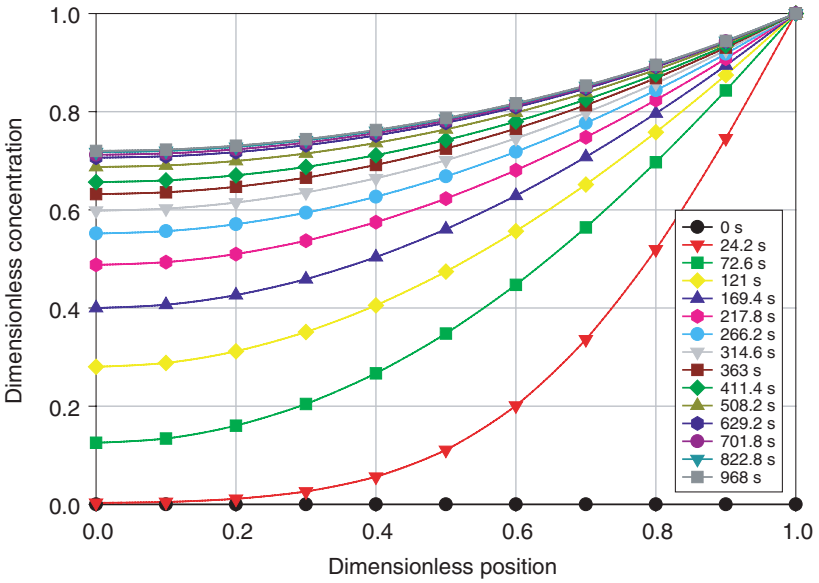

Fig. E11.1d Results of Eq. E11.1-3 for the coupled diffusion-reaction process of the initially segregated "powder" sample.

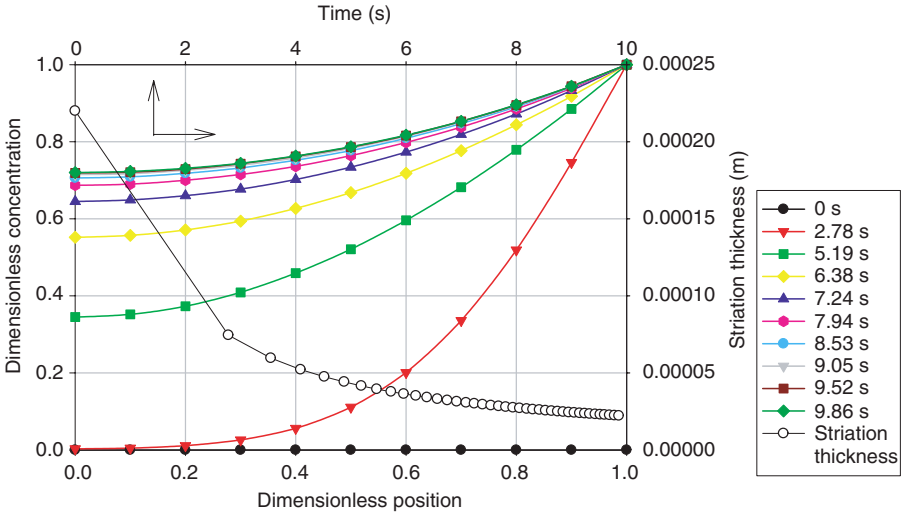

Fig. E11.1e The coupled diffusion-reaction process while applying a steady torsional parallel-disk flow of $\dot{\gamma} = 1\,\mathrm{s}^{-1}$ to the initially segregated sample.

Example 11.2 Investigation of the Effects of Interfacial Cross-linking, Diffusion, and Area Generation Rates on Multilayer Miscible (PE-8% GMA)/PE-4% MAH) Films on the Extensional Rheometry of Such Films. Saito and Macosko (54) prepared multilayer films of two low density polyethylene (LDPE) miscible copolymers: a random copolymer of

ethylene and 8% glycidyl methacrylate (PE-GMA) and an LDPE randomly grafted with 4% maleic anhydride (MAH) (PE-MAH). The 256-layer films were produced in layer multiplication dies of Schrenk and Alfrey (55) at 220°C with a die residence time of 180 s and then cooled to room temperature, T_{room}. Strips were cut whose ends were clamped by the Rheometrics extension rheometer (RME) grips (56), allowed to come to thermal equilibrium under a blanket of nitrogen at 140°C, and then forced to undergo constant extensional strain-rate deformations at 0.01–0.05 s^{-1}. The length, width, and thickness of the strip $(l(t), W(t), H(t))$ (see Chapter 3) vary with time as follows:

$$\begin{aligned} l(t) &= l_0 \exp(\dot{\varepsilon} t) \\ W(t) &= W_0 \exp\left(-\frac{1}{2}\dot{\varepsilon} t\right) \\ H(t) &= H_0 \exp\left(-\frac{1}{2}\dot{\varepsilon} t\right) \end{aligned} \tag{E11.2-1}$$

If, during the extensional multilayer film deformation, the interfacial layers remain continuous, then the interfacial area *per unit film volume*, A_I, increases exponentially. For N layers

$$A_I(t) = \frac{N-1}{H_0} \exp\left(\frac{1}{2}\dot{\varepsilon} t\right) \tag{E11.2-2}$$

Because the consecutive stacked film layers are miscible, it is expected that a typical two-layer sample can be represented morphologically, as shown on Fig. E11.2a. The thickness of the interface layer, δ_I, increases with time, provided that the adjacent layers are molten, as is the case during the residence in the die (220°C), as well as during the time of thermal conditioning and stretching in the RME (140°C). Assuming an Arrhenius-type temperature dependence of the diffusivity (57),

$$\mathscr{D}_{AB}(T) = \mathscr{D}_{AB_0} \exp\left(-\frac{E_D}{RT}\right) \tag{E11.2-3}$$

with $E_D = 24\,\text{kJ/mole}$ for PE, they converted the 180-s residence in the die to an equivalent (longer) time at 140°C and added the 180-s conditioning time in the RME; they

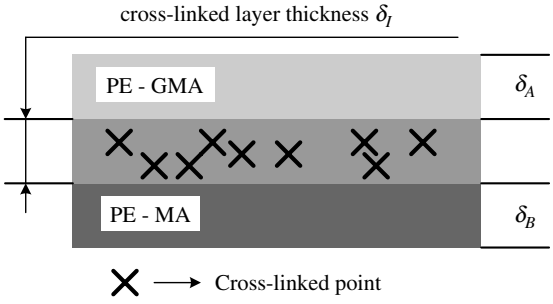

Fig. E11.2a Schematic representation of an adjacent pair of PE-GMA/PE-MAH layers. δ_I, the reacting interphase with cross-linked (branched) LDPE increases with time because of diffusion, at the expense of both δ_A and δ_B; note that $\delta_A + \delta_I + \delta_B = \delta_{A_0} + \delta_{B_0}$

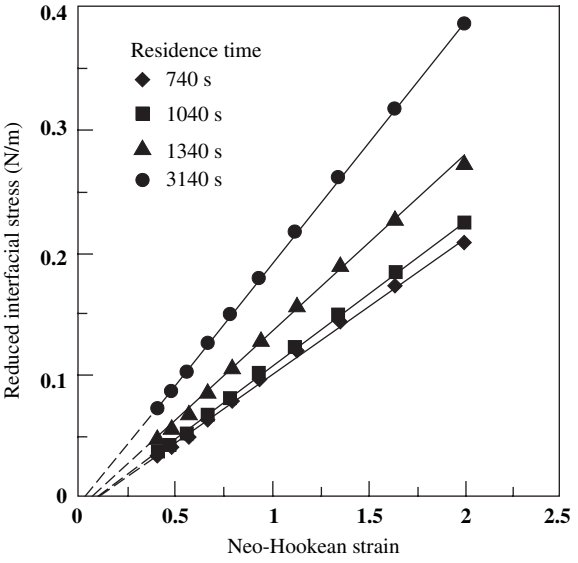

Fig. E11.2b Interfacial stress versus Neo-Hookean strain for three samples of different total residence times at 140°C, showing, δ_I thickening. [Reproduced by permission from T. Saito and C. W. Macosko, ''Interfacial Cross-linking and Diffusion via Extensional Rheometry,'' *Polym. Eng. Sci.*, **42**, 1–9 (2002).]

estimated the residence time at 140°C to be 740 s before any extensional deformation in the RME. Increasing the total residence time increases, δ_I, and, since the interphase is a cross-linked PE, the elongational stress–strain measured by the RME increases with total residence time, as shown on Fig. E11.2b. The measured force (stress) of the deforming multilayer film is

$$F_{\text{multilayer}} = \left\{\frac{1}{2}N\left(\delta_a - \frac{1}{2}\delta_i\right)\sigma_a + \frac{1}{2}N\left(\delta_b - \frac{1}{2}\delta_i\right)\sigma_b + (N-1)\delta_i\sigma_i\right\}W(t) \qquad \text{(E11.2-4)}$$

where N is the number of layers, σ is the tensile stress, δ is the layer thickness, W is the width, and a, b, and i are the subscripts denoting each polymer and the cross-linked interlayer, respectively. Since $\delta_i < \delta_{a,b}$ and $\sigma_i \gg \sigma_{a,b}$, Eq. E11.2-4 can be simplified to

$$F_{\text{multilayer}} = \left\{\frac{1}{2}N(\delta_a\sigma_a + \delta_b\sigma_b) + (N-1)\delta_i\sigma_i\right\}W(t) \qquad \text{(E11.2-5)}$$

The independent contributions of PE-GMA, A, and PE-MAH, B, depend on their volume factions ϕ_A and ϕ_B and therefore:

$$\frac{1}{2}N(\delta_a\sigma_a + \delta_b\sigma_b)W(t) = \phi_a F_a(t) + \phi_b F_b(t) \qquad \text{(E11.2-6)}$$

where F_a and F_b are measured independently and are shown on Fig. E11.2c together with the ten times larger force of the multilayer film.

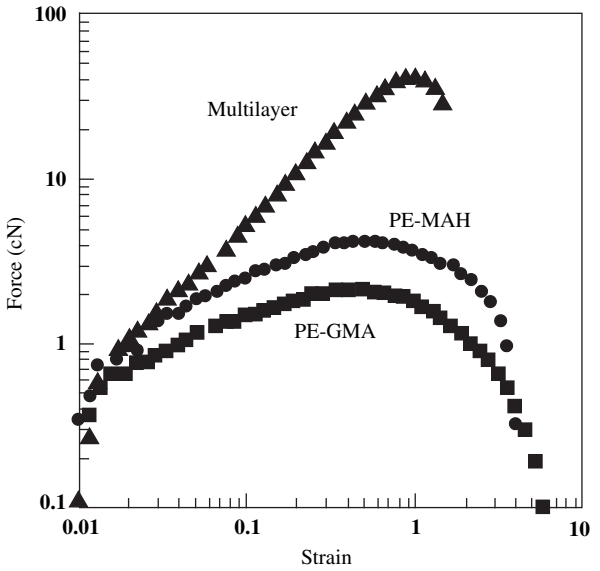

Fig. E11.2c Extensional stress–strain response of the PE-GMA, PE-MAH, and 256 multilayer films at 140°C and extension rate of $0.1\,s^{-1}$. [Reproduced by permission from T. Saito and C. W. Macosko, ''Interfacial Cross-linking and Diffusion via Extensional Rheometry,'' *Polym. Eng. Sci*., **42**, 1–9 (2002).]

The contribution of all the δ_I cross-linked interlayers is found from the difference between Eqs. E11.2-5 and E11.2-6

$$F_I(t) = (N-1)\delta_I\sigma_I W(t) = F_{\text{multilayer}} - [\phi_A F_A(t) + \phi_B F_B(t)] \tag{E11.2-7}$$

From the first part of the preceding equation the tensile stress per unit width of any interlayer is

$$\delta_I\sigma_I(t) = \frac{F_I(t)}{(N-1)W(t)} \tag{E11.2-8}$$

Using Eq. E11.2-1 and Eq. E11.2-8 the ''reduced'' interfacial stress can be calculated and plotted on Fig. E11.2b for various residence times at 140°C. There the ''Neo-Hookean'' strain ε^{NH}

$$\varepsilon^{NH} = \exp(2\dot{\varepsilon}t) - \exp(-\dot{\varepsilon}t) = \frac{l^2(t)}{l_0} - \frac{l_0}{l(t)} \tag{E11.2-9}$$

If a Neo-Hookean constitutive equation is used to describe the tensile behavior of the cross-linked interlayer

$$\sigma(t) = G\varepsilon(t)^{NH} \tag{E11.2-10}$$

then $\delta_i\sigma_i = \delta_i E\varepsilon(t)^{NH}$. The modulus E was evaluated from tensile experiments of well cross-linked PE-MAH and PE-GMA samples and found to be 1.6×10^5 Pa. Using this value with

the 740 s, curve of Fig. E11.2b, which plots the reduced interfacial stress, $\sigma_i\delta_i$, we evaluate the interfacial thickness to be 0.7 μm. In addition, 740 s is the time in the RME before the start of the extensional deformation. From the curves, at higher times in the RME, we can obtain the increase in the interlayer thickness, which was found to grow in a diffusion-controlled manner with time.

In this example of ''model'' reactive polymer processing of two immiscible blend components, as with Example 11.1, we have three characteristic process times: t_D, t_r, and the time to increase the interfacial area, all affecting the RME results. This example of stacked miscible layers is appealing because of the simple and direct connection between the interfacial layer and the stress required to stretch the multilayer sample. In Example 11.1 the initially segregated samples do create with time at 270°C an interfacial layer around each PET particulate, but the torsional dynamic steady deformation torques can not be simply related to the thickness of the interfacial layer, δ_I. However, the initially segregated morphology of the ''powder'' samples of Example 11.1 are more representative of real particulate blend reaction systems.

11.4 REACTIVE PROCESSING OF MULTICOMPONENT IMMISCIBLE AND COMPATIBILIZED IMMISCIBLE POLYMER SYSTEMS

As discussed in Chapter 1, the majority of ''new'' polymers have been blends of existing commodity or engineering polymers. Blends account for roughly 30% of all polymer sales (12). Most polymer pairs used in blends are practically *immiscible* and, as such, in principle their morphology and properties are unstable. Thus, commercial blends are made by *reactively* forming a block copolymer at the interface during reactive polymer processing operations. The interfacial reactions require that the homopolymer blend components are functionalized. We have reviewed some of them in Section 11.1 and there are a number of specific and informative general references (11,12,58). Block copolymers, synthesized in polymerization reactors, are functioning much like a ''third'' surfactant-type component of the blend, since one part of the block is immiscible to one component, while the other immiscible with the second blend component (59,60). They therefore, ''compatibilize'' the two immiscible components. These compatibilizers improve blend morphology and stability, but because of viscosity differences, their addition may sometimes lead to the formation of compatibilizer micelles inside one of the homopolymer, creating the so-called ''salami'' morphologies (61,62).

Blends are produced by the intensive mixing that takes place in the processing equipment. In Chapter 7 we dealt with mixing of both miscible and immiscible blends. With *miscible systems*, we discussed both the mechanisms and rates of mixing (rates of interfacial area increase), which are relatively straightforward, since they depend primarily on the flow kinematics. In discussing mixing of immiscible blends we concentrated, not so much on the rates of droplet and filament breakup, but on the physical mechanisms associated with the breakup process, and with the final morphology in both shear and extensional flows. In the next section, we discuss the rates of melt droplet and filament breakup, through ''carcass'' analysis in compounding equipment, mainly twin rotor devices, and relate it to both the melting and mixing phenomena, deformations, and flows in such equipment.

In dealing with the reactive processing (blending) of multicomponent immiscible systems we must, however, also consider chemical reaction rates. Thus, we have to

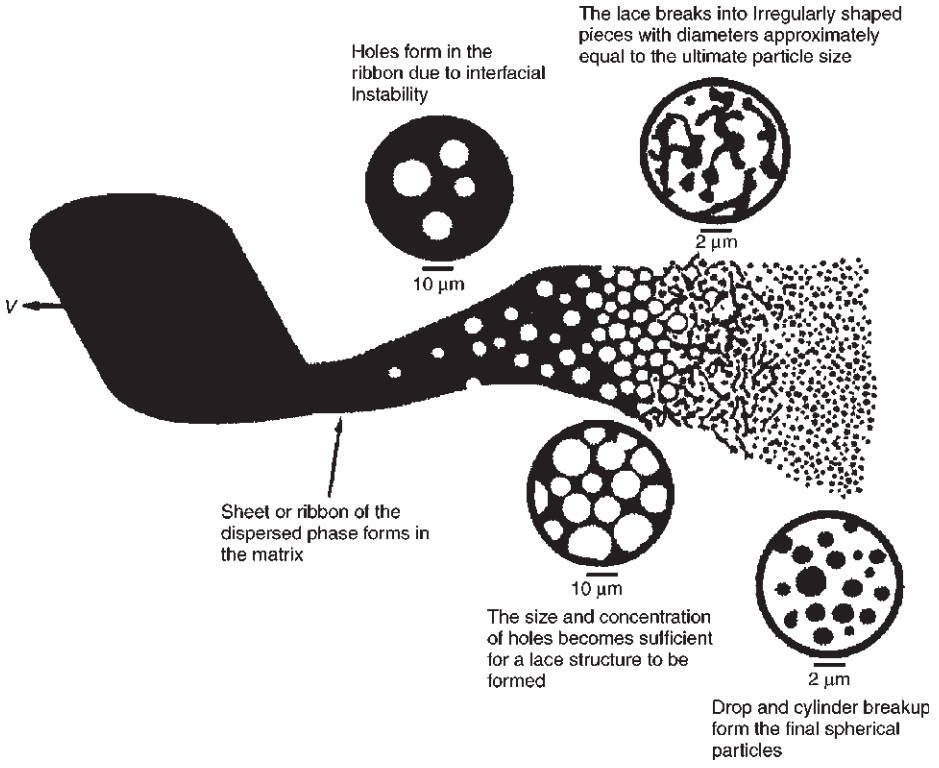

Fig. 11.17 The melting mechanism of immiscible blends, showing in cartoon form the evolution of blend morphology during and following melting in twin rotor devices. [Reprinted by permission from C. E. Scott and C. W. Macosko, "Morphology Development During the Initial Stages of Polymer–polymer Blending," *Polymer*, **36**, 461–470, (1995).]

consider *three* characteristic times: the melt dispersive *mixing* characteristic time, t_{mix}, from the time of melting of the blend components to the time of attainment of a final and stable morphology; the *reaction* time, $t_r(T)$, and the time it takes to achieve the very limited *diffusion* needed for the reaction, t_D, at the interface, creating exceedingly thin, but beneficial, interphases. Scott and Macosko (63) studied the evolving blend morphologies in a Co-TSE, with the results shown in "cartoon" form in Fig. 11.17 and in batch-intensive mixers by taking samples at various mixing times and analyzing them with scanning electron micrography (SEM) (64). Five model blends were used. In all of them the minor dispersed phase was DuPont Nylon Zytel 330, which is a partially aromatic amorphous Nylon [polyamide (PA)] capped at both ends with reactive amine groups. Five matrices were used in the blends of 20% Zytel 330: three are not reactive and immiscible, and two are reactive and initially immiscible. They are: (a) functionalized polystyrene (PS) through copolymerization with 1% vinyl oxazoline and reactive with the amine groups of PA; (DOW RPS X U.S. 4005601) (PS-Ox); (b) styrene-maleic anhydride copolymer (ARCO Dylark 29), with a reported reactive MAH content of 17% (SMA); (c) Dow's PS (Styron 666D), not reactive with Zytel 330; (d) amorphous low MW copolyester (Eastman Chemical Kodar 6763), nonreactive with the amine end-capped PA (PETG), and (e) Dow general-purpose polycarbonate, also nonreactive with the end-capped PA (PC).

It was found (64) that for all five systems, reactive and nonreactive, the melting mechanism giving rise to the evolution of the blend morphology is identical in the initial stages of mixing, namely, the formation of molten *sheet, lace*, *filaments*, and finally *droplets*, as schematically shown in Fig. 11.17. In terms of ratios of characteristic times, the identical initial morphology of both reactive and nonreactive blends requires that $t_{\text{mix}}/t_r \leq 10^{-1}$. At longer mixing times, however, after the formation of dispersed PA droplets it is observed that the mean droplet diameter is 5–10 times *smaller* and *stable* for the reactive blends, because of the compatibilizing products of the chemical reaction at the interface. One can conclude from these results that, for the two reactive blends just cited, *mixing is not controlling* the morphology development down to the droplet level, since the morphology evolution completion time is very small; at longer times droplets will decrease in size as the concentration of the interfacial reactions increases, decreasing the interfacial tension. Furthermore, Marič and Macosko (65) working with aminoterminated PS and anhydride-terminated polydimethylsiloxane (PDMS) blends, observed that this reactive immiscible blend gives a fine and stable droplet morphology that is insensitive to the mixing device used; nonreactive blends, on the other hand, have mixing device-sensitive morphologies.

We have previously used the term ''interfacial reaction'' to describe mixing between two reactive blend components. In reality, as we have seen in the Example 11.2, there is an interphase that is formed on the surface of the dispersed phase where molecules of both components can be found and react (66,67). If the nonfunctionalized blend components have high immiscibility, then the thickness, δ_I, of the interphase around the droplets, as well as the volume of the interphase, V_I, will be small and, thus, the probability of the functional groups to react forming compatibilizing products will be low, giving rise to coarse and not very stable morphologies. Helfand (66) defines δ_I as

$$\delta_I = \frac{2\langle b \rangle}{\sqrt{6\chi_{AB}}} \tag{11.4-1}$$

where $\langle b \rangle$ is the mean segment length of the formed block copolymer, and χ_{AB} is the Flory–Huggins interaction parameter between components A and B (68):

$$\chi_{AB} = \frac{\overline{V}}{RT}(\delta_A - \delta_B)^2 \tag{11.4-2}$$

where $\overline{V}$ is the molar volume and δ_A and δ_B are the solubility parameters. The mean length $\langle b \rangle$ can be calculated from chain dimensions data and estimated as the geometric mean of the homopolymer segment lengths b_A and b_B (69,70)

$$\langle b \rangle = (b_A b_B)^{1/2} \tag{11.4-3}$$

Macosko and his co-workers have estimated δ_I for a number of immiscible uncompatibilized polymer pairs in the Table 11.1.

A blend between two highly immiscible polymers, 20% PDMS in Nylon 6 (PA6) has a very thin interphase thickness of 2Å, as shown on Table 11.1, and, as a result a coarse dispersed morphology of about 10μm. Similarly coarse morphology in obtained when PDMS is blended with PA 6 amine-functionalized at each chain end to form PA 6/diamine.

TABLE 11.1 Calculated Interphase Thicknesses δ_I for Four Pairs of Immiscible Polymers

Blend Component	δ_I(A)	T (°C)
PS/PDMS	10	200
PS/PI	23	180
PS/PMMA	68	180
PA6/PDMS	2	235

Apparently, with a very small interphase thickness the two end-cap groups are too few and not easily accessible to affect compatibilization. On the other hand, when four anhydride (An) groups are attached, randomly on each PDMS chain, then the blend of 20% PDMS/4-An and PA 6/di-amine have a very fine and stable morphology (ca 0.5 μm). Thus, the amount of interfacial reaction product, although diminished by small δ_I values of the unmodified polymer components, is promoted by the larger number and more ''accessible'' functional groups in either or both of the reactive components. Finally, Macosko and co-workers (62) have estimated that the minimum fraction of the interphase that has to be covered by reacted compatibilization products to achieve fine and stable morphologies is about 0.2.

11.5 POLYMER COMPOUNDING

As stated in Chapter 1, polymer processing is the engineering activity concerned with operations carried out on polymeric materials or material systems to increase their utility. While the early objective of the field was the shaping (forming) of finished products, polymer processing has long dealt with and made large technological strides by using the processing equipment to carry out compounding and chemical reactions in order to achieve macromolecular modifications, creation of multicomponent and multiphase structures, and morphology stabilization. All these lead toward technologically and commercially desired ''value added'' products. Figure 1.9 depicts schematically the transformation of feed streams of polymers, additives, and reactants into microstructured ''designer pellets,'' which are, in turn, used in shaping products with enhanced properties.

Compounding is associated mainly with the dispersive and distributive mixing of additives into a single polymer matrix, or the creation of stable physical blends of two or more polymers. Often, before entering the compounding equipment, solid components are surface modified to improve dispersive mixing during compounding and products with enhanced mechanical properties. Also in physical blend compounding, interfacial modifiers and compatibilizers are introduced to achieve stable and finely dispersed blends. Reactive processing, on the other hand, utilizes chemical reactions that modify the macromolecular structure of polymers to achieve the same designer pellets as in compounding. The only difference between compounding and reactive processing is that interfacial modifications are through reactions that, subject to the associated heats of reactions, are carried out *in situ* in the processing equipment. The equipment of choice for carrying out both reactive processing and compounding are twin rotor devices. The reasons for this choice, as discussed in Chapter 10, are their ability to achieve rapid melting and efficient chaotic laminar mixing.

Polymer Additives and Modifiers Used in Compounding

In earlier chapters we mentioned that all commercial plastics are compounds of polymerization reactor-generated macromolecules and a number of additives and modifiers that impart chemical stability, facilitation of processing and fabrication, as well as desired product properties. Although arriving at a specific additives formulation package may be the result of accumulated practical experience, specific and general statements can be made concerning their role or functionality in affecting dispersive and distributive mixing, as well as their effect on processing material variables, such as the viscoelastic nature of the processed stream, at least after mixing is complete and uniform. Mascia (71) and Mascia and Xanthos (72) and recently Xanthos (73,74) have suggested that additives and modifiers be classified according to their *function*, *miscibility*, and *concentration*. We follow this classification in Tables 11.2, 11.3, and 11.4, as presented by Xanthos (73).

The additives in the tables below can be either *rigid* (fillers, reinforcing agents, inorganic flame retardants, pigments, etc.) or *deformable* (polymeric impact modifiers, compatibilizers, dyes, etc.). For rigid particulate additives, as discussed in Chapter 7, the dominant mixing mechanism determining compounding quality is *dispersive mixing*, which depends on many operational and physical property variables, such as the cohesive strength of the particle, its shape, size, and size distribution, and the volume fraction of the additive. In addition, the surface area and surface treatment to alter surface tension and improve wetting and particulate adhesion to the matrix play an important role. For *deformable additives* deformation and breakup by the polymer matrix depends on

TABLE 11.2 Examples of Additives that Modify Mechanical Properties, Electrical Conductivity, and Flame Retardancy

Functions	Examples
Fillers/reinforcements	
Inorganics	Oxides (glass, MgO, SiO_2, Al_2O_3)
	Hydroxides ($Al(OH)_3$)
	Salts ($CaCO_3$, $BaSO_4$, $CaSO_4$, phosphates)
	Silicates (talc, mica, kaolin, woolastonite)
	Metals (boron, steel fibers)
Organics	Carbon-graphite, cellulose, PA, PET, PE, PVA and aramid fibers, wood starch
Plasticizers	Phthalate esters, trialkyl phosphates, adipates, chlorinated paraffins, high molecular-weight polyesters, epoxy derivatives
Impact modifiers	EPR, EPDM, NBR, NR, EVA, MBS, CPE, various elastomers
Cross-linking agents	Organic peroxides, rubber curatives
Flame retardants and smoke suppressants	Sb_2O_3, chlorinated paraffins, $Al(OH)_3$, $Mg(OH)_2$, organophosphate esters, MoO_3, zinc barate, brominated organic compounds, molybdate salts
Conductive additives	Carbon black, carbon-graphite fibers, metals, metallized fillers/reinforcements

Source: Reprinted by permission from M. Xanthos, "The Physical and Chemical Nature of Plastics Additives," in *Mixing and Compounding of Polymers*, I. Manas-Zloczower and Z. Tadmor, Eds. Hanser 1994.]

TABLE 11.3 Examples of Processing and Antiaging Additives

Functions	Examples
Processing Additive	
Stabilizers	Primary antioxidants (sterically hindered phenols, *sec*-arylamines) hydroperoxide decomposers (organophosphites, thioesters), acid absorbers (lead salts, Ca/Ba-Ba/Cd-Ba/Sn salts, organotins, epoxidized oils)
Lubricants	High molecular weight fatty acids and derivatives, paraffin waxes, metal soaps, ester and amide waxes, silicones, polyfluorocarbons
Flow and fusion promoters	PMMA and acrylate ester copolymers, MBS
Thixotropic agents	Fumed silica, clays
Antiaging	
Antioxidants	Sterically hindered phenols, *sec*-aromatic amines, phosphates, thioethers
Metal deactivators	Chelating agents (hydrazones, oxamindes, hydrazides, phosphates, phosphines)
Light Stabilizers	Pigments (carbon black, iron oxides), UV absorbers (hydroxyphenones, benzotriazoles), excited-state quenchers (organic Ni complexes), free-radical scavengers Hindered amine light stabilizers [piperidines, hindered amine light stabilizers (HALS)]
Biostabilizers	Copper quinolinolate, phenoxarsines, phthalimides, thio compounds

Source: Reprinted by permission from M. Xanthos, "The Physical and Chemical Nature of Plastics Additives," in *Mixing and Compounding of Polymers*, I. Manas-Zloczower and Z. Tadmor Eds. Hanser, New York, 1994.

TABLE 11.4 Examples of Surface Modifiers, Optical Property Modifiers, and Blowing Agents

Functions	Examples
Surface modifiers	
Antistats	Ethoxylated amines and quatemary ammonium salts, phosphate esters, glycerides
Antifoggers	Fatty chain glycol and polyether surfactants
Antiblocking agents, slip additives	Silica, amide waxes, oleamide
Antiwear additives	Graphite, MoS_2, polytetrafluoroethylene (PTFE)
Wetting agents	Ionic and nonionic surfactants
Adhesion promoters	Silanes, titanates, block and graft copolymers
Optical property modifiers	
Pigments	*Inorganic:* Ti, Fe, and Cr oxides, Cd, Ba, and Pb sulfides, sulfates, and chromates *Organic:* carbon black, phthalocyanines, quinacridones, flavanthrones, azo pigments
Dyes	Anthraquinones, azo and bisazo compounds, nigrosines
Nucleating agents	SiO_2, talc, sodium benzoate, polymers
Blowing agents	
Physical	Hydrocarbons, halocarbons, CO_2, N_2
Chemical	Bicarbonates, azodicarbonamide, benzene sulfonylhydrazides, tetrazoles

Source: Reprinted by permission from M. Xanthos, "The Physical and Chemical Nature of Plastics Additives" in *Mixing and Compounding of Polymers*, I. Manas-Zloczower and Z. Tadmor Eds., Hanser, 1994.

interfacial tension—which influences miscibility—volume fraction, and the viscosity and elasticity ratios of the additives to the matrix at processing conditions. The *distributive mixing* aspect of compounding depends primarily, almost exclusively, on the flow field generated by the compounding equipment in partially and fully filled sections.

Effects of Additives and Modifiers on the Rheology and Processing of Compounded Systems

The effect of additives and modifiers on product properties will not be discussed here because it is beyond the scope of this textbook. We must emphasize, however, that the ultimate objective of compounding additives and modifiers in polymer matrices is to obtain specific multicomponent and multiphase structures and morphologies needed to obtain certain desired product properties. We will only discuss their effects on the compounded systems rheology and, mainly, the shear flow viscosity, and their effects on compounding equipment and processes.

The Rheology of Solid Particulate-Filled Polymer Matrices

For polymer matrices filled with particulate additives of dimensional aspect ratio near unity, that is, nearly spherical, the rheological behavior at low volume fraction concentrations $\phi_v < 10\%$ resembles the shear thinning nature of the unfilled polymer matrix, except that the viscosity is higher and increases with particulate concentration. In other words, as expected from suspension theory, the suspended particulates do not interact strongly and do not form a particulate *network structure*. At higher particulate volume fractions, on the other hand, such suspended particulate networks are formed and become stronger, increasingly dominating the rheology of the suspension. The above are illustrated in Fig. 11.18 for PS–carbon black filled melts (75).

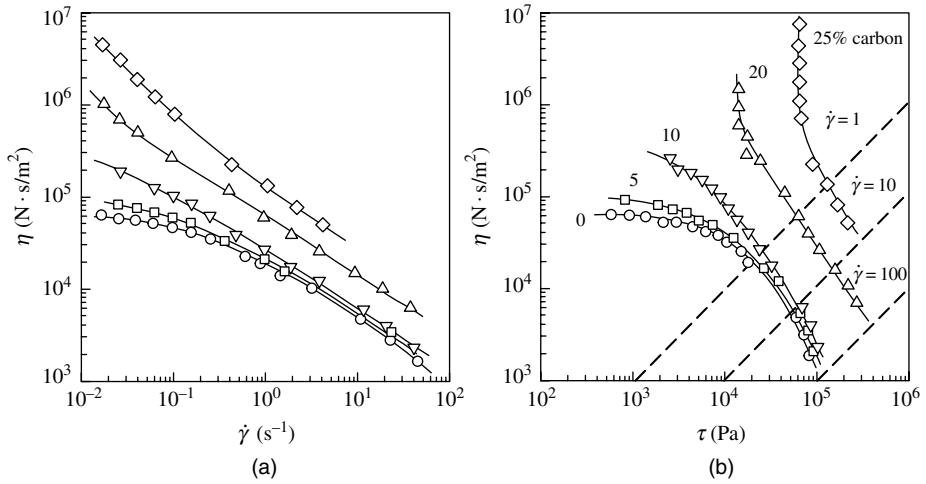

Fig. 11.18 (a) The steady state shear rate and (b) shear stress-dependent viscosity of carbon black filled PS melts; $\overline{M}_W = 214,000$, carbon black surface are a 124 m^2/g area. [Reprinted by permission from V. M. Lobe and J. L. White, "An Experimental Study of the Influence of Carbon Black on the Rheological Properties of a Polystyrene Melt," *Polym. Eng. Sci*., **19**, 617 (1979).]

We observe that at 5% volume concentration carbon black has a very small effect: shear thinning is preserved and no yield is exhibited. On the other hand, at and above 20% and in the very low shear rate region $10^{-2} < \dot{\gamma} < 1\,s^{-1}$ network yielding is evident, as well as very large viscosity increases—two orders of magnitude higher than the polystyrene matrix at $\dot{\gamma} = 10^{-2}\,s^{-1}$. It is noteworthy that at processing shear rates, which generally are above $10\,s^{-1}$, the network structure of the carbon black particulates is destroyed: at the onset of flow the network is strained until it yields; thus, the rate of network junctions' destruction is much larger than the rate of creation. At steady state, normal shear thinning is established, indicating that now the rheological nature of the matrix dominates. Also noteworthy is that at the two higher loadings, the viscosity increase with increasing ϕ is more pronounced.

Figure 11.19(a) and 11.19(b) plot relative viscosities of suspensions of monodispersed-size spheres in Newtonian liquids. Figure 11.19(a) was constructed by Bigg (76) from data obtained by Lewis and Nielsen (77), who investigated the viscosity of glass-sphere suspensions in Aroclor Type 1254, a Monsanto chlorinated bisphenyl liquid with Newtonian viscosity of 80 poise at 25°C. As we will see later, Lewis and Nielsen investigated the effect of glass sphere agglomeration on suspension viscosity. Rutgers (78) has also presented similar results.

Figure 11.19(b) plots the steady state ratio of the viscosities of suspensions of spherical particles in Newtonian liquids, μ_s, to the viscosity of the Newtonian fluid, μ_f. It was constructed by Thomas (79) using the data of a number of investigators. A variety of uniform-sized particles having diameters of 1–400 μm were used. They included PS and

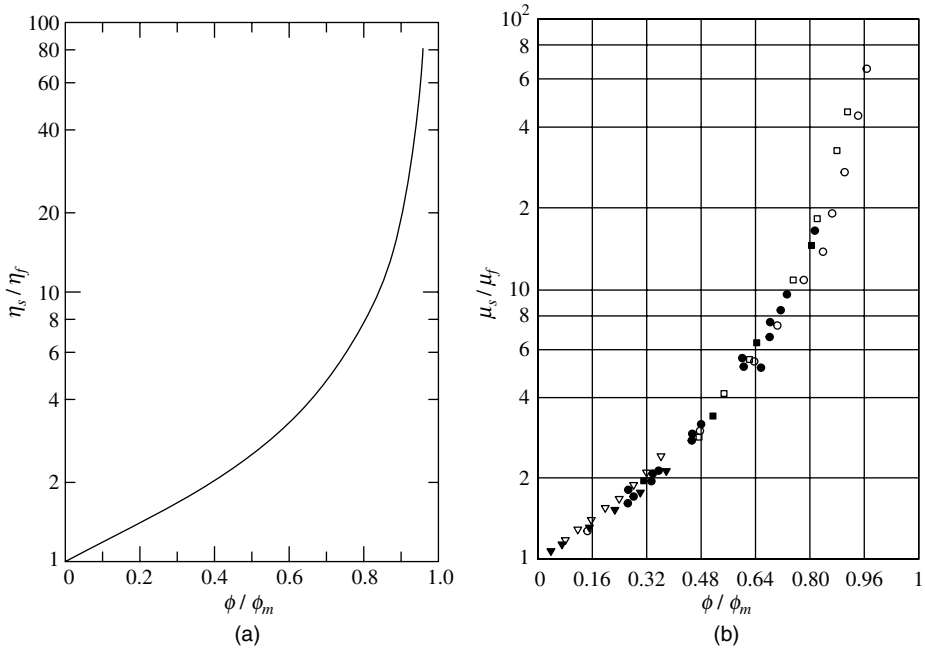

Fig. 11.19 Viscosity of suspensions of spherical particles in Newtonian fluids. (a) Curve constructed by Bigg. [Reprinted by permission from D. M. Bigg, ''Rheological Behavior of Highly Filled Polymer Melts,'' *Polym. Eng. Sci*, **23**, 206 (1983).] (b) Curves presented by Thomas (79).

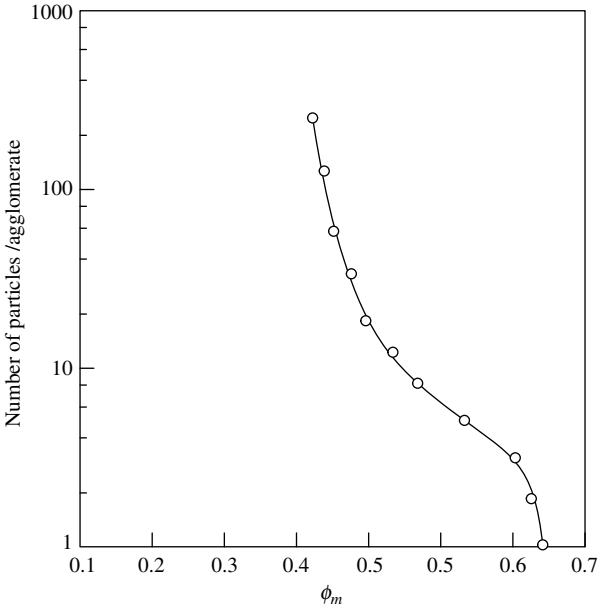

Fig. 11.20 Relationship between the number of spherical particulates in an average agglomerate and ϕ_m, plotted by Bigg from data by Lewis and Nielsen (77), on glass spheres in Aroclor with various degrees of agglomeration. [Reprinted by permission from D. M. Bigg, "Rheological Behavior of Highly Filled Polymer Melts," *Polym. Eng. Sci*, **23**, 206 (1983).]

polymethyl methacrylate (PMMA) beads, rubber latex, and glass spheres. To avoid settling, either the density of the suspending medium was adjusted or a medium of high viscosity was used. The maximum packing density was determined by extrapolating a plot of $1/[(\mu_s/\mu_f) - 1]$ vs. ϕ to zero, giving $\phi_m = 0.625$, very close to that of randomly packed spheres of equal size. Frankel and Acrivos (80) have developed and reviewed theories describing the viscosity behavior of concentrated Newtonian fluid suspensions. Thus ϕ_m is an important parameter in determining the viscosity of filled systems. It depends on the particle size distribution and shape of the fillers, plus the degree of agglomeration. Small size fillers, with large surface-to-volume ratios agglomerate under the influence of interparticle forces. Agglomeration decreases the maximum packing volume fraction, as shown on Fig. 11.20. Thus, agglomeration increases the viscosity of particulate filled melts.

Surface treatment of fillers normally reduces the interparticle forces, the degree of agglomeration, which in turn increases the maximum packing density, ϕ_m, and decreases the viscosity at any given level. This is shown on Fig. 11.21 for LDPE filled with uncoated and stearic acid-coated $CaCO_3$ (81,82) and for PP filled with uncoated and titanate-coated $CaCO_3$ (83,84). The viscosity is reduced by coating $CaCO_3$ with a physical coupling agent (stearate) or a reactive coupling agent (titanate), where X is the reactive group. Both compounds are bifunctional with one end adhering to the matrix and the other to the particulate filer. In the case of titanate coated $CaCO_3$ there is an apparent suppression of the yield stress. It is generally observed that filled polymer melts are "less elastic" than their matrices, resulting in lower extrudate swell and depressed melt fracture (81). Indeed, the results in Fig. 11.21(b) indicate that at constant stress the first normal stress coefficient decreases appreciably with the addition of $CaCO_3$, and this is evidence of the decrease in

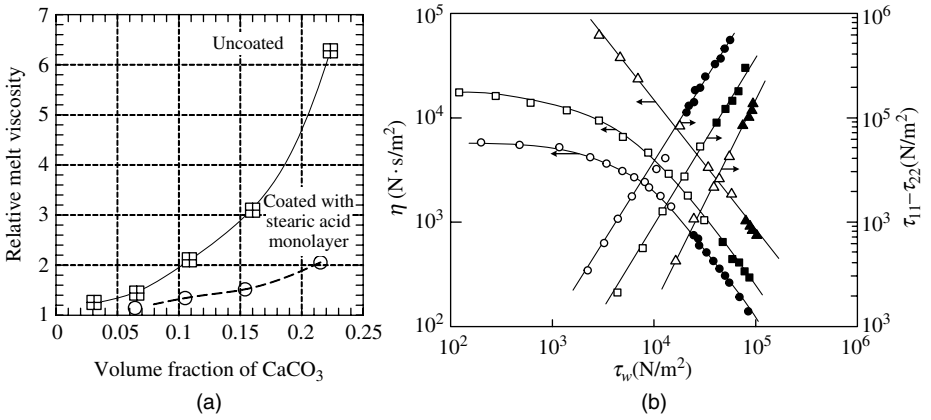

Fig. 11.21 Increases in viscosity brought about by (a) the deagglomerating effect of coating $CaCO_3$ filler particulates with calcium stearate [reprinted by permission from Y. Bomal and P. Goddard, ''Melt Viscosity of $CaCO_3$-filled Low Density Polyethylene: Influence of Matrix-filler and Particle–particle Interactions,'' *Polym. Eng. Sci.*, **36**, 237–243 (1996)], and (b) a titanate RO-Ti-$(OX)_3$. Viscosity and first normal stress difference vs. shear stress for $CaCO_3$-filled polypropylene with titanate coupling agent TTS (isopropyl triisosotearoyl titanate) at 200°C. (○ ●) PP; (△ ▲) PP/$CaCO_3$; (□ ■) PP CaCO3/TTS. Data with open symbols were obtained with a Weissenberg rheogoniometer, and data with closed symbols were obtained with the Han slit/capillary rheometer. [Reprinted by permission from C. D. Han et al., ''Effects of Coupling Agents on the Rheological Properties Processability and Mechanical Properties of Filled PP,'' *Polym. Eng. Sci.*, **21**, 196 (1981).]

elasticity. The reason behind the smaller decrease in N_1 with the titanate-coated $CaCO_3$ shown in the figure may be related to better matrix–particulate adhesion.

Next we turn to *anisotropic fillers* such as glass fibers and explore their effect on the rheology of polymer matrices. Fibers, like spherical particulates cause an increase in viscosity and a decrease in elasticity. They are also coated with coupling agents to decrease agglomeration and increase adhesion between the fibers and the matrix. This is especially desirable for glass fiber reinforced final products. They decrease solid state debonding from both thermoplastic polymers, thus becoming true load-bearing components of such composite structures. But unlike nearly spherical fillers, randomly suspended rodlike *fibers* get oriented during flow start-up. In nondilute fiber-filled polymer matrices fiber orientation is in the direction of flow, with a distribution similar to that of rodlike fillers in Newtonian fluids (82). Fiber motions in non-Newtonian fluids have been the main focus of theoretical studies (83–86). Experimental steady state glass fiber orientation distributions in viscometric pressure flow are shown on Fig. 11.22. Fiber orientation distribution is narrow and below 5° away from the shear plane at low shear rates, and it narrows to even smaller angles with increasing shear rate. Thus, there is a major fiber network destruction that results in lowering the viscous energy dissipation and allowing the matrix to be the major contributor to the shear thinning behavior of the glass-filled melt (87–89). This is shown on Fig. 11.23 for a 30% wt glass-filled LDPE melt.

We note that in the entire range of processing shear rates (10^1–10^3 s^{-1}) the viscosity of the glass-filled melt seems to be dominated by the matrix in its shear-thinning property, but has an absolute value of about 50% higher than the matrix at this loading level. The filler aspect ratio (i.e., length to diameter ratio) affects the low shear rate viscosity of glass-filled melts, as shown on Fig. 11.24 for a series of loadings with a low viscosity Nylon-6. Above

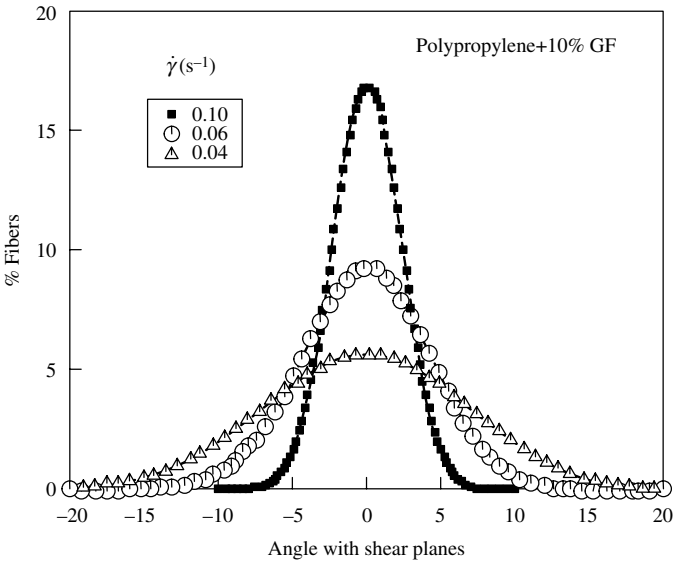

Fig. 11.22 Steady state fiber orientation with respect to shear planes for GF-filled PP. [Reprinted by permission from A. T. Mutel, Ph.D. Thesis, Department of Chemical Engineering, McGill University, Montreal, Canada (1989).]

fiber *L/D* ratio of 10 and shear rates up to about $1\,s^{-1}$ the effect is more pronounced, indicating possible network formation. Furthermore, Nylon-6 with longer fibers is more shear thinning than the Newtonian matrix and matrix filled with shorter fibers. This is an indication of the destruction of remnants of long-fiber networks, albeit weak.

The flow-induced destruction of networks of both near-spherical and rodlike particulates suspended in polymer matrices can be reversed with time in quiescent conditions. It is of limited interest, since it may take hours, which will cause thermal degradation. Larson (90)

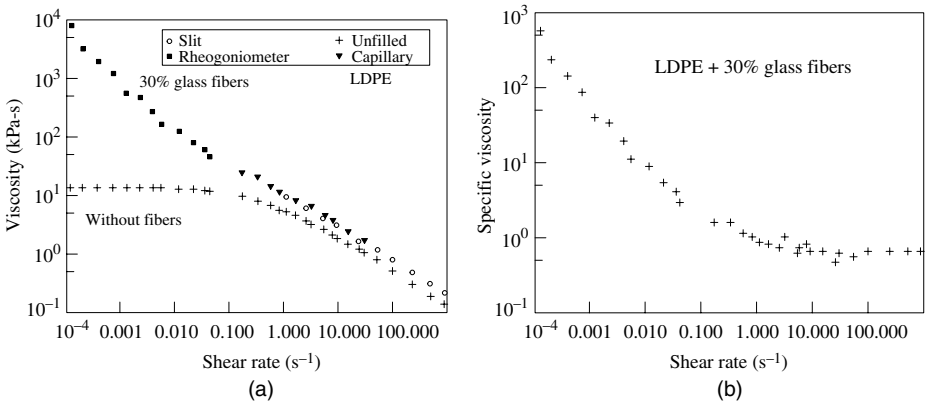

Fig. 11.23 (a) The shear flow viscosity of the matrix and 30% wt glass-filled PP, and (b) the specific viscosity, equal to the ratio of the glass-filled LDPE to the unfilled LDPE viscosities at the same shear rate. [Reprinted by permission from H. M. Laun, "Orientation Effects and Rheology of Short Glass Fiber-reinforced Thermoplastics," *Colloid Polym. Sci.*, **262**, 257 (1984).]

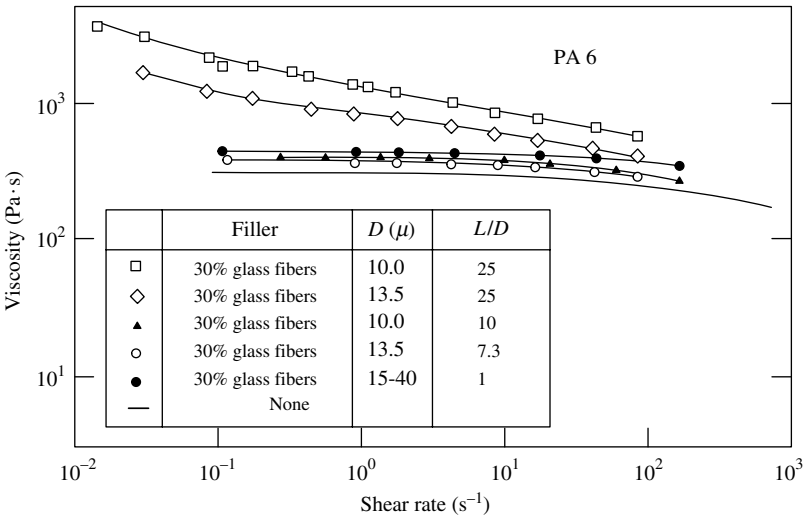

Fig. 11.24 The effects of the fiber aspect ratio, at constant 30% wt loading, on glass-filled polyamide-6. [Reprinted by permission from H. M. Laun, ''Orientation Effects and Rheology of Short Glass Fiber-reinforced Thermoplastics,'' *Colloid Polym. Sci*., **267**, 257 (1984).]

estimates that the diffusion time, $t_D \approx \eta d^3/k_b$ for a 1-μm-diameter particle in a melt of viscosity 10^3 Pa·s is very long, of the order of 10 h! This phenomenon is *thixotropy*, which is shear-thinning with time at constant deformation rate.

Finally, at higher particulate loadings, above 50% vol, the rheological behavior of filled melts is dominated by particle-to-particle interactions, due to both interparticle forces and physical flow–caused movement hindrances of the suspended particulates, particularly during pressure flows. One consequence of this is the creation of a particulate-free wall film that creates a lubricity slip layer and pluglike flows. Such slip velocities have to be considered in flow rate versus pressure drop design expressions, as well as the viscometric rheological characterization (91).

In summary, the following effects of particulates on the viscosity of filled melts are observed: at very low shear rates and with $\phi_v > 0.1$–0.2, very large effects are observed, indicative of the presence of interparticle networks; the destruction of these networks at the entire processing shear-rate region results in the fact that the matrix shear-thinning nature is preserved, but with viscosities increasing with increasing ϕ_v; coating particulates with bifunctional coupling agents decrease agglomerization, increasing ϕ_m, and therefore decreasing the shear viscosity; at higher ϕ_v particulate-free wall-slip layers are formed during flow, resulting in wall-slip velocities; filled melts are less elastic, resulting in low extrudate swelling and delayed onset of melt fracture; finally, filled melts are thixotropic. The preceding collection of rheological attributes of particulate-filled polymer melts renders them to be ''complex'' fluids.

Compounding of Particulate-Filled Systems

Let us now turn to the question of the consequences of the previously discussed rheological behavior to polymers compounding operations. In continuous compounding equipment we have to answer this question for each of the elementary steps involved.

Solids Handling Feeding and solids transport can benefit from coating particulates with physical and chemical coupling agents, since they reduce agglomeration and make particulates free flowing, but feeding polymer pellets or stabilized reactive powder with solid particulates of different size and density may result in feed-constituent segregation. In general, feeding of dry particulate ingredients requires preblending, which is carried out in simple ribbon blenders with the blend transferred to a metering feeder in twin rotor compounders and a gravity or force feeder in a SSE. However, feeding large amounts of filler may also be carried out by preblending via separately metered joint feeding, or by sequential addition of the filler through feed ports after melting has taken place (92). Feeding a mix of a liquid additive with solid particulates is facilitated by preparing a concentrate in an intensive mixer, for example, a Henschel mixer. The high speed rotors generate very vigorous flow, coating, and collisions, leading to a rise in temperature and absorption of the liquid component by the solid particulates, often resulting in a free-flowing system.

Feeding fibers together with polymer pellets or powder does lead to feeding complications as well as component segregation. Furthermore, the high fiber aspect ratio together with their abrasive nature will result in excessive machine wear in those channel segments that are full of solids (solids transport and early melting sections). For these reasons continuous glass rovings or ''chopped'' fibers are fed or ''stuffed'' at a location downstream of the melting section, as shown on Fig. 11.25 (93), requiring only deagglomeration and dispersive mixing by the laminar flow stresses. Within the machine, downstream from the feeding port, near-spherical particulates may get agglomerated or

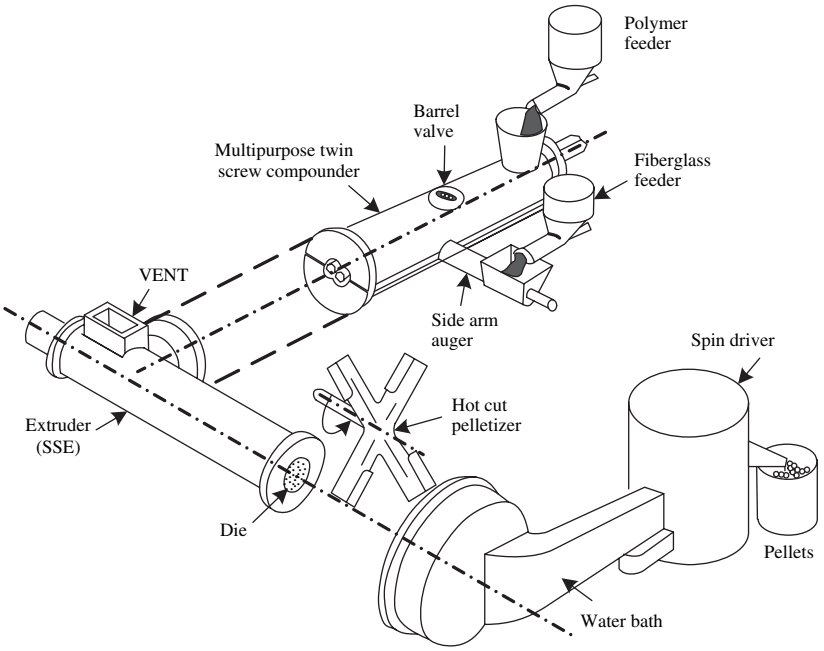

Fig. 11.25 Schematic of twin-screw compounding system for producing glass-reinforced polymer pellets. [Reprinted by permission from D. B. Todd and D. K. Baumann, ''Twin Srew Reinforced Plastics Compounding,'' *Polym. Eng. Sci.*, **18**, 321–325 (1978).]

"briquetted" by compressive forces, thus hindering the tasks of dispersive mixing following melting. On the other hand, very small and "fluffy" particulate additives, such as carbon black, are pelletized into moderate density 0.3–0.5-g/cm^3 pellets and transported in bulk or bags. The process conditions must "navigate between *Scylla* and *Charybdis*"[2] (94) in making pellets with enough cohesive strength to endure bulk handling, but weak enough to be dispersed by laminar flow stresses during compounding. Additives that will be compounded with water sensitive polymers (e.g., polyamides and polyesters) must be thoroughly dried, and a nitrogen blanket is required for compounding into polymers sensitive to oxidative degradation (e.g., LDPE).

The presence of particulate fillers in polymer systems, which are compounded in twin rotor equipment, does not affect *solids transport*, since that section of the device is partially filled and, in the case of co-rotating twin extruders, self-wiping. By contrast, in single-rotor processing equipment, compressed-particulate solids beds are formed soon after gravity-fed hoppers. They slide in a pluglike fashion downstream, under the frictional forces at the barrel–solid bed interface. There, the filler particulates in contact with the barrel, bring about a higher apparent coefficient of friction, $f_{w,ps}$ above that without the filler, f_w. This results in an increase in frictional forces, which in turn leads to increased transport capability, to increased torque and power consumption, as well as more machine wear since most fillers are abrasive. The extra frictional force is

$$F(z) = P(z)A_{ps}(z)(f_{w,ps} - f_w) \tag{11.5-1}$$

where $A_{ps}(z)$ is the area of effective contact between particulates and the barrel. The extra mechanical power is

$$\dot{W}(z) = F(z)(V_b - V_{\text{plug}}) \tag{11.5-2}$$

where V_{plug} is the solids bed plug velocity (see Section 4.9). Higher $\dot{W}$ will generate, in a shorter down-channel distance, the thickness needed for melting to begin, and thus reduce the length of the "delay zone," discussed in Chapter 9. The preceding effects increase with increasing filler loadings.

Melting The effects of particulate fillers on melting are appreciable in both single and twin rotor compounding equipment. In single rotor devices, melting occurs by *conduction* with *drag-induced melt removal* (see Section 5.7). The two heating contributors are conduction from the barrel and viscous energy dissipation (VED) generated in the sheared molten film (see Eq. 5.7-38 for "Newtonian" melts). The VED source term increases linearly with viscosity. Turning to Fig. 11.18 we observe at a shear-rate value of $10^2\ \text{s}^{-1}$ an order-of-magnitude increase in the viscosity at 20% by volume of carbon black–filled PS compared to PS. Since in compounding it is reasonable to assume that VED is the dominant contributor, the melting rate also may increase by an order of magnitude.

2. Ulysses had been warned by Circe of the two monsters Scylla and Charybdis. Scylla dwelt in a cave high up on the cliff, from whence she was accustomed to thrust forth her long necks (for she had six heads), and in each of her mouths to seize one of the crew of every vessel passing within reach. The other terror, Charybdis, was a gulf nearly on a level with the water. Thrice each day the water rushed into a frightful chasm, and thrice was disgorged. *The Odyssey* by Homer.

Similar, but lower increases are observed on Fig. 11.21(a), with 20% loading of uncoated $CaCO_3$ giving a fivefold viscosity increase and a twofold increase with the coated filler in LDPE. The denominator in Eq. 5.7-38 represents the amount of thermal energy needed to raise the temperature of the feed to the processing melt temperatures. Note that the filler does not have to undergo melting; thus, the needed thermal energy may be lower, also contributing to higher melting rates.

In twin rotor compounding equipment melting takes place very rapidly in the melting section, which is filled by compacted particulate-filled polymers. The initial melting mechanisms (see Section 5.9) are frictional energy dissipation (FED) and plastic energy dissipation (PED). After partial melting, the unmelted pellets/powder form ''suspensions'' in the particulate-filled fresh melt. Thus, VED in the molten regions now becomes an important melting contributor. The presence of particulates has the following effects: an appreciable increase of the FED, since frictional forces between deforming filler-coated assemblies are larger, or much larger, than with only polymer particulate assemblies; thus FED, which is usually much smaller than PED in unfilled systems becomes a strong contributor to melting at the polymer–particulate surfaces. This, coupled with PED, stemming from solid pellet deformations, results in more rapid melting both initially and during the VED stage. This is shown on Fig. 11.26 for a system of PP powder filled with only 2% by weight of clay melted in the Twin Screw Melting Element Evaluator[3] (TSMEE) and a Brabender internal mixer (95). The melting length in the TSMEE is reduced by 17% and the melting peak in the Brabender internal mixer is reduced from 18 s to 6 s. It is also noteworthy that addition of 5% PE wax lubricant increases the melting length, for example, for PP powder from 1.6 *L/D* to 2.2. *L/D*.

Dispersive Mixing The objective of dispersive mixers is to break down agglomerates. This is discussed in detail in Section 7.1. Yet, as mentioned earlier in this section, particulate fillers may undergo agglomeration by the high-frequency pressure generated by the kneading paddles, and if this happens it will generally be difficult to deagglomerate in the downstream mixing section. The degree of agglomeration, or rather the lack of dispersive deagglomeration, at any uniform global concentration will affect the mechanical properties of the product as well as its visual appearance when analyzed at small enough scale of examination.

An example of agglomeration in a $CaCO_3$-filled PP sample is shown on Fig. 11.27 (96). The SEM photograph shows that the 8% filled (by volume) sample is packed with agglomerates of different sizes. The degree of agglomeration can be appreciated by the fact that an agglomerate of size $d_1 \approx 15\,\mu m$, contains approximately 10^6 primary $CaCO_3$ particles of size $d_2 \approx 0.15\,\mu m$. Yet, the main function of mixers is to disperse the agglomerates into smaller agglomerates, or preferably into the primary particles and distribute them throughout the volume of a batch mixer, or the discharge of a continuous mixer.

In Section 7.1 we show that the criterion for a spherical agglomerate breakup in viscous flow depends on parameter Z defined as:

$$Z = \frac{8}{9}\chi\mu\dot{\gamma}\left(\frac{\varepsilon}{1-\varepsilon}\right)\frac{d}{C_0} \tag{11.5-3}$$

3. The TSMEE is an experimental device developed to study melting and mixing in twin rotor mixers during the Polymer Mixing Study conducted at the Polymer Processing Institute (95).

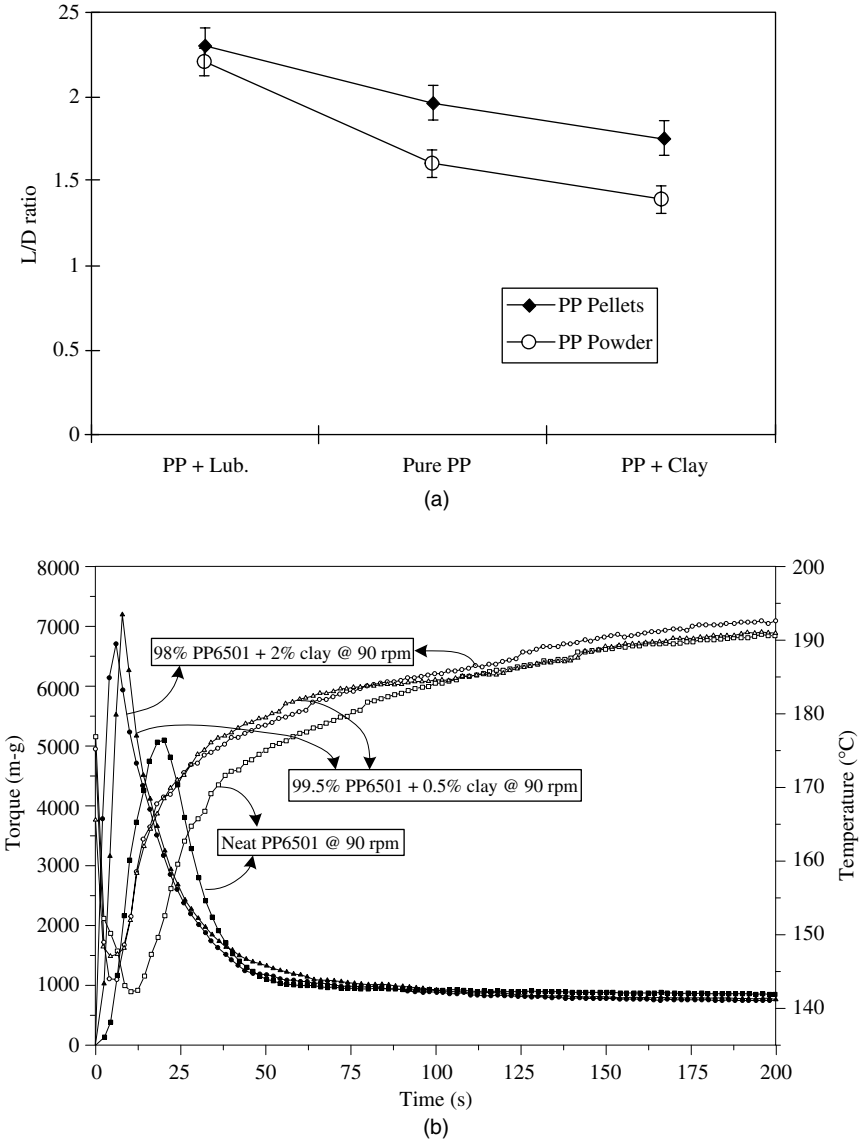

Fig. 11.26 (a) The length-to-diameter ratio, *L/D*, required for melting of PP Montell (6523) pellets and the same powder: PP only, PP with 2% wt clay, and PP with 5% wt PE wax lubricant. (b) The evolution of torque and temperature in a Brabender internal mixer for neat and clay-filled powder. [Reprinted by permission from M. Kim and C. G. Gogos, "The Roles of Clay and PE Wax Lubricants on the Evolution of Melting in PP Powder and Pellets," *Proceedings of the 11th Polymer Mixing Study Meeting*, Polymer Processing Institute, Hoboken, NJ (1995).]

Agglomerate breakup will occur at $Z > 2$ in shear flow; in biaxial extensional and uniaxial extensional flow, it will occur at $Z > 1$ and $Z > 0.5$, respectively. Breakup does not depend on agglomerate size, but on the size of the primary particle. Clearly, the smaller the primary particle is, the higher the shear stresses needed to reach breakup. It is worth noting

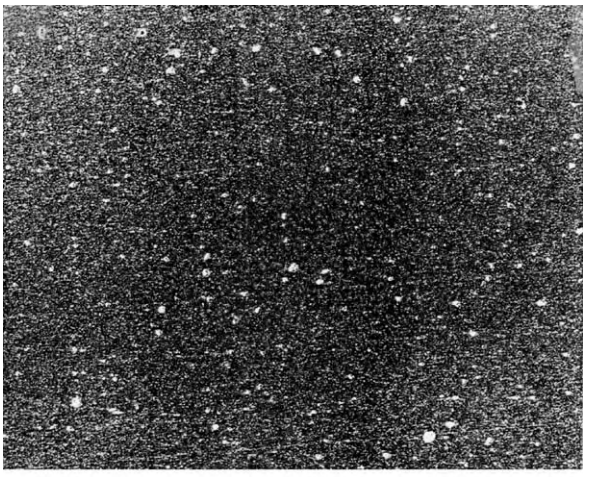

Fig. 11.27 Scanning electron micrograph of calcium carbonate–filled polypropylene: the primary particle size is 0.15 μm; the volume fraction of filler 0.08. [Reprinted by permission from Y. Suetsugu, "State of Dispersion-Mechanical Properties Correlation in Small Particle Polymer Composites," *Int. Polym. Process.*, **5**, 184 (1990).]

that the dimensionless number Z is the agglomerate equivalent of the capillary number. Both are parameters representing the ratio of hydrodynamic surface forces acting to break up the particle/droplet to the cohesive forces that hold them together. In agglomerates these are van der Waals forces between the primary particles; whereas, in droplets it is the surface tension.

We have shown in Section 7.1 that hard agglomerate breakup requires fairly high shear stresses. Yet, because of power and heat transfer limitations, mixers for both rubbers and plastics, continuous or batch, cannot be designed to impose high stress levels throughout the mixer volume. All dispersive mixers are therefore designed to have the following characteristics: (a) high stress regions of relatively small volume with good heat-removal characteristics; (b) a flow pattern that circulates the fluid repeatedly through the high shear regions; and (c) an overall geometrical configuration that ensures very good distributive mixing, frequently stemming from chaotic flow patterns in the mixers. In classic Banbury-type batch mixers, the high-stress region is the radial clearance between the tip of the rotating blades and the wall of the mixer. In the continuous twin screw–type of mixers it is the clearance between the tip of a flight or a kneading-type element and the barrel surface, or any other geometrical configuration with narrow clearance.

Clearly, if these conditions are met, different fluid particles experience a different number of passes (for a given time in a batch mixer, or over a certain length in a continuous one), and we can only compute the probability of a fluid particle to experience a given number of passages. This is what the number of passage distribution (NPD) functions discussed in Section 7.3 accomplish. Now, having the criterion of breakup, and assuming midplane cleavage when it occurs, and using the NPD functions, Manas-Zloczower, Nir, and Tadmor (97) derived a complete model for batch mixers.

They adopted the well-stirred vessel with recirculation as a model for internal Banbury-type mixers. They derived the NPD function, combined it with a physical and hydrodynamic model to describe the rupture of an individual freely suspended axisymmetric solid particle, and derived the ultimate particle size distribution of the solid. They tested the model with experimental results on carbon black dispersion in rubber and showed very good agreement. The good agreement was attributed to the capture by the NPD function of the key element of the very complex mixing process. Indeed they suggested (98) as a mixer scale-up criterion the mean number of passages coupled with securing a given threshold shear stress value in the high shear region between the tip of the rotor and the chamber wall.

Example 11.3 The Two-Zone Theoretical Model for Agglomerate Dispersion in a Batch Intensive Mixer In this example we calculate the agglomerate size distributions, a function of mixing time in a dispersive batch mixer following the two-zone model developed by Manas-Zloczower et al. (97,98). According to this model the mixer of volume V is divided into two functional zones: *Zone 1* occupies virtually all of the mixer and it is considered to be a stirred tank, implying uniform composition at all times; whereas, *Zone 2* occupies the small narrow gap high shear regions. A constant steady stream q exits the first zone, passes through the high-shear second zone, and is recirculated to the first zone. We assume constant shear stress drag flow in the gap. Therefore, since we have shown in Section 7.1 that for agglomerates with uniform porosity rupture is independent of size, there are only two outcomes for agglomerates passing in Zone 2: they either rupture or not. Of course, dispersive mixing occurs only in the former case. We further assume that the rupture of agglomerates is a repetitive process until the ultimate particle size is reached, which can no longer rupture. The initial agglomerates are spherical in diameter size, D_0, and when they rupture two equal size spherical smaller agglomerates are formed of size D_1, and so on. Thus, the size of the agglomerate after $k+1$ ruptures is given by

$$D_{k+1} = \frac{D_k}{2^{1/3}} \tag{E11.3-1}$$

and in terms of the initial size

$$D_k = \frac{D_0}{2^{k/3}} \tag{E11.3-2}$$

Initially a fluid particle in the mixer contains a volume fraction v_0 of agglomerates of size D_0. After the fluid particle passes Zone 2 once, it will contain the same volume fraction of particles of size D_1, and so on. But, as discussed in Section 7.3, at any time, t, we find fluid particles in Zone 1 that never passed through Zone 2, fluid particles that passed once, twice, or k times. Therefore, as soon as mixing begins, at any given mixing time, t, we find a *distribution* of agglomerate sizes in the mixer. In Section 7.3 we showed that the volume fraction of fluid that has experienced k passes in a recirculating stirred vessel is given by

$$g_k = \left[\frac{1}{k!}\left(\frac{t}{\bar{t}}\right)^k\right] e^{-t/\bar{t}} \tag{E11.3-3}$$

where $\bar{t}$ is the mean residence time in Zone 1, between passes through Zone 2, and is given by

$$\bar{t} = \frac{V}{q} \tag{E11.3-4}$$

Equation E11.3-3 provides the required size distribution of the agglomerates, because the direct correspondence between the number of passes in Zone 2 and the resulting agglomerate size as given in Eq. E11.3-2. Thus, at a given mixing time, t, the fraction of fluid volume that never passed Zone 2, and, therefore, contains only agglomerates of size D_0, according to Eq. E11.3-3 decreases exponentially with time:

$$g_0 = e^{-t/\bar{t}} \tag{E11.3-5}$$

The volume fraction that contains agglomerates that passed through Zone 2 once and, therefore contains agglomerates of size of D_1, is

$$g_1 = \left(\frac{t}{\bar{t}}\right) e^{-t/\bar{t}} \tag{E11.3-6}$$

We note that the volume fraction of fluid with agglomerates of this size begins with zero and passes through a maximum at a mixing time $t/\bar{t} = 1$ and then drops exponentially. Similarly, all fractions at $k > 1$ will exhibit the same type of behavior, but with the maxima at increasingly longer mixing times.

The quality requirements of dispersive mixing generally require that the fraction of agglomerate above a critical size be below a certain set value. For carbon black dispersion in rubber, for example, generally the requirement is that the fraction of agglomerates above 10 μm be less than 1%. In terms of distribution function the mixing time needed to meet such a criterion is given by

$$\sum_{i=0}^{L} g_i = \sum_{i=0}^{L} \left(\frac{1}{i!}\right)\left(\frac{t}{\bar{t}}\right)^i e^{-t/\bar{t}} < \psi \tag{E11.3-7}$$

where L is the minimum number of passes needed to reach the critical size of the agglomerate, and ψ is the quality criterion (e.g., 0.01 for carbon black). If, for example, $L = 10$, and the mean residence time is 10 s, the mixing time needed to meet a criterion of $\psi = 0.01$ is $t = 529$ s. That is, 8.8 min are needed to secure that 99% of the agglomerates experience more than 10 passages.

From the preceding equations, we can also calculate the discreet agglomerate size distribution at any mixing time. The total initial number of agglomerates is

$$N_0 = \frac{v_0 V}{4\pi D_0^3/3} \tag{E11.3-8}$$

The number of initial-size agglomerates decreases with time, as given by Eq. E11.3-5:

$$N_0(t) = N_0 e^{-t/\bar{t}} \tag{E11.3-9}$$

In a fluid particle that passes k times the *size* of the particle according to Eq. 11.3-2 reduces to D_k, and the *number* of particles doubles every pass to $N_k = 2^k N_0$. Thus, the number of agglomerates of size D_k in the mixer at time t is

$$\begin{aligned} N_k(t) &= 2^k N_0(0) g_k \\ &= 2^k N_0(0) \left[\frac{1}{k!} \left(\frac{t}{\bar{t}} \right)^k \right] e^{-t/\bar{t}} \end{aligned} \tag{E11.3-10}$$

The fraction of agglomerate of size k is

$$Y_k = \frac{N_k(t)}{\sum_0^L N_k(t)} \tag{E11.3-11}$$

There is a series of additional factors that we have not taken into account in this example. These, however, do not change the concept, but make the model somewhat more complicated.

The first factor is that the agglomerates are not necessarily spherical in shape. A more general representation would be to assume that they are spheroids in shape with fore and aft symmetry. This case was treated in detail by Manas-Zloczower et al. (97). These particles enter the high shear zone in random orientation, and therefore some may rupture and others will pass without rupturing. The fraction of particles that rupture in a given set of condition can be calculated.

The second factor is that the flow field is not pure drag flow, because upstream from the high shear zone there is a tapered region that generates pressure and affects the flow field. The pressure is necessary to prevent slip in the narrow gap. Moreover, elongational flow develops in the tapered section, which by itself helps separate closely spaced particles and even leads to rupture. Clearly, if the flow field in the narrow-gap is a combination of drag and pressure flow, the shear stress will no longer be uniform and consequently not all agglomerates may rupture, because some may pass the narrow gap region at locations where the shear stress is below the critical value. This factor can be incorporated into the model, too.

The third factor is the nonuniform temperature field in the gap, because the outside wall is cooled to secure high enough stresses in the gap, but the rotor is not cooled; moreover, viscous dissipation generates heat. All these led to a nonuniform stress field, which once again affects performance.

Finally, the fourth factor in the size-dependent cohesion of agglomerates (99), discussed in Section 7.1.

Example 11.4 Revisiting the SSE as a Dispersive Mixer In Section 9.2 we discussed the Manas-Zloczower and Tadmor (100) NPD model for an SSE, which indicates that the common SSE is an inherently poor dispersive mixer. In this example we examine the NPD in an SSE with a larger flight clearance providing for more circulation over the flight. The model is based on a continuous-plug-like flow system with recirculation shown schematically in Fig. E11.4 where an axial slice of material considered a well-mixed tank, with recirculation over the flight, moves along the axis of the SSE.

The NPD is given by Eq. 9.2-44 (which is equivalent to Eq. E11.3-3) where $\lambda = t/\bar{t}$ is given in Eq. 9.2-47, and it is the ratio of residence time in the extruder (given by the ratio of free volume of the screw to SSE volumetric flow rate, V/Q) to the mean circulation time over the flight zone (given by the ratio of the free volume of the screw to the total (drag) flow rate

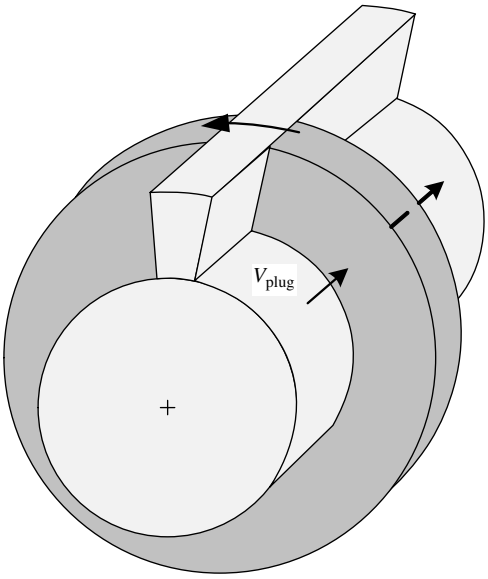

Fig. E11.4 A shaded axial slice of the screw extruder of volume v, which is assumed to move axially in a plug-like mode. The barrel drags melt from the well-mixed annular region over the flight back to the annular well-mixed region.

over the flight, V/Q_f). If we neglect the effect of the flight width on the free volume of the screw, λ is given by Eq. 9.2-47

$$\lambda = \frac{Q_f}{Q} \tag{E11.4-1}$$

As an example consider a single-flighted 60-mm diameter extruder with length-to-diameter ratio of 20 and a relatively large flight clearance of 0.05 cm to allow high rates of flow over the flight (and thus increase the number of passages) with the screw rotating at 60 rpm and extruding 50 1/h melt.

The flow rate of the flight from Eq. 9.2-47 is

$$Q_f = \frac{1}{2}\pi\left(\frac{60}{60}\right)(20 \times 0.06)(0.06)(0.5 \times 10^{-3}) = 0.565 \times 10^{-4} m^3/s$$

And the volumetric flow rate is

$$Q = 50 l/h = \frac{50 \times 10^{-3}}{3600} = 0.13889 \times 10^{-4} m^3/s$$

Which results in $\lambda = 4.068$ and the NPD is

g_0	1.71%
g_1	6.96%
g_2	14.15%
g_3	19.20%
g_4	19.50%
g_5	15.87%
g_6	10.76%

Results indicate that although only 1.7% of the exiting flow rate never passes the flight, 61.5% of the material passes less than five times. Keeping in mind that for good dispersion we need some 25 passages, clearly the SSE is a poor dispersive mixer. Moreover, the melt in the screw channel, though mixed by the circulatory flow pattern that ensues in the channel, cannot be considered well-mixed and chances are that much of the same melt is recirculated; the velocity profile in the flight clearance is not pure drag flow, but because of temperature effect it is distorted, reducing the flow rate across the flight; the barrel is hot and the melt is heated further by viscous dissipation, reducing shear stresses in the flight; and, finally, there is no tapered entrance into the narrow flight gap, generating pressure to avoid slip in the flight. In view of all this one cannot expect that the SSE be dispersive mixers. However, using a very different screw geometry and design, as shown by Tadmor (101), SSEs can be converted into dispersive mixers.

Finally, along similar lines, Canedo and Valsamis (102) analyzed and modeled the nonintermeshing twin rotor Farrell Continuous Mixer (FCM) as a continuous plug-flow system with recirculation. These authors calculate the average number of passages in the FCM machine to be in the range of 20–50, despite the relative short residence time of the material. By modeling flow over the clearance they compute the maximum shear stress, and they propose to quantify mixing performance of continuous mixers in terms of the maximum shear stress, the mean number of passages, and the mean residence time. Dispersive mixing requirements with fiber additives are more complex. On the one hand, we wish to wet and break bunches of fibers into individual fibers and then distribute them throughout the volume. Yet, the need of dispersion must be carefully balanced with the risk of fiber length breakdown. Indeed, brittle fiber additives suffer length breakdown mainly during melting, but also during the subsequent mixing flows, as seen on Fig. 11.28, tracking the breakdown of glass fibers in an SSE (103). For this reason fibers are fed (stuffed) at a feed location downstream melting in both single- and twin-rotor continuous compounders. Figure 11.29 (104) depicts the original fiber length distribution of magnesium oxysulfate (MOS) whiskers in the extruder when MOS is dry-blended with PP pellets (feed A) and those when MOS is fed after melting has taken place (feed B). In the former, fiber breakdown is much larger than in the latter. Nevertheless, fiber feeding after melting also results in appreciable length breakdown. Turkovich and Erwin (103) found no significant effect of processing variables and filler concentration (in the range of 1% to 20%) of 6-mm glass fibers on breakdown of the fiber; this indicates that for the given initial length and for the equipment size used, fiber–fiber interactions are not responsible for the breakdown. Gogos et al. (105) studied the effect of preheating 10–15-mm-long pulltruded polyamid pellets containing 50% wt E-glass fibers, during injection molding. Figure 11.30 shows clearly the benefits of feed preheating by analyzing "carcass" samples taken at the screw tip, which contained almost an order of magnitude more fibers that were over 6 mm long. This was attributed to melting under lower shearing stresses. Of course, during the mold filling flow considerable glass-fiber attrition will take place.

Distributive Mixing Distributive mixing of solid particulate fillers is, to a first approximation, the same as with homogeneous melts: the flow kinematics, not laminar stresses dictate it, with chaos-conducive stretching and folding patterns being the most efficient (see Section 7.1). In the SSE distributive mixing can be greatly improved by a host of mixing elements. These are being extensively used not only because they improve distributive mixing, but primarily because they help complete the melting process, which

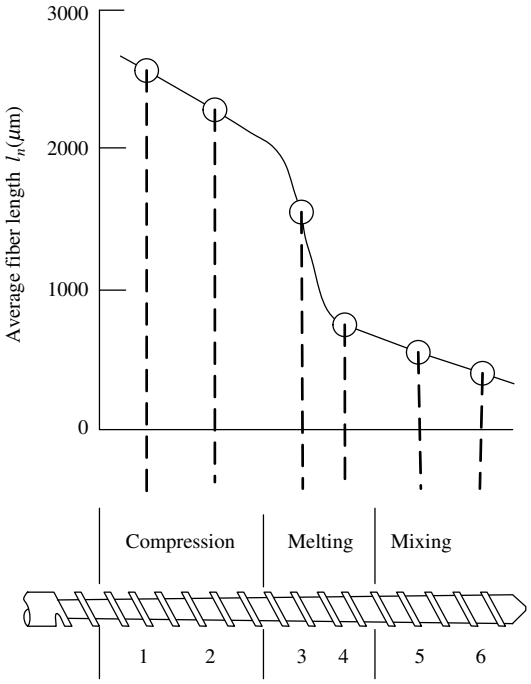

Fig. 11.28 The number average fiber length at various axial positions of an injection molding screw. DuPont Alathon 2010 pellets preblended with 3.2 mm chopped fibers and extruded in a 0.75 in diameter, 20.1 *L/D*, with 3:1 compression ratio extruder. [Reprinted by permission from R. von Turkovich and L. Erwin, "Fiber Fracture in Reinforced Thermoplastic Processing," *Polym. Eng. Sci*., **23**, 743 (1983).]

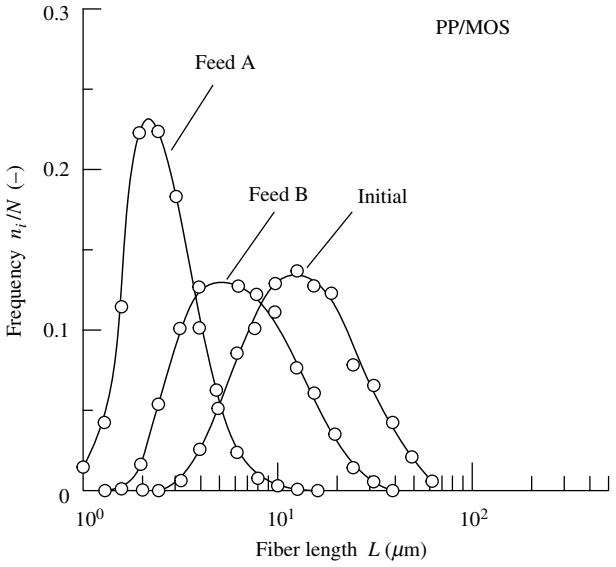

Fig. 11.29 Fiber-length distribution of MOS and feeding protocol for MOS-filled PP containing ethylene-propylene copolymer. [Reprinted by permission from Y. Suetsugu, "The Effect of Mixing on Some Properties of Compounds and Composites," in *Mixing and Compounding of Polymers*, I. Manas-Zloczower and Z. Tadmor, Eds., Hanser, Munich, 1994.]

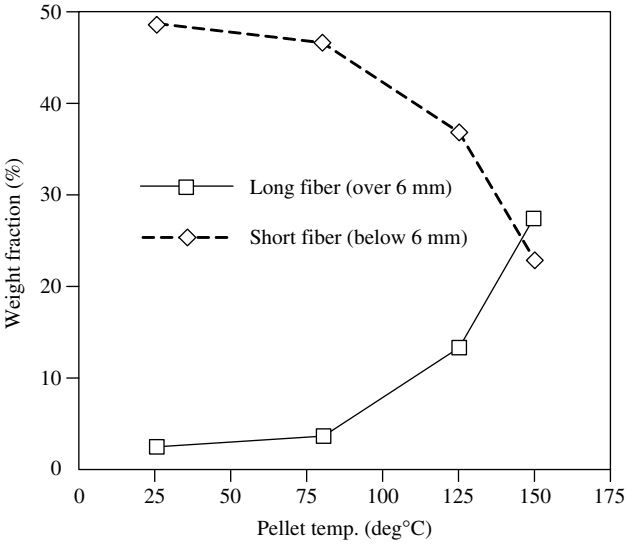

Fig. 11.30 Effect of preheating 50% by weight E-glass fiber–filled polyamide pulltruded pellets on fiber lengths at the screw tip of a 300-ton 23.86-oz reciprocating injection molding machine. [Reprinted by permission from C. G. Gogos, C. K. Yoon, and J. Brizzolara, "Injection Molding Process Development for Long Fiber Reinforced Thermoplastics," *SPE ANTEC Tech. Papers*, **40**, 384 (1994).]

if uncompleted, is the major source of both composition and thermal nonuniformity. An extruder having a screw equipped with suitable mixing sections, though it lacks the dispersive capability of twin-rotor mixers, is a very good compounder. Rauwendaal (106) reviewed the commonly used mixing elements in SSEs. A single-rotor extruder with exceptionally good distributive capability is the Ko-kneader-type rotating and reciprocating machine (107). The barrel in these machines has rows of pins and the screw flights are slotted to allow the barrel pins to pass through the flight slots. This results in stretching and folding flows by the relative and reciprocating motions of barrel pins and screw slots (108). Andersen (109) relates distributive mixing in co-rotating TSEs to mixing practices and distributive mixing elements, which generate stretching and folding chaotic flows, as well as splitting and recombination, leading to spatial redistribution of the compounded stream. As discussed in Chapter 10, simulations of the stretching and folding flows in full kneading elements in co-rotating TSEs have been carried out by a number of investigators, notably, Kiani and Samann (110) and Bravo et al. (111).

Compounding of Polymer Blends

Commercially available important *miscible* polymer blends are rare, the most notable and commercially important example being General Electric's original Noryl^{TM} polyphenylene oxide (PPO)/PS composition (112). Producing such blends commercially in compounding equipment is best carried out with chaotic flows following melting of the two components. With no interfacial forces, the two components flow with shear rates that are inversely proportional to their viscosities, since $\tau = \eta_A \dot{\gamma}_A = \eta_B \dot{\gamma}_B$. Thus, unless there is a very large

disparity in the viscosities, for example, a ratio greater than 100, chaotic flows will normally create small and spatially uniform striation thicknesses within short mixing times, t_m, enabling molecular diffusion to complete mixing on a molecular level. Twin rotor continuous and, of course, batch equipment are capable of creating rapid and uniform distributive mixing, and thus they are the preferred equipment for this type of compounding.

However, the majority of commercial blends is *immiscible* and are either physically or chemically *compatibilized* to improve and maintain, or rather to ''lock in'' the morphology developed during compounding and forming flows. The two components are morphologically segregated, coexisting as (a) *dispersions* at low ''minor'' component concentrations; (b) *cocontinuous* at nearly equal component concentration or *phase-inverted suspensions*, where the ''major'' is dispersed because the minor-to-major viscosity ratio is very small; and (c) composite-droplet, or ''salami,'' or droplet-within-droplet morphologies (113–116). The compatibilizing component(s), being amphiphilic, is (are) concentrated at the *interfaces* between the two polymer components.

It is axiomatic that compounding laminar flows are the cause of component domain breakup, since laminar stresses are the sources for breakup. On the other hand, their specific effects cannot be easily quantified because the flows are mostly nonviscometric and most often time-varying, the blend components are viscoelastic, and the stress transfer across the interfaces is ill-understood as a result of ''dynamic'' nonequillibrium interfacial tension. In addition, the domain cohesive strength, resisting laminar stress dispersion, has in addition to the surfaces stresses due to interfacial tension, as discussed in Section 7.1, plus a second component due to ''melt strength'' of the whole bulk of the dispersed domain. Thus, both the evolution of morphology during compounding and its final state are difficult to predict. Nevertheless, the mechanisms described in Section 7.1 do provide insight into the nature of the process. These are sequential liquid droplet breakup at some critical capillary number and extension of the dispersed phase into filaments and subsequent breakup of the filament into droplet, as depicted in Fig. 7.23. It is the latter that is the dominant mechanism in creating polymer blends.

In both batch and continuous mixers the elongational flow, conducive to filament stretching and breakup, occurs at the tapered entrance regions to narrow gaps between blades and wall and between kneading elements of the co-rotating intermeshing twin screw compounders. Past the narrow gap the material is mixed with the bulk. Thus, the global model for blending compounders is identical conceptually to the ''two-zone'' model of dispersion of solids previously discussed[4] in which material circulates between a *strong* zone, where affine stretching and thread breakup in flow take place, and a *weak* zone, where thread breakup at rest continues and drop coalescence may take place. Thus, the mechanism of liquid breakup is more complex than that of solid breakup. In the latter case, the criterion for agglomerate breakup is a simple yes/no, depending on the stress levels in the gap, and there is no size dependence; whereas, in liquid breakup local time scales in the gap and beyond play a distinctive role and breakup is size dependent. Yet, as shown by Janssen and Meijer (117), this complex mechanism can be modeled with reasonable accuracy.

The most commonly used equipment for continuous blending is the co-rotating intermeshing TSEs. In these machines the kneading flows produce two-dimensional

4. The name ''two-zone model'' was coined by H. E. H Meijer in his chapter ''Processing for Properties'' in R. W. Cahn, P. Haasen, and E. J. Kramer, Eds., *Material Science and Technology*, Vol. 18, Wiley-VCH, New York, 1997.

sheets, which progress to become ligaments and then fine droplets. The SSE is more limited in its capability to process blends for the same reasons it is limited in dispersive mixing. As pointed out earlier for dispersive mixing, certain screw designs (101) should at least partially overcome this limitation.

We conclude this chapter by reviewing in some detail an experimental mixing program entitled ''Polymer Mixing Study,'' which was led by one of the authors.[5] The study focused on the central complexities of compounding polymeric blends during melting and mixing. Two experimental laboratory-size compounders were developed and used to study the mixing mechanisms in continuous compounders. One was the *Single Screw Mixing Element Evaluator* (SSMEE)^{TM} and the other the *Co-rotating Twin Screw Mixing Element Evaluator* (TSMEE)^{TM}. Both experimental devices share the following features:

1. They are designed with split barrels, each half having extensive cooling channels; these two features enable quick quenching of the processed stream and easy opening of the barrel for morphological examination of the solidified ''carcass'' to study the evolution of dispersive mixing.
2. They can operate in two mixing modes: the first is the *melt–melt mixing* (M–M) mode, where the two blend components are fed into two separate ports as melts, using two SSE pumps. The two melt streams are mixed at the entrance of the mixing element to be evaluated for a given component blend. The second is the *dissipative-mix melting* (DMM) mode, where the two blend components are fed in pellet or powder form as a dry blend to be melted and mixed by the melting/mixing element used. Thus, in the DMM mode, the device can also be used to evaluate melting performance.
3. Downstream from the mixing element section there are two separate inverse SSEs (see Section 6.2) that have the helical channel machined into the barrel, thus needing only rotating shafts to convey the material. Two pressure transducers, one diameter apart, record the pressure built up at closed discharge, a parameter that can be used to measure the viscosity of the molten blend at various shear rates. This ''rheometry'' section is the forerunner of the *Helical Barrel Rheometer* (HBR)^{TM} of the Polymer Processing Institute (118).
4. A portion of the exiting stream of the molten blend is diverted into the Flow Cell^{TM}, where Nomarsky reflection microscopy is carried out in a thin slit, the bottom plate of which is reflective polished steel and the top is a quartz window. The microscope, the rapid image data acquisition device, and analyzer are capable of producing dispersion data down to sizes of one micrometer. The TSMEE is shown schematically for both the (M–M) and DMM) modes in Fig. 11.31 (119–121).

These experimental mixers enabled the study of the role of the rheological properties of the individual blend components on the mechanisms and rates of dispersive mixing. Three commercial polymers: Dow Chemical Company polystyrene (PS686) and low density polyethylene (PE 132) and Chevron low density polyethylene (PE 1409) were used in the study. Figure 11.32 (a) shows the viscosities of the three polymers at 200°C (121). PS 685

5. This industrially cosponsored program was carried out through the 1990s at the Polymer Processing Institute at New Jersey Institute of Technology, Hoboken, NJ, and directed by one of the authors.

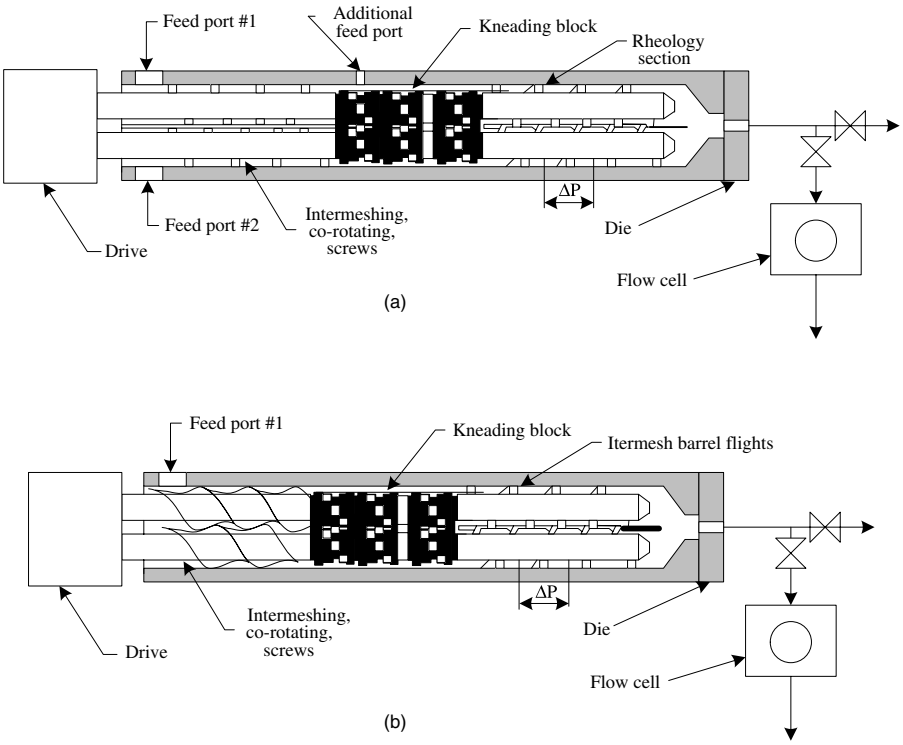

Fig. 11.31 Schematic representation of the Twin Screw Mixing Element Evaluator (TSMEE) in (a) the melt-melt (M–M) mode, and (b) the dissipative mix-melting (DMM) mode. The last section of both the M–M and DME modes consists of two separate HBRs. The mixing element sequences are a "design" variable. [Reprinted with permission from *Proceedings of the Sixth Semi-annual Meeting of the Polymer Mixing Study*, Polymer Processing Institute, Hoboken, NJ (1993).]

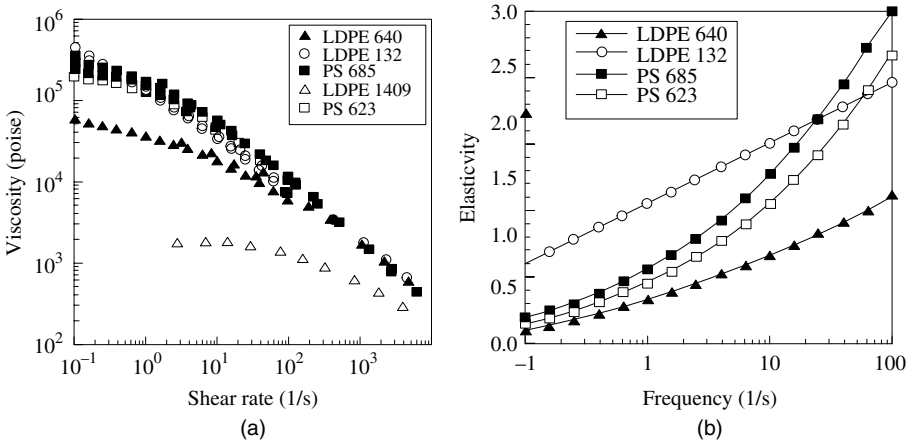

Fig. 11.32 The rheological properties of the polymer resins used in the polymer mixing study at 200°C. (a) The shear viscosity. (b) The elasticity parameter ($\frac{\tau_{11}-\tau_{22}}{\tau_{12}}$). [*Proceedings of the Sixth Semi-annual Meeting of the Polymer Mixing Study*, Polymer Processing Institute, Hoboken, NJ (1993).]

and PE132 are *equiviscous*. On the other hand, PE 1409 has a much lower viscosity as compared to PS 685. Furthermore, as shown in Fig. 11.32(b), PS 685 and PE 132 are elastic, while PE 1409 is almost totally nonelastic. The blends PS 685/PE 132 are *rheologically matched*, while those of PS 685/PE1409 are *rheologically mismatched*, yet they are both equally immiscible. The following PS/LDPE blends were used to study the ''rheology driven'' dispersion mechanisms (121):

Blend 1	10% PS	90% PE 1409
Blend 2	10% PS	90% PE132
Blend 3a	90% PS	10% PE 1409
Blend 3b	98% PS	2% PE 1409
Blend 3c	75% PS	25% PE 1409

The TSMEE in the M–M mixing mode was used with three kneading blocks of 5/45/42 forwarding elements. Experiments were conducted at two melt temperatures, 180° and 140°C, and two rotor speeds, 60 and 120 rpm. The results and conclusions that emerged from the study are discussed in the following subsections.

Equiviscous Blend 2 Earlier we postulated that the compression/expansion cycles in fully melt-filled kneading elements of Co-TSEs in fact superpose a periodic axial stretching flow to the steady flow generated by the shaft rotation (110,111). This results in time-varying velocity components in both the axial and radial directions, which, in turn, produce a two-dimensional stretching flow, which is effective for dispersive mixing. We have observed experimentally the effect of the flow pattern just described at the blend microstructure level when analyzing blend ''carcasses.'' Morphology images taken from samples of equiviscous systems have shown clear evidence of this complex nature of the flow as evidenced by the affine deformation of the minor phase. The minor, following the matrix flow field, undergoes stretching and folding before breaking into smaller domains, as shown in Fig. 11.33. This affine deformation of the dispersed phase was observed *only* in the equiviscous Blend 2. The dispersion mechanism for this blend in the stretching/folding flow field is by the sequential formulation of sheets with holes that reduce the interfacial area, ligament formation, and stretching of the ligaments, which leads to breakup formation of fine droplets, as seen on Fig. 11.34. The rate of dispersive mixing in this equiviscous blend is very rapid, as shown on Fig. 11.35, becoming complete by the eighth lobe, that is, half way into the middle kneading block.

Also noteworthy is the appreciable *coalescence* caused by the shear flows in the single screws, of the ''rheology'' section of the TSMEE following the mixing element section. Flow of dispersed immiscible blends involves continuous breakdown and coalescence of the dispersed domains (122). Shear flows, where droplet-to-droplet collisions are frequent—in contrast to extensional flows—favor coalescence over dispersion. The presence of compatibilizers shifts the balance toward reduced coalescence rate. Macosko et al. (123) attribute this to the entropic repulsion of the compatibilizer molecules located at the interface as they balance the van der Waals forces and reduce coalescence, as shown on Fig. 11.36.

The addition of a very small amount of styrene-isoprene-styrene (SIS) triblock compatibilizer, introduced as a compounded pellet with PS 685, suppresses the shear flow-induced coalescence appreciably, as seen by comparing Fig. 11.35 with Fig. 11.37. On the other hand, there is no effect of this very small amount of SIS on the dispersion rate.

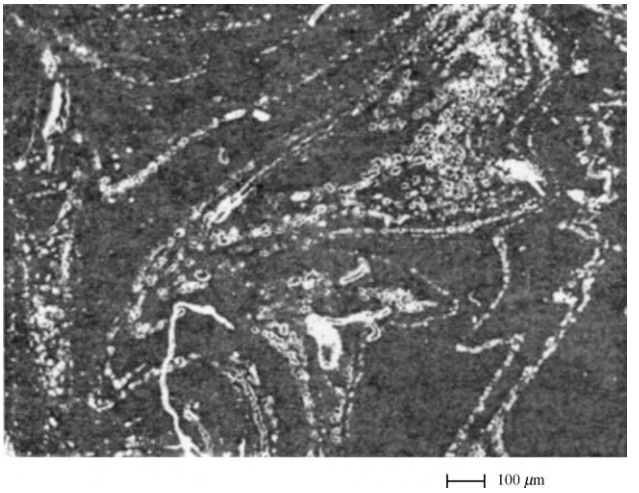

Fig. 11.33 Dispersed PS 685 streaks of ligaments and droplets in the equiviscous Blend 2. PS is flowing/deforming in an affine fashion in the expected stretching and folding pattern. Experiments were conducted at 180°C and 120 rpm. [Reprinted with permission from *Proceedings of the Tenth Semi-annual Meeting of the Polymer Mixing Study*, Polymer Processing Institute, Hoboken, NJ (1995).]

When the melt–melt mixing temperature is reduced to 140°C and at 120 rpm, there is still stretching of PS, but the stretched morphology is different; not smooth, but rather jagged PS domains stretched into jagged ''finger-like'' ligaments, followed by shedding of droplets. This is shown on Fig. 11.38. The fact that at 140°C PS is a rubbery melt, in

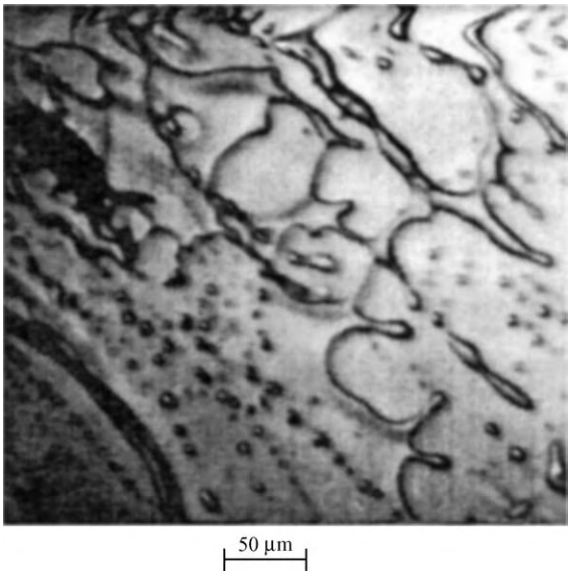

Fig. 11.34 The dispersive mixing mechanism of the equiviscous Blend 2 at 180°C and 120 rpm. Repeated stretching and folding is evident, which result in sheets that have holes, ligaments, and droplets. [Reprinted with permission from *Proceedings of the Eighth Semi-annual Meeting of the Polymer Mixing Study*, Polymer Processing Institute, Hoboken, NJ (1994).]

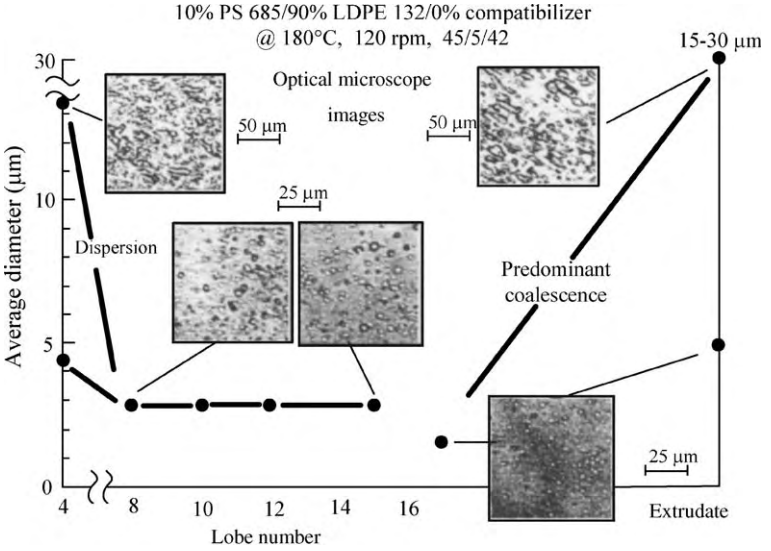

Fig. 11.35 Dispersion rate of Blend 2 obtained through carcass analysis: TSMEE at 180°C and 120 rpm. [Reprinted with permission from *Proceedings of the Tenth Semi-annual Meeting of the Polymer Mixing Study*, Polymer Processing Institute, Hoboken, NJ (1995).]

the Williams–Landel–Ferry (WLF) regime (124), explains the PS domain's resistance to form smooth sheets and ligaments. Figure 11.39 tracks the evolution of dispersion and 140°C. Compared to Blend 2 dispersed at 180°C, shown on Fig. 11.37, the dispersed morphology is coarser and with a wide size distribution. It was also found that, when

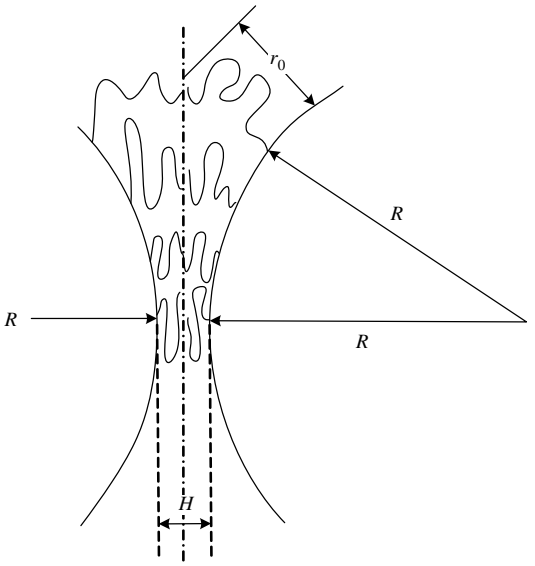

Fig. 11.36 Schematic representation of the effect of compatibilizer chains between two dispersed droplets. The entropic decrease near the pinch distance H repulses ''the droplets,'' decreasing coalescence.

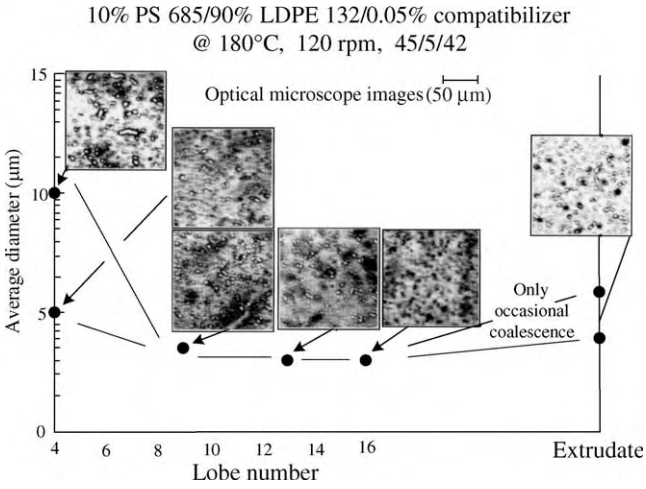

Fig. 11.37 Suppression of shear flow–induced coalescence by incorporating a very low concentration of SIS triblock compatibilizer into the equiviscous Blend 2. [Reprinted by permission from the *Proceedings of the Tenth Semi-annual Meeting of the Polymer Mixing Study*, Polymer Processing Institute, Hoboken, NJ (1995).]

operating the TSMEE in the *dissipative mix-melting* mode at 180°C and 120 rpm, the morphology obtained is closer to that in Fig. 11.39, mix-melting carried out at 140°C. For the equiviscous Blend 2, M–M mixing results in finer morphologies than those obtained at the same conditions with dissipative mix-melting. On the other hand,

Fig. 11.38 Blend 2 at 140°C and 120 rpm. Early morphology development reveals rough PS surfaces and ''fingers'' indicative of the rubber-like nature of PS at 140°C. [Reprinted by permission from the *Proceedings of the Seventh Semi-annual Meeting of the Polymer Mixing Study*, Polymer Processing Institute, Hoboken, NJ (1993).]

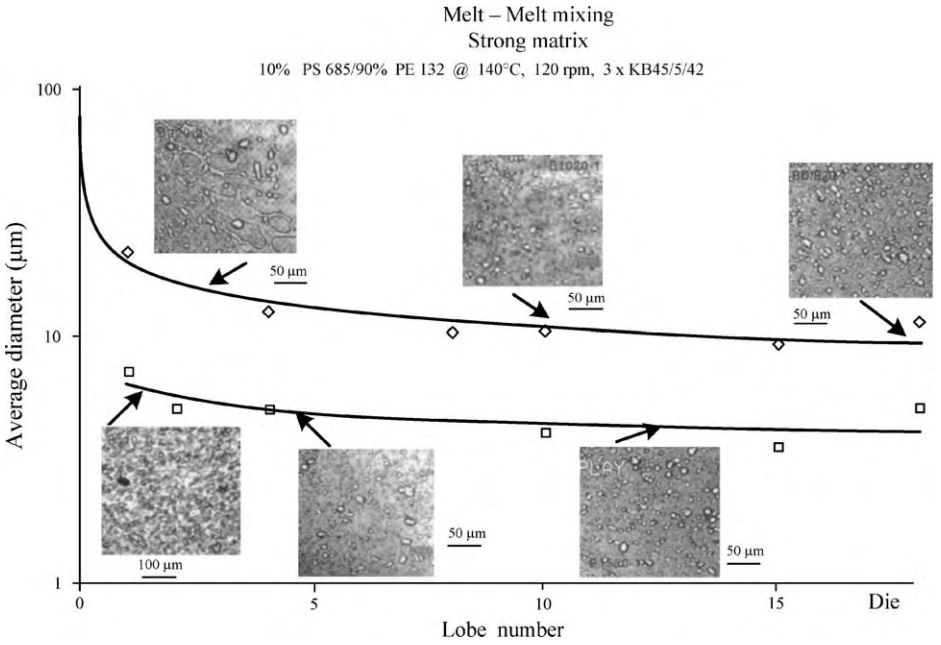

Fig. 11.39 Melt–melt dispersive mixing Blend 2 in the TSMEE at 140°C and 120 rpm. [Reprinted by permission from the *Proceedings of the Thirteenth Semi-annual Meeting of the Polymer Mixing Study*, Polymer Processing Institute, Hoboken, NJ (1996).]

incorporation of 1–5% SIS compatibilizer into Blend 2 mixed in the dissipative mix-melting made at 180°C and 120 rpm makes the morphology finer, much like the one shown on Fig. 11.37. At this level of compatibilizer the transfer of laminar stresses improves and the interfacial tension decreases, both conducive to finer dispersions.

Weak Matrix Blend 1 Blend 1 consists of a high viscosity and elasticity rheologically robust PS resin, in a low-viscosity inelastic rheologically weak LDPE. The viscosity ratio $\eta_d/\eta_m \approx 50$. The composition of this blend does not favor good dispersion, because the dispersed PS has both bulk elastic strength and high surface tension that resists breakup, and the matrix has a weak Newtonian viscosity. Thus, only extensional flows, whose dispersing ability is only weakly dependent on the viscosity ratio, would achieve dispersive mixing. Figure 11.40 shows the extrudate emerging from the SSMEE using a 3.5 L/D Maddock mixing element, at 140°C and 90 rpm. A gross unmixed lump of the rubbery PS, about 100 μm in size, attests to the fact that, even after passing through the "barrier" region of this dispersive mixer with a flow that has some elongational component, the prevailing shear flow in the mixing element is unable to affect dispersion. Single rotor devices are not compounding equipment of choice for dispersing systems like Blend 1. With the TSMEE in the M–M mixing mode, two-dimensional extensional flows are generated in full kneading disks. The results at the following operating conditions—140°C and 60 rpm; 140°C and 120 rpm; 180°C and 120 rpm—are shown in Fig. 11.41(a)–Fig. 11.41(c), respectively. Under all three operating conditions there is strong evidence of

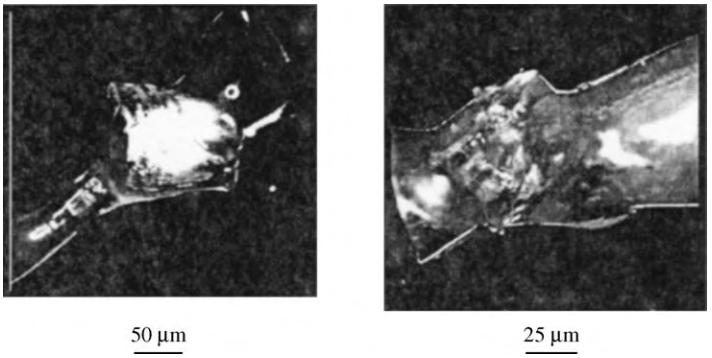

Fig. 11.40 Extrudate of Blend 1 emerging from the SSMEE with a 3.5 *L*/*D* Maddock mixer operating at 140°C and 90 rpm. [Reprinted by permission from the *Proceedings of the Fourth Semi-annual Meeting of the Polymer Mixing Study*, Polymer Processing Institute, Hoboken, NJ (1992).]

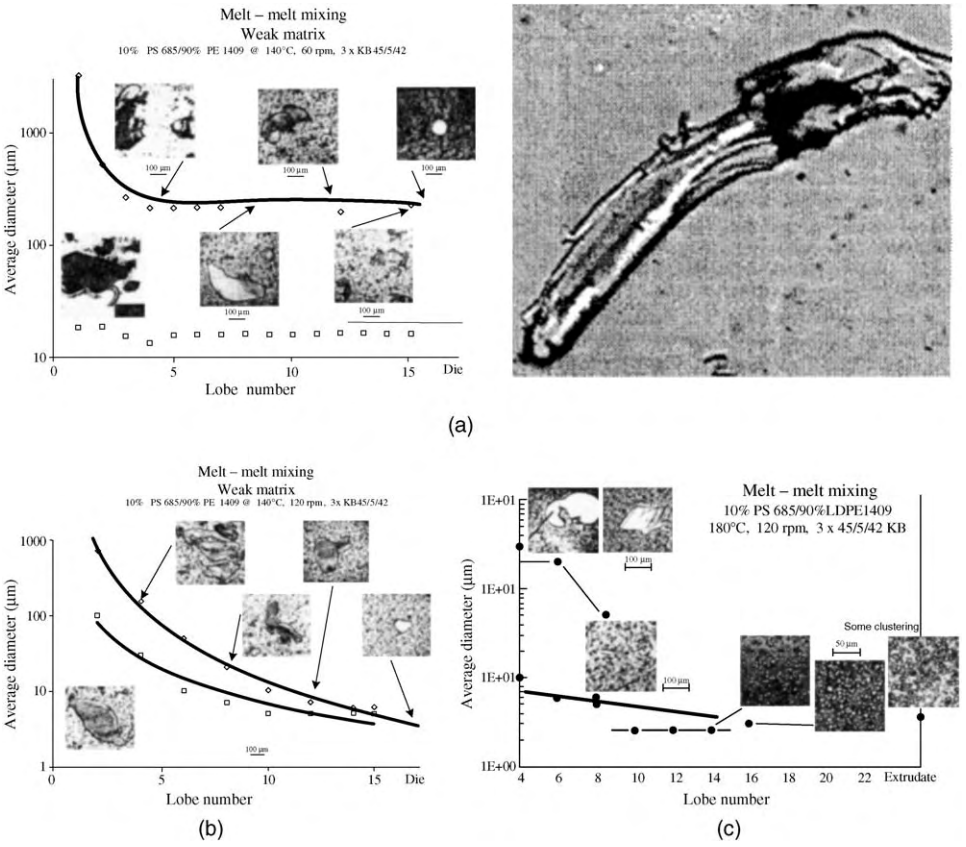

Fig. 11.41 Evolution of the dispersed morphology along the TSMEE mixing element at three operating conditions of the weak matrix Blend 1: (a) 140°C and 60 rpm; (b) 140°C and 120 rpm; (c) 180°C and 120 rpm. [Reprinted by permission from the *Proceedings of the Thirteenth Semi-annual Meeting of the Polymer Mixing Study*, Polymer Processing Institute, Hoboken, NJ (1996).]

dispersion by "brittle" fracture. Initially in the PS breakup, the domains are being stretched and form *fragments with sharp edges*. This is most prevalent at 140°C and 60 rpm; with the brittle features becoming milder and more toward thick stretched sheets only with increasing melt temperature. That is, brittle fracture becomes less dominant as the Deborah number, $De = \lambda/t_{exp}$, becomes smaller, rendering the dispersed domain less elastic.

For both the 140°C dispersive experiments there is evidence of small–large size bimodal dispersion with a fair number of "escapees," that is, large undispersed PS regions, present in the extrudate. This is, of course, a practically unacceptable dispersion, albeit common with weak matrix blends. At 180°C, Fig. 11.41(c), bimodal dispersion is present only in the early lobes where large sheets and droplets coexist. The sheets and extrudate escapees disappear because PS is now less elastic. It is worth noting in this figure that the degree of coalescence is smaller than with Blend 2, possibly due to the ease with which droplets avoid "collisions" in the low viscosity shear flow. On the other hand, clustering of neighboring droplets, which were not forced to coalesce by strong matrix laminar shear stresses becomes more prominent, possibly because the low matrix viscosity allows quiescent diffusional droplet motion. Finally, using the TSMEE in the dissipative mix melting mode at 180°C and 120°C we obtain both strong brittle fracture features, but the presence of PS extrudate escapees persists with dispersion bimodal results, as seen on Fig. 11.42. PED melting, taking place in the dissipative mix-melting mode with the weak

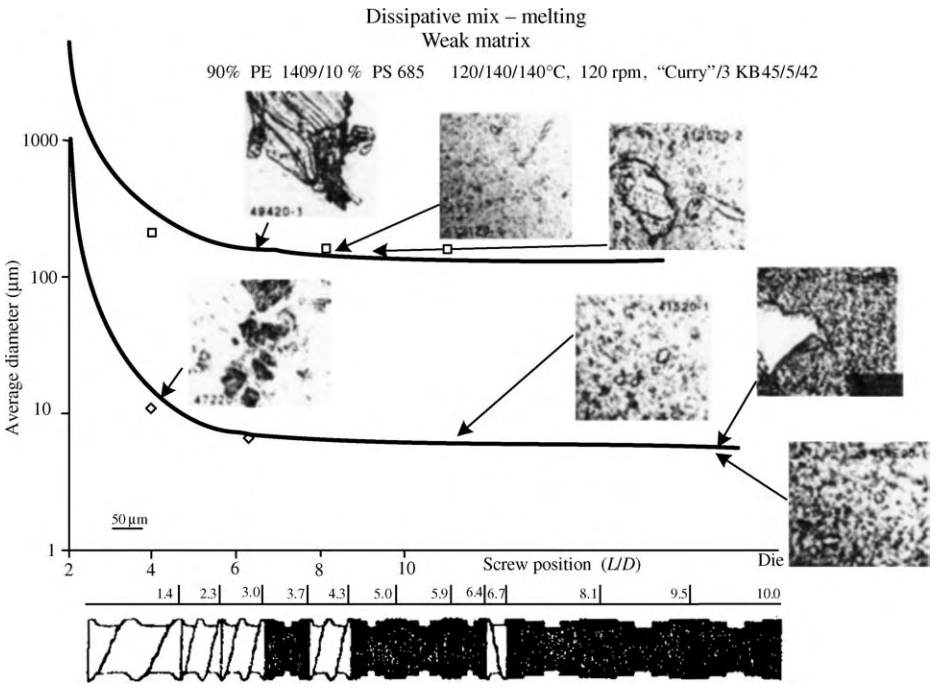

Fig. 11.42 Weak matrix Blend 1. Evolution of dispersed morphology in dissipative mix-melting mode at 180°C and 120°C. [Reprinted by permission from the *Proceedings of the Thirteenth Semi-annual Meeting of the Polymer Mixing Study*, Polymer Processing Institute, Hoboken, NJ (1996).]

matrix Blend 1 is inefficient, resulting in chunks of cooler PS domains entering the TSMEE mixing element. This is the reason for being plagued with such escapees in industrial scale compounding of weak matrix blends compounded in twin rotor equipment.

Let us examine the preceding from the point of view of the PED melting phenomena taking place in the PS/LDPE pellet blend system. In contrast with the PED melting of the single component PS, where its high modulus creates high PED heating/melting rates and complete melting over a short kneading element distance, PS/LDPE blends were found to melt differently. The stiffer polymer, which normally melts faster (i.e., has a much shorter melting length in the full kneading element region of the Co-TSE) when melted alone, is not the faster melting component in blends. This is because in blends, not unlike stacked cylinders of the blend components undergoing unconfined compressive deformation, the softer component LDPE is the component that responds first and predominantly to the forced applied deformations caused by the kneading element corotation. Thus, LDPE ''absorbs'' most of the plastic deformation energy, melts, and surrounds the mostly unmolten PS. Melting of the PS particulate suspension in LDPE can now take place primarily by VED. If the viscosity of the molten LDPE matrix is high (as is the case with Blend 2), the PS will melt completely; if the viscosity is low (as in Blend 1), PS melting will be incomplete, resulting in ''escapees.'' In conclusion, we can state that the relative rates of the *initial* heating/melting of the blend components depend inversely on their individual modulus and mechanical strength at high deformation levels; furthermore, complete melting of the strong modulus component occurs only when the melt viscosity of the weak modulus component, which melts first, is high, promoting vigorous VED. This mechanism is corroborated by the compressive stress–strain behavior of two stacked molded disks, one PS and one LLDPE, and is depicted in Fig. 11.43 (125). As the stack is

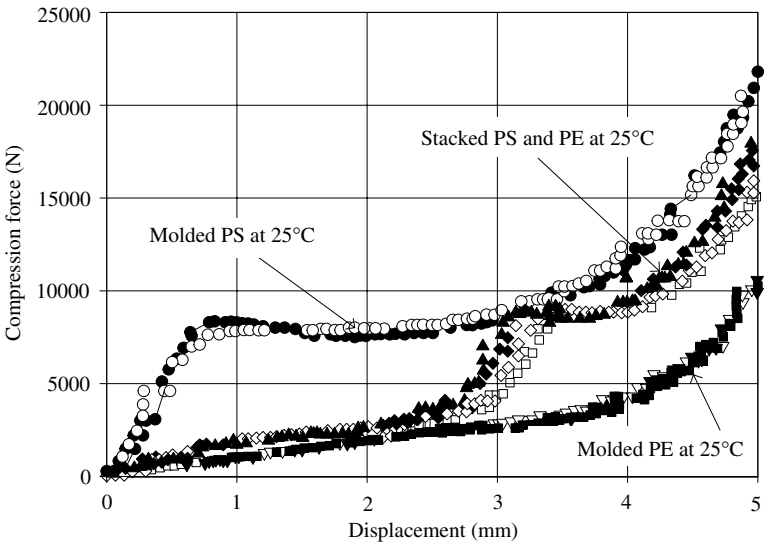

Fig. 11.43 The compressive force versus displacement of stacked PS and LLDPE cylinders at 25°C. Note that initially the stack deformation force tracks that of the more deformable LLDPE, before, at 3 mm, beginning to deform the PS cylinder. [Reprinted by permission from B. Qian, D. B. Todd, and C. G. Gogos, ''Plastic Energy Dissipation and Its Role on Heating/melting of Single-component Polymers and Multi-component Polymer Blends,'' *Adv. Polym. Technol.*, **22**, 85 (2003).]

compressed it is only the weaker modulus LLDPE that deforms and gets heated by PED, while PS is not affected, and it is only when the LLDPE is almost fully flattened that PS deformation starts. With the weak matrix Blend 1 in full kneading disks, PS will be deformed after PE 1409 is melted. But, as previously discussed, the PS pellets now will be suspended in a low viscosity matrix that will allow for reduced PED and certainly greatly reduced VED because of the low LDPE 1409 viscosity; the result is incompletely heated and incompletely melted PS particulates that become ''escapees.''

Blends 3 (a,b,c) Rheologically Robust Matrix and Weak Dispersed Components Since PE 1409 is a low viscosity nearly Newtonian polymer melt, its dispersive behavior is uncomplicated and more Newtonian like. Blend 3a forms a small (3–5-μm) droplet dispersion morphology, and Blend 3b is even finer (1–2 μm), becoming, only below 2% concentration, less subject to flow-induced coalescence. The TSMEE-obtained dispersions are finer than those from the TSMEE, with a variety of kneading elements (126). What is noteworthy about these blends is the early stages of the dispersion process, shown on Fig. 11.44, obtained with Blend 3a using the TSMEE at 180°C and 120 rpm.

The low viscosity PE 1409 breaks up into large ''odd looking'' domains which, when they break up to sizes around 10 μm, become rounder, progressively becoming fine droplets of size 2–3 μm, by the repeated breakdown mechanisms indicated on Fig. 7.23. Finally, Blend 3c forms phase-inverted morphology in the SSMEE, as shown on Fig. 11.45, where the minor low viscosity, dark region PE 1409, engulfs the major PS. In shear devices sequential addition of low-viscosity blend components is required to achieve fine dispersions; whereas, TSMEEs do not have this limitation to the same extent.

Fig. 11.44 Early-stage morphology developed with Blend 3a in the TSMEE at 180°C and 120 rpm. [Reprinted by permission from the *Proceedings of the Sixth Semi-annual Meeting of the Polymer Meeting Study*, Polymer Processing Institute, Hoboken, NJ (1993).]

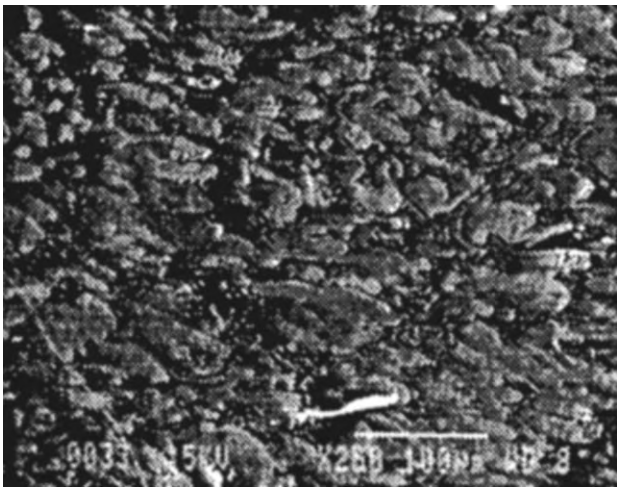

Fig. 11.45 Blend 3a morphology developed in the SSMEE at 180°C and 80 rpm. SEM image of the carcass. [Reprinted by permission from the *Proceedings of the Sixth Semi-annual Meeting, Polymer Mixing Study*, Polymer Processing Institute, Hoboken, NJ (1993).]

REFERENCES

1. J. A. Biesenberger and C. G. Gogos, Guest Eds., *Polymer Topics Issue on Reactive Polymer Processing*, *Polym. Eng. Sci*., **20**, 837 (1980).
2. D. B. Todd, ''Features of Extruder Reactors,'' in *Reactive Extrusion,* M. Xanthos, Ed., Hanser, New York, 1992, Chapter 5.
3. J. A. Biesenberger, Ed., *Devolatilization of Polymers,* Hanser, Munich, 1983.
4. J. A. Biesenberger, ''Principles of Reaction Engineering,'' in *Reactive Extrusion*, M. Xanthos, Ed., Hanser, New York, 1992, Chapter 6.
5. J. A. Biesenberger and D. H. Sebastian*, Principles of Polymerization Engineering*, Wiley, New York, 1983.
6. D. H. Sebastian ''Non-Isothermal Effects in Polymer Reaction Engineering,'' in *Temperature Control Principles for Process Engineers*, E. P. Dougherty, Ed., Hanser, Munich, 1993.
7. R. C. Kowalski, ''Fit the Reactor to the Chemistry,'' in *Reactive Extrusion*, M. Xanthos, Ed., Hanser, New York, 1992.
8. N. G. Gaylord, ''Reactive Extrusion in the Preparation of Carboxyl – containing Polymers and their Utilization as Compatibilizers,'' in *Reactive Extrusion*, M. Xanthos, Ed., Hanser, New York, 1992, Chapter 3.
9. R. C. Kowalski, ''Fit the Reactor to the Chemistry,'' in *Reactive Extrusion*, M. Xanthos, Ed., Hanser, New York, 1992.
10. S. Datta and D. J. Lohse, *Polymeric Compatibilizers*: *Uses and Benefits in Polymer Blends*, Hanser, New York, 1996.
11. H. R. Brown, ''Strengthening Polymer-Polymer Interfaces,'' in *Polymer Blends Volume 2: Performance*, D. R. Paul and G. B. Bueknall, Eds., Wiley, New York, 2000, Chapter 23.
12. L. A. Utracki, *Polymer Alloys and Blends*, Hanser, New York, 1989.
13. N. G. Gaylord, ''Poly(maleic Anhydride),'' *J. Macromol. Sci.–Rev. Macromol. Chem.*, **C13**(2), 235–261 (1975).
14. B. N. Epstein, U.S. Patent 4,174,538, DuPont (1979); U.S. Patent 4,172,859, DuPont (1979).

15. B. N. Epstein and R. U. Pagilagan, U.S. Patent 4,410,661, DuPont (1983).
16. R. A. Steinkamp and T. J. Grail, U.S. Patent 3,862,265, Exxon Res. and Eng. (1975): US 3,953,655, Exxon Res. and Eng. (1976).
17. N. G. Gaylord and J. Y. Koo, ''Participation of Cationic Intermediates in Radical-induced Homopolymerization of Maleic Anhydride,'' *J. Polym. Sci. Polym Lett. Ed.*, **19**, 107–112 (1981).
18. N. G. Gaylord and R. Mehta, ''Peroxide-catalyzed Grafting of Maleic Anhydride onto Molten Polyethylene in the Presence of Polar Organic Compounds,'' *J. Polym. Sci.: Part A: Polym. Chem*., **26**, 1189–1198 (1988).
19. P. J. Flory, *Principles of Polymer Chemistry*, Cornell University Press, Ithaca, NY, 1953.
20. G. Odian, *Principles of Polymerization*, *Second Edition*, Wiley, New York, 1981.
21. R. C. Kowalski, Ph.D. Dissertation, Department of Chemical Engineering, Polytechnic Institute of Brooklyn, Brooklyn, NY, 1983.
22. J. C. Statton, J. P. Keller, R. C. Kowalski, and J. Harrison, U.S. Patent 3,551,943, Esso (1971).
23. R. C. Kowalski, U.S. Patent 3,563,972, Esso (1971).
24. J. Beauxis and R. C. Kowalski, U.S. Patent 3,593,011 Esso Res. and Eng. Co. (1971).
25. R. C. Kowalski, J. W. Starrison, J. C. Staton, and J. P. Kener, U.S. Patent 3,608,001, Esso (1971).
26. M. Xanthos, ''Process Analysis from Reaction Fundamentals,'' in *Reactive Extrusion*, M.Xanthos, Ed., Hanser, New York, 1992.
27. A. Dreiblatt, H. Herrmann, and H. J. Nettelnbrecker, ''ON-line Quality Control for Improved Compounding,'' *Plast. Eng*., **43**, 31–34 (1987).
28. J. Curry, S. Jackson, B. Stroehrer, and A. VanderVeen, ''Free Radical Degradation of Polypropylene,'' *Chem. Eng. Prog*., **84**, 43–46 (1988).
29. J. G. Andersen and M. J. Kenny, *SPE RETEC: Polyolefins VI, Tech. Papers*, Huston, TX, 1988, p.186.
30. T. Hertlein and H. G. Fritz, *Kunstst. Ger. Plast*., **78**, 606 (1988).
31. A. Pabedinskas, W. R. Clmett, and S. T. Balke, ''Process Control for Polypropylene Degradation during Reactive Extrusion,'' *Polym. Eng. Sci*., **29**, 993–1003 (1989).
32. M. Dorn, ''Modification of Molecular Weight and Flow Properties of Thermoplastics,'' *Adv. Polym. Tech*., **5**, 82–98 (1995).
33. C. Tzoganakis, J. Vlachopoulos, and A. E. Hamielec, ''Production of Controlled-rheology Polypropylene Resins by Peroxide Promoted Degradation during Extrusion,'' *Polym. Eng. Sci*., **28**, 170–180 (1988).
34. Atochem, Product Bulletin, ''Half-life: Peroxide Selection Based on Half–life,'' Buffalo, NY (1990).
35. Pennwalt Corp., Lucidal Division Product Bulletin ''DialkylPeroxides,'' Buffalo, NY (1989).
36. D. W. Yu, Ph.D Dissertation, Department of Chemical Engineering, Stevens Institute of Technology, Hoboken, NJ 1991.
37. S. H. Ryu, C. G. Gogos, and M. Xanthos, ''Kinetic Studies on the Peroxide Initiated Polypropylene Controlled Degradation,'' *SPE ANTEC Tech. Papers*, **35**, 879–881 (1989).
38. M. Xanthos, C. G. Gogos, and S. H. Ryu, ''Kinetic Studies on the Peroxide Initiated Polypropylene Controlled Degradation,'' *Proc. Polym. Process Soc., Meeting,* Paper 7F, Amherst, MA, 879–882 (August 1989).
39. R. Dhavalkikar, Ph.D. Dissertation, Department of Chemical Engineering, New Jersey Institute of Technology, Newark, NJ 2002; also, R. Dhavalkikar and M. Xanthos, ''Monitoring the Evolution of PET Branching through Chemorheology,'' *Polym. Eng. Sci.*, **44**, 474 (2004).
40. W. N. Semenov, *Some Problems in Chemical Kinetics and Reactivity,* Princeton University Press, Princeton, NJ, 1958, p. 87.

41. S. K. Dey, Ph.D Dissertation, ''Reactive Extrusion of Methyl Methacrylate,'' Department of Chemical Engineering, Stevens Institute of Technology, Hoboken, NJ, 1987.
42. S. K. Dey and J. A. Biesenberger, ''Reactive Extrusion of Methyl Methacrylate,'' *SPE, ANTEC Tech. Papers*, **45**, 133–135 (1987).
43. D. A. Frank-Kamenetskii, *Diffusion and Heat Exchange in Chemical Kinetics*, Princeton Univ. Press, Princeton, NJ, 1955, pp. 202–266.
44. T. Vomkarman, *Nachr. Ges. Wiss*. Gottingen, Math-physic. K1 (1930).
45. Y. Lu, Ph.D. Dissertation, Department of Chemical Engineering, Stevens Institute of Technology, Hoboken, NJ, 1993.
46. Y. Lu, J. A. Biesenberger, and D. B. Todd, ''A Backmix Drag-flow Reactor,'' *SPE. ANTEC, Tech. Papers*, **51**, 27–29 (1993); also Y. Lu, J. A. Biesenberger, and D. B. Todd, ''Continuous Polymerization in a back-mixed Drag Flow reactor,'' *SPE. ANTEC Tech. Papers*, **52**, 113–115 (1994).
47. J. A. Biesenberger and D. B. Todd, U.S. Patent 5, 372,418 (1994).
48. J. Grenci and D. B. Todd, ''Effect of Conversion on Chain Addition Copolymerizations Performed in a Backmixed Drag Flow Extruder Reactor,'' *Int. Polym. Process*., **15**, 147–156 (2000).
49. J. M. Ottino, C. W. Leong, H. Rising, and P. D. Swanson, ''Morphological Structures Produced by Mixing in Chaotic Flows,'' *Nature*, **333**, 419–425 (1988).
50. J. M. Ottino, *The Kinematics of Mixing: Stretching, Chaos and Transport*, Cambridge University Press, London, 1989.
51. F. H. Ling and S. Widagdo, *Polymer Mixing Study,* Vol. 1, Polymer Processing Institute, 1991.
52. T. Brouwer, D. B. Todd, and L. P. B. M. Janssen, ''Flow Characteristics of Screws and Special Mixing Enhancers in a Co-rotating Twin Screw Extruder,'' *Int. Polym. Process*., **18**, 26 (2002).
53. B. Jeong and C. G. Gogos, ''Reactive Extrusion of Initially Segregated Miscible Blends with a Time Reducing Striation Thickness,'' Submitted *Adv. Polym. Technol*. (2005).
54. T. Saito and C. W. Macosko, ''Interfacial Crosslinking and Diffusion via Extensional Rheometry,'' *Polym. Eng. Sci*., **42**, 1–9 (2002).
55. W. J. Schrenk and T. Alfrey, ''Some Physical Properties of Multilayered Films,'' *Polym. Eng. Sci*., **9**, 393–399 (1969).
56. J. Meissner and J. Hostettler, ''A New Elongational Rheometer for Polymer Melts and Other Highly Viscoelastic Liquids,'' *Rheol. Acta*, **33**, 1–21 (1994).
57. J. Klein, D. Fletcher, and L. J. Fetters, ''Dynamics of Entangled Star-branched Polymers,'' *Faraday Symp. Chem*., **18**, 159–171 (1983).
58. D. R. Paul and C. B. Bucknall, Eds*., Polymer Blends Vols. I and II*, Wiley, New York, 2000.
59. S. H. Anastasiades, I. Ganattz, and J. T. Koberstein, ''Compatibilizing Effect of Block Copolymers Added to the Polymer/polymer Interface,'' *Macromolecules*, **22**, 1449–1453 (1989).
60. W. Hu, J. T. Koberstein, J. P. Lingelser, and Y. Gallot, ''Interfacial Tension Reduction in Polystyrene/Poly(dimethylsiloxane) Blends by the Addition of Poly(styrene-b-dimethylsiloxane),'' *Macromolecules*, **28**, 5209–5214 (1995).
61. G. Kim and M. Libera ''Microstructural Analysis of Compatibilizer Distribution in LDPE/PS Blends with SIS,'' *Proceed. Eleventh Semi-annual Polymer Mixing Study*, Polymer Processing Institute, Hoboken, NJ, 1996.
62. C. W. Macosko, P. Gueram, A. K. Khandpur, A. Nakayama, and P. Marechal, ''Compatibilizers for Melt Blending: Premade Block Copolymers,'' *Macromolecules*, **29**, 5590–5598 (1996).
63. C. E. Scott and C. W. Macosko, ''Morphology Development during the Initial Stages of Polymer-polymer Blending,'' *Polymer*, **36**, 461–470, (1995).

64. C. E. Scott and C. W. Macosko, ''Model Experiments Concerning Morphology Development during the Initial Stages of Polymer Blending,'' *Polym. Bull*., **26**, 341–348 (1991).
65. M. Marič and C. W. Macosko, ''Improving Polymer Blend Dispersion in Mini-mixers,'' *Polym. Eng. Sci.*, **41**, 118–130 (2001).
66. E. Helfand and Y. Tagami, ''Theory of the Interface between Immiscible Polymers. II,'' *J. Chem. Phys.*, **56**, 3592 (1972).
67. J. Noolandi and K. M. Hong, ''Interfacial Properties of Immiscible Homopolymer Blends in the Presence of Block Copolymers,'' *Macromolecules*, **15**, 482–492 (1982)
68. J. Brandrup and E. H. Immergut, Eds., *Polymer Handbook*, Third Edition, Wiley, New York, 1985.
69. L. J. Fetters, D. J. Lohse, D. Richter, T. A. Witten, and A. Zirkel, ''Connection between Polymer Molecular Weight, Density, Chain Dimensions, and Melt Viscoelastic Properties,'' *Macromolecules*, **27**, 4639–4647 (1994).
70. M. Marič, N. Ashuror, and C. W. Macosko, ''Reactive Blending of Poly- (dimethylsiloxane) with Nylon 6 and Poly (styrene): Effect of Reactivity on Morphology,'' *Polym. Eng. Sci*., **41**, 631–642 (2001).
71. L. Mascia, *The Role of Additives in Plastics*, Edward Arnold, London, 1972.
72. L. Mascia and M. Xanthos, ''An Overview of Additives and Modifiers for Polymer Blends: Facts, Deductions, and Uncertainties,'' *Adv. Polym. Technol.*, **11**, 237–248 (1992).
73. M. Xanthos, ''The Physical and Chemical Nature of Plastics Additives,'' in *Mixing and Compounding of Polymers,* I. Manas-Zloczower and Z. Tadmor Eds. Hanser, Munich, 1994.
74. M. Xanthos *Functional Fillers for Plastics*, Wiley-VCH, New York, 2005.
75. V. M. Lobe and J. L. White, ''An Experimental Study of the Influence of Carbon Black on the Rheological Properties of a Polystyrene Melt,'' *Polym. Eng. Sci*., **19**, 617–624 (1979).
76. D. M. Bigg, ''Rheological Behavior of Highly Filled Polymer Melts,'' *Polym. Eng. Sci*, **23**, 206–210 (1983).
77. T. B. Lewis and L. E. Nielsen, ''Viscosity of Dispersed and Aggregated Suspensions of Spheres,'' *Trans. Soc. Rheol*., **12**, 421–443 (1968).
78. I. L. Rutgers, *Rheol. Acta*., **2**, 202, (1962); also, I. L. Rutgers, *Rheol. Acta*., **2**, 305, (1962).
79. D. G. Thomas, ''Transport Characteristics of Suspension: VIII. A Note on the Viscosity of Newtonian Suspensions of Uniform Spherical Particles,'' *J. Colloid Sci.*, **20**, 267–277 (1965).
80. N. A. Frankel and A. Acrivos, ''On the Viscosity of a Concentrated Suspension of Solid Spheres,'' *Chem. Eng. Sci*., **22**, 847–853 (1967).
81. Y. Bomal and P. Goddard, ''Melt Viscosity of Calcium–carbonate-filled Low Density Polyethylene: Influence of Matrix-filler and Particle-particle Interactions,'' *Polym. Eng. Sci*., **36**, 237–243 (1996).
82. G. Wypych, ''Effects of Fillers on Rheolgoical Properties of Filled Materials,'' in *Handbook of Fillers*, *Second Edition*, Plastic Design Library, Toronto, Canada, 1999, Chapter 9.
83. C. D. Han, *Multiphase Flow in Polymer Processing*, Academic Press, New York, 1981.
84. C. D. Han, T. Van-den Weghe, P. Shete, and J. R. Haw, ''Effects of Coupling Agents on the Rheological Properties, Processability, and Mechanical Properties of Filled Polypropylene,'' *Polym. Eng. Sci*., **21**, 196–204 (1981).
85. Y. Iso, D. L. Kuch, and C. Cohen, ''Orientation in Simple Shear Flow of Semi-dilute Fiber Suspensions 1. Weakly Elastic Fluids,'' *J. Non-Newt. Fluid Mech*., **62**, 115–134 (1996).
86. L. G. Leal, ''The Motion of Small Particles in Non-Newtonian Fluids,'' *J. Non-Newt. Fluid. Mech*., **5**, 33–78 (1979).
87. A. T. Mutel, Ph.D. Thesis, Department of Chemical Engineering, McGill University, Montreal, Canada, 1989.

88. H. M. Laun, ''Orientation Effects and Rheology of Short Glass Fiber-reinforced Thermoplastics,'' *Colloid Polym. Sci*., **262**, 257–269 (1984).
89. A. T. Mutel and M. R. Kamal ''Rheological Properties of Fiber-reinforced Polymer Melts,'' in *Two-phase Polymer Systems*, L. A. U. Utracki, Ed., Hanser, New York, 1991.
90. R. G. Larson, *The Structure and Rheology of Complex Fluids*, Oxford University Press, Oxford, 1999.
91. P. Yaras, U. Yilmazer, and D. M. Kalyon, ''Ustable Flow of Concentrated Suspensions in Tube Flow,'' *SPE ANTEC Tech. Papers*, **39**, 2604–2606 (1993); also B. Aral and D. M. Kalyon, ''Time-dependent Development of Wall Slip in Shear Flows of Concentrated Suspensions,'' *SPE ANTEC Tech. Papers*, **39**, 2607–2610 (1993).
92. D. B. Todd, ''Introduction to Compounding,'' in *Plastics Compounding*, D. B. Todd, Ed., Hanser, Munich, 1998.
93. D. B. Todd and D. K. Baumann, ''Twin Screw Reinforced Plastics Compounding,'' *Polym. Eng. Sci*., **18**, 321–325 (1978).
94. G. Wypych, *Handbook of Fillers, Second Edition*, Plastics Design Library, 1999.
95. M. Kim and C. G. Gogos, ''The Roles of Clay and PE Wax Lubricants on the Evolution of Melting in PP Powder and Pellets,'' *Proc..11th Polymer Mixing Study Meeting*, Polymer Processing Institute, Hoboken, NJ (1995).
96. Y. Suetsugu, ''State of Dispersion – Mechanical Properties Correlation in Small Particle Filled Polymer composites,'' *Int. Polym. Process*., **5**, 184–190 (1990).
97. I. Manas-Zloczower, A. Nir, and Z. Tadmor, ''Dispersive Mixing in Internal Mixers—A Theoretical Model Based on Agglomerate Rupture,'' *Rubber Chem. Technol*. **55**, 1250–1285 (1982); also, I. Manas-Zloczower, I. Nir, and Z. Tadmor, ''Dispersive Mixing in Roll-mills,'' *Polym. Compos*., **6**, 222 (1985).
98. I. Manas-Zloczower and Z. Tadmor, ''Scale-up of Internal Mixers,'' *Rubber Chem. Technol.*, **57**, 49–54 (1984).
99. V. Collin and E. Peuvrel-Disdier, ''Disperion Mechanisms of Carbon Black in an Elastomer Matrix,'' *Elastomery*, Vol. 9 (2005) Special Edition JSSN PL 1427-3519; see also V. Collin and E. Peuvrel-Disdier, presentation at the Conference of European Rubber Research ''Practical Improvements of Mixing Processer,'' Paterborn, Germany, January 25-26 (2005), pp. 219–241
100. I. Manas-Zloczower and Z. Tadmor, ''The Distribution of Number of Passes over the Flights in Single Screw Melt Extruders,'' *Adv. Plasti. Technol*., **3**, 213–221 (1983).
101. Z. Tadmor, ''Screw Elements Having Shearing and Scraping Devices'' U.S. Patent 5,356,208, October 18, 1994; also, Z. Tadmor, ''Machine Invention, Innovation and Elementary Steps,'' *Adv. Polym. Technol.,* **21**, 87–97, 2002.
102. E. L. Canedo and L. N. Valsamis, ''Modeling Mixing in Continuous Mixers,'' *SPE ANTEC Tech. Papers*, **35**, 116 (1989).
103. R. Turkovich and L. Erwin, ''Fiber Fracture in Reinforced Thermoplastic Processing,'' *Polym. Eng. Sci*., **23**, 743–749 (1983).
104. Y. Suetsugu, ''The Effect of Mixing on Some Properties of Compounds and Composites,'' in *Mixing and Compounding of Polymers*, I. Manas-Zloczower and Z. Tadmor, Eds., Hanser, Munich, 1994.
105. C. G. Gogos, C. K. Yoon, and J. Brizzolara, ''Injection Molding Process Development for Long Fiber Reinforced Thermoplastics,'' *SPE ANTEC Tech. Papers*, **40**, 384 (1994).
106. C. Rauwendaal, ''Mixing in Single Screw Extruders,'' in *Mixing and Compou*nding *of Polymers*, I. Manas-Zloczower and Z. Tadmor, Eds., Hanser, Munich, 1994.
107. C. Rauwendaal, ''Mixing in Reciprocating Extruders,'' in Mixing and Compounding of Polymers, I. Manas-Zloczower and Z. Tadmor, Eds., Hanser, Munich, 1994.

108. R. Brzowski, T. Kumazawa, and J. L. White, ''A Model of Flow in the Mixing Section of the List KoKneader,'' *Int. Polym. Process*., **6**, 136 (1991).

109. P. G. Andersen, ''Mixing Practices in Corotating Twin Screw Extruders," in *Mixing and Compounding of Polymers*, I. Manas-Zloczower and Z. Tadmor, Eds., Hanser, Munich, 1994.

110. A. Kiani and H. J. Samann, ''Transient Flow Calculation of Co-rorating Twin Screw Extruders,'' *SPE ANTEC Tech. Papers*, **39**, 2758–2762 (1993).

111. V. L. Bravo, A. N. Hrymak, and J. D. Wright, ''Numerical Simulation of Pressure and Velocity Profiles in Kneading Elements of a Co-rotating Twin Screw Extruder,'' *Polym. Eng. Sci*., **40**, 525–541 (2000).

112. A. F. Yee, ''Mechanical Properties of Mixtures of Two Compatible Polymers,'' *Polym. Eng. Sci.,* **17**, 213–219 (1977).

113. B. D. Favis, ''Factors Influencing the Morphology of Immiscible Polymer Blends in melt Processing,'' in *Polymer Blends*, Vol. I, D. R. Paul and C. B. Bucknall, Eds., Wiley-Interscience, New York, 1999.

114. D. R. Paul and J. W. Barlow, ''Polymer Blends (or Alloys),'' *J. Macromol. Sci., Rev. Macromol. Chem*., **C18**, 109–168 (1980).

115. G. N. Avgeropoulos, F. C. Weissert, P. H. Biddisow, and G. G. A, Böhm, ''Heterogeneous Blends of Polymers. Rheology and Morphology,'' *Rubber Chem. Technol.*, **49**, 93–104 (1976).

116. L. A. Utracki, ''On the Viscosity-concentration Dependence of Immiscible Polymer Blends,'' *J. Rheol.*, **35**, 1615–1637 (1991).

117. J. M. H. Janssen and H. E. H. Meijer, ''Dynamics of Liquid-liquid Mixing: A 2-zone Model,'' *Polym. Eng. Sci*. **35**, 1766–1780 (1995).

118. D. B. Todd, C. G. Gogos, and D. N. Charalambopoulos, U.S. Patent 5,708, 197 (1998).

119. C. G. Gogos, M. Esseghir, B. David, D. B. Todd, and D. H. Sebastian, ''The Mixing Element Evaluator,'' *SPE ANTEC Tech. Papers*, **39**, 1542–1545 (1993).

120. C. G. Gogos, M. Esseghir, D.W. Yu, D. B. Todd, and J. E. Curry, ''The Twin-screw Mixing Element Evaluator: On-line Performance Evaluation of Modular Twin-Screw Mixing Elements,'' *SPE ANTEC Tech. Papers*, **40**, 270–276 (1994).

121. M. Esseghir, D.W. Yu, and C. G. Gogos ''Rheology-driven Mixing Mechanisms in TSMEE Kneading Blocks,'' *SPE ANTEC Tech. Papers*, **41**, 1994 (1995).

122. N. Tokita, ''Analysis of Morphology Formation in Elastomer Blends,'' *Rubber Chem. Technol*., **50**, 292–300 (1977).

123. C. W. Macosko, P. Guégan, A. K. Khandpur, A. Nakayama, P. Marechal, and T. Inoue, ''Compatibilizers for Melt Blending: Premade Block Copolymers,'' *Macromolecules*, **29**, 5590–5598 (1996).

124. M. L. Williams, R. F. Landel, and J. D. Ferry, ''The Temperature Dependence of Relaxation Mechanisms in Amorphous Polymers and Other Glass-forming Liquids,'' *J. Am. Chem. Soc*., **77**, 3701–3707 (1955).

125. B. Qian, D. B. Todd, and C. G. Gogos, ''Plastic Energy Dissipation and Its Role on Heating/melting of Single-component Polymers and Multi-component Polymer Blends,'' *Adv. Polym. Technol.,* **22**, 85–95 (2003).

126. M. Esseghir and D. W. Yu, *Proc. 4th Semi-annual Meet. of the Polymer Mixing Study,* Polymer Processing Institute, Hoboken, August 1992.

PROBLEMS

11.1 ***Complete POX Decomposition Requirements at Various Temperatures*** If we define, functionally, complete POX decomposition to be after a reaction time, t_f, at

constant reaction temperature, when the POX concentration $C(t_f) \cong 4 \times 10^{-2}[C_0]$. (a) Calculate t_f for POXs B and E on Fig. 11.3 at 180° and 240°C. (b) Calculate t_f for POX B in a dilute solution of decane in a reaction vessel, where the temperature is increased at the following rate: $T(t) = 180 + At$, where $A = 2 \times 10^{-1}[°\text{C} \cdot \text{s}^{-1}]$. Use the reported $t_{1/2}$ activation energy.

11.2 ***Rate-Controlling Phenomena in Reactive Processing*** Figure 11.4 indicates that the rate of decomposition in dodecane at 180°C of a commonly used POX in PP viscracking, Lupersol 101 is very close to the rate of decrease of the torque of a PP melt mixed with this POX in a laboratory scale Brabender internal laminar mixer. The reduction of the Brabender rotor torque is related to the reduction of the effective melt viscosity, due to the reduction of $\overline{M}_w$ and narrowing of the MWD, both consequences of the *controlled rheology polypropylene* (CR-PP) or viscracking reaction. (a) The text states that this similarity in the reduction rates of the POX concentration in dodecane and torque in the Bradender indicates that the POX decomposition kinetics is *rate controlling* the CR-PP reaction. What is meant by this statement? (b) In view of the kinetics of decomposition presented for the three POXs on Fig. 11.3, and keeping in mind their constant decomposition activation energy, would you expect POX decomposition to be *rate controlling* with the PP-Lupersol 101 reaction carried out at 240°C? If not, what would be the most probable rate-controlling process? What would be the effect of increasing the rotor speed? (c) At the POX concentration levels used with the reaction depticled on Fig. 11.4, what would you expect the order of magnitude of (t_G/t_R), Eqs. 11.2-5 and 11.2-6 to be?

11.3 ***Physical Significance and Reactive Processing Consequences of Process Characteristic Time Ratios*** A number of reactive processing characteristic times were presented in Sections 11.2–11.4. Following Biesenberger and Sebastian (5) and Sebastian (6), our discussion of reactive processing utilizes considerations of the physical significance of *ratios* of competing process characteristic times of processes involved in reactive polymer processing. Discuss the following ratios of characteristic times; in particular on how and why their order-of-magnitude values determine the rate-controlling processes in reactive processing, as well as how they affect process stability: (a) t_G/t_R or $t_G/(t_R + t_H)$ (b) $\text{Da} = t_{\text{res}}/t_r$ (c) t_D/t_r (d) t_D/t_{res} (e) t_D/t_{mix}

11.4 ***Advantages and Limitations of Polymer Processing Equipment as Polymer System "Reactors"*** Consider the following reacting systems involving polymers. Conduct the necessary literature[6] searches on the reaction mechanisms, kinetics, and heats of reaction for each system and discuss it as a candidate to be carried in polymer processing equipment, considering both batch and continuous processors. (a) Polymerization of methylmethacrylate monomer into high MW PMMA. (b) Polymerization of PMMA prepolymer into high MW PMMA. (c) Condensation polymerization of PET. (d) Halogenation (both chlorination and bromination) of polyolefins. (e) Grafting of AA onto PE or PP.

6. An excellent source of references on reactions carried out in polymer processing equipment is S. B. Brown, "Reactive Extrusion: A Survey of Chemical Reaction of Monomers and Polymers, during Extrusion Processing," in *Reactive Processing*, M. Xanthos, Ed., Hanser, Munich, 1992.

11.5 ***Carrying out Controlled Rheology Polypropylene (CR-PP) Viscracking Reactions in Single Screw and Twin Screw Extruders*** Historically the early CR-PP reactions were carried in SSEs with the POX mixed into the feed PP reactor granules or in a smaller-scale reactive extrusion process by mixing PP-POX masterbatch pellets with PP pellets. Currently, this process is carried out, almost exclusively, in TSEs and most often by coating the PP particulates with the required amount of POX. You are asked to: (a) Discuss the differences in carrying out the CR-PP reaction in SSEs and Co-TSE, from the points of view of the different melting and mixing mechanisms in each. (b)Which of the preceding ''reactors'' will yield lower $\overline{M}_w$ and narrower MWD viscracked PP product? Why? (c) If the POX were to be introduced in both extruders as a separate reactant stream *after* melting, which of the two will yield a lower $\overline{M}_w$ and narrower MWD? Will the difference become larger or small at higher melt temperatures? Why?

11.6 ***Estimation of the Effective Diffusivity of POX in PP Melts*** Ryu et al. (37), as discussed in Section 11.1, coated 200–300 μm diameter PP granules with POX, compressed them to prepare thin films and used the films to carry out CR-PP reactions by placing them in a constant-temperature oven, withdrawing the samples after specified reaction times, and obtaining $\overline{M}_w$ and MWD; POX ''E,'' (see Fig. 11.3) was used. They found no measurable macromolecular structure changes after reaction times of (6–7) $t_{1/2}$ of POX ''E.'' They concluded that the process of diffusion of POX ''E'' into the PP melt was not rate controlling. (a) What is the basis for this conclusion? (b) Can one obtain an estimate of the effective diffusivity of POX ''E'' in the PP melt by specifying the order of magnitude of the ratio of diffusion to reaction characteristics times (t_D/t_r)?

11.7 ***Effect of Compositional Nonuniformities on the "Unifying" Ability of Characteristic Time Ratios to Analyze the Dynamic State of Reactions*** Figure 11.10, plotting the dimensionless initial reactant concentration as a function of the Damkohler number, $\mathrm{Da} = t_{\mathrm{res}}/t_r$ for both batch and continuous reactors. This analysis assumes a well-mixed reacting system. (a) What will the effects of poor mixing be and how will they influence this analysis? (b) What is the maximum allowable striation thickness between the reacting species for the system to be considered well mixed?

11.8 ***Physicochemical Mechanisms Responsible for the Beneficial Actions of Polymer Additives*** Tables 11.2–11.4 list examples of common polymer additives by their beneficial action(s) to the polymers during processing and products during their product life.

1. You are invited to search for and examine the physicochemical mechanisms responsible for such beneficial actions for the following additives: (a) Sterically hindered phenol antioxidants; (b) Carbon black, as a light stabilizer (e.g., rubber tires); (c) Carbon black, as an electrically conductive additive; (d) Silanes, as glass fiber–coating adhesion promoter with thermosets and thermoplastic reinforced systems; (e) Quaternary ammonium salts as antistatic agents; (f) Azodicarbonamide as a chemical blowing agent; (g) CO_2 as a physical blowing agent; (h) Hydrocarbons as physical blowing agents (e.g., LDPE foams)

2. Are there critical maximum distances between adjacent dispersed additive cites, above which the additives are not effective? Discuss, with example(s).

11.9 ***Modeling Melt-Full Kneading Elements by the Two-Zone Theoretical Model*** The two-zone model to treat dispersive mixing was developed by Manas-Zloczower et al.[7] for internal batch mixers. An example of this work is presented in this chapter, Example 11.3 and, as extended to the continuous SSE, viewed as a dispersive mixer, in Example 11.4. You are invited to consider the melt-full, kneading elements, Fig.10.11, from a two-zone dispersive mixer point of view. Comment on the gradual and cyclical reduction/extension of the available cross-sectional area between a pair of opposing kneading disks and the barrel.

11.10 ***Fiber Length Attrition during the Single Screw Extrusion of PE Pellets Mixed with 3.2-mm Chopped Glass Fibers*** Figure 11.28 presents experimental results of von Turkovich and Erwin (103) on the fiber number average length attrition along the single screw in the downstream direction of solids conveying, compression, melting, and metering/mixing sections. (a) What analytical procedures can be used to measure the number average fiber length using the SSE carcass along the screw length? (b) Comment on the observed results, that is, what fiber breaking phenomena are at play at each section? (c) Would you expect different results in a larger SSE, say a 4-in-diameter, where the channel dimensions are an order of magnitude larger than the fiber and pellet dimensions? (d) Will the glass-fiber attrition rate be different if they were coated with a silane compound?

7. *Rubber Chem. Technol.*, **55**, 1250–1285 (1982); *Polym. Compos.*, **6**, 222 (1985).